UNIVERSITA' DEGLI STUDI DI MILANO-BICOCCA
Facoltà di scienze Matematiche, Fisiche e Naturali
Scuola di dottorato in Biologia
XXII ciclo

STUDIES ON THE MECHANISM AND PHYSIOLOGICAL ROLE(S) OF THE INTERACTION OF ATAXIN-3 WITH TUBULIN

Docente guida: prof. Paolo Tortora

Mazzucchelli Serena
Matr.040591

Anno accademico 2008/2009

A mio marito e
al piccolo Pietro

Abbreviations

Abs	absorbance
AD	alzheimer disease
Amp	ampicillin
AR	androgen receptor
AT3	ataxin-3
BBF	bromophenol blue
BDNF	brain-derived neurotrophic factor
Bis-acrilammide	N,N′-methylen-bisacrilamide
bp	base pair
BSA	bovine serum albumine
Caf	chloramphenicol
CAPS	3-cyclohexylaminopropan-1-sulphonic acid
CBP	cAMP response element-binding protein
CD	circular dicroism
CK-II	casein kinase II
CRE	cAMP repressor element
CREB	CRE-binding protein huntington disease
DMEM	Dulbecco's modified eagle medium
dNTP	deoxyribonucleotide triphosphate
DRPLA	dentatorubroluysian atrophy
DTT	dithiotreitol
EDTA	etilendiaminetetraacetic acid
ERAD	endoplasmic-reticulum associated degradation

EST	expressed sequence tags
EtBr	etidium bromide
FBS	bovine foetal serum
FTIR	fourier-transformated infrared spectroscopy
GFP	green fluorescent protein
GST	gluthatione S-transferase
JD	josephin domain
H	hours
HA	hemagglutinin
HD	huntington disease
HDAC6	histone deacetylase 6
Kan	kanamicin
kDa	kilodalton
IF	intermediate filament
LB	Luria-Bertani
MAP2	microtubule associated protein 2
min	minutes
MT	microtubule
MTOC	microtubule organizing center
MJD	Machado-Joseph's disease
NES	nuclear export signal
NI	nuclear inclusion
NLS	nulear localization signal
NRSE	neuron restrictive silencer element
PAGE	polyacrylamide gel electrophoresis

PBS	phosphate buffer
PD	parkinson disease
PMSF	phenilmethansulphonilfluoride
REST	repressor element-1 transcription factor
SBMA	spinobulbar myotonic atrophy
SCA	spinocerebellar ataxia
SDS	sodium dodecilsulfate
sec	seconds
SPR	surface plasmon resonance
TAE	tris-acetate-EDTA buffer
TEMED	N,N,N′,N′tetramethylethylendiamine
TRIS	tris [hydroxymetil] aminomethane
Ub	ubiquitin
UPP	ubiquitin-proteasome pathway
UIM	ubiquitin interacting motif
UCH	ubiquitin C-terminal hydrolase
UBP	ubiquitin specific protease
VCP	valosin-containing protein
VIMP	VCP interacting membrane protein

Abstract

Ataxin-3 (AT3) is a protein consisting of an N-terminal globular Josephin domain and an unstructured C-terminal region that contains a stretch of consecutive glutamines. When its length is beyond a critical threshold, it triggers an inherited neurodegenerative disease, spinocerebellar ataxia type 3. The pathology results from protein misfolding and intracellular accumulation of fibrillar amyloid-like aggregates. Plenty of work has been carried out to elucidate the protein's physiological role(s), which has shown that AT3 is multifunctional protein. It acts as transcriptional repressor and also carries out its normal function on protein surveillance pathways. In fact, AT3 interacts with RAD23, which shuttles ubiquitinated protein to proteasome, and also with VCP that seems to be involved in the degradation pathway ubiquitin-proteasome dependent and in the retrotranslocation of ERAD substrates. In addition, a recent report suggests that it participates in sorting misfolded protein to aggresomes. Furthermore, it was shown that AT3 binds ubiquitin chains through its ubiquitin-binding motifs and also has, in the Josephin domain, the catalytic triad of thiol proteases that in this protein sustains ubiquitin cleavage. Since a thorough understanding of the protein's physiological role(s) requires the identification of all the molecular partners interacting with AT3, we pursued this goal by taking advantage of two-dimensional chromatography coupled to tandem mass spectrometry. We found that different AT3 constructs,

including the sole Josephin domain, bound α- and β-tubulin from soluble rat brain extracts. Coimmunoprecipitation experiments confirmed this interaction. Also, normal AT3 overexpressed in COS-7 cultured cells partially colocalized with microtubules, whereas an expanded variant only occasionally did so, probably due to aggregation. Furthermore, by surface plasmon resonance (SPR) we determined a dissociation constant of 50–70 nM between AT3 and tubulin dimer, which strongly supports the hypothesis of a direct interaction of this protein with microtubules in vivo. Since misfolded protein is sorted to aggresome via microtubules under conditions where proteasome is overloaded or its function compromised, our finding suggests an involvement of AT3 in directing aggregated protein to aggresome.

In further experiments, we assessed by SPR the binding affinity of AT3 with either Lys^{48}-linked or Lys^{63}-linked polyubiquitin chains. We observed that either chains were bound with high affinity by AT3. However, we also found that binding of Lys^{48}-polyubiquitin and tubulin were mutually exclusive, whereas Lys^{63}-polyubiquitin and tubulin could be bound simultaneously. Protein Lys^{48}- and Lys^{63}-polyubiquitination are signals that direct to proteasome and aggresome, respectively. Thus, our findings point to a model whereby AT3 sorts tagged protein to either goals, depending on the type of ubiquitin bound. In the former case, AT3 cannot bind to tubulin so it is prevented from being directed to aggresome; in the latter it sorts misfolded protein to aggresome. In keeping with this hypothesis, we

also found that AT3 binds to histone deacetylase 6 with nanomolar affinity. Actually, the latter protein is indispensable for aggresome formation, as it also binds Lys^{63}-polyubiquitylated proteins and interacts with the dynein complex, which transports misfolded protein cargo to aggresomes via microtubules.

Finally, we also investigated the mode of interaction between AT3 and tubulin by producing several truncated AT3 variants, and determining their affinity towards tubulin. These studies highlight the occurrence of three different tubulin-binding sites: in the Josephin domain, in the disordered stretch upstream of the polyQ tract, and at the C-terminus, at the very end of the polypeptide chain.

Index

1 Introduction

1.1 Pathologies associated with triplet expansions

Investigations on the human eukaryotic genome showed the presence of numerous microsatellite DNA, which are very short (less than 13 bp) tandem repeated sequences (Richards and Sutherland, 1997). These repeats were once thought to be commonplace iterations in the genome, but now we know that these apparently "benign" streches of DNA can sometimes expand and cause disease (Cummings, and Zoghbi, 2000). Triplet expansions can be found inside or outside protein-encoding regions. If they are outside, an alteration of protein expression may occur. On the other hand, if the trinucleotide repeat lies in a protein-encoding region, this results in synthesis of abnormal, mostly misfolded proteins, which in turn may alter cellular metabolism (Richards and Sutherland, 1997).

The occurrence of triplet expansions in the coding sequences may be responsible for such pathologies. Thus, proteins associated with triplet expansions may loose their physiological function, acquire a toxic one resulting from aggregation. Triplet expansions is responsible for several pathologies that, all together, are referred to as triplet expansion diseases (Richards and Sutherland, 1997).

Several defining features are shared among disorders caused by trinucleotide expansions. First, the mutant repeats show both somatic and germline instability and, more frequently, they expand rather than contract in successive transmissions (Ross, 1995; Perutz, 1996).

1

Expansions arise from unequal crossing-over or from a defective performance of DNA polymerase during replication. The underlying mechanism relies upon loops or hairpins formation in DNA repeats when they are located in single-stranded DNA stretches, with resulting insertion of additional triplets (Mandel, 1997). Secondly, an earlier age of onset and increasing severity of phenotype in subsequent generations (anticipation) generally are correlated with larger repeat length. Finally, the parental origin of disease allele can often influence anticipation, with paternal transmissions carrying a greater risk of expansion for many of these disorders (Cummings and Zoghbi, 2000).

The pathologies associated to the triplet expansions can be divided in two main subclasses, based on the relative location of the trinucleotide repeat to a gene. The first subclass, presently accounting for six diseases, has its repeats in non-coding sequences. The non-coding trinucleotide repeats diseases typically are characterized by large and variable repeat expansions that result in multiple tissue disfunction or degeneration. The trinucleotide repeat sequences vary in this subclass (CGG, GCC, GAA, CTG and CAG), and it is clear that the particular trinucleotide sequence, as well as its location with respect to a gene, are important defining factors in dictating the unique mechanism of pathogenesis for each disease. The pathogenic mechanism also varies from disease to disease, depending on the consequences of the lost function of the respective proteins or, in some cases, acquired function of a toxic transcript. Such pathologies include the X-fragile syndrome, Myotonic dystrophy, Friedrich ataxia, Fragile

XE MR, Spinocerebellar ataxia type 8 and 12 (Cummings and Zoghbi, 2000).

The second subclass is characterized by exonic $(CAG)_n$ repeats that code for polyglutamine tracts. The latter group is referred to collectively as "polyglutamine diseases" (Cummings and Zoghbi, 2000). In this class, are included Huntington's disease (HD), DRPLA (dentatorubropallidoluysian atrophy), Kennedy's disease, different types of spinobulbar muscular atrophy and five types of ataxias (ataxia 1, 2, 3, 6, 7) (Mandel, 1997). The two classes also differ in the length of the expansions, class II generally involving a smaller number of repeats (Mandel, 1997).

1.2 Role of CAG repeats in pathogenesis

Possible mechanisms by which the expansions are involved in the pathogenesis of triplet expansions diseases fall into three categories. The gain-of-function mechanism is characteristic for diseases caused by CAG repeat expansions in translated sequences. The loss-of-function mechanism is represented by the fragile X syndrome and the Friedrich ataxia in which the transcriptional silencing of the FMR-I gene and transcriptional interference in the case of X-25 gene result in reduced levels of their protein products. The third category includes the gain-of-function mechanism known for dominantly inherited myotonic dystrophy, which is caused by trinucleotide repeat expansion in a non-coding sequence (Jasinska *et al.*, 2003).

In the myotonic dystrophy (class I neurodegenerative disease), which is caused by the expansion of either repeats CTG in the *DMPK* gene, or CCTG repeats in the ZNF1 gene within the untranslated sequence, the pathogenic effects are postulated to occurs predominantly at the RNA level (Wang *et al.*, 1995). The transcript with the expanded CUG repeat alters the functioning of RNA binding proteins which results in the disrupted processing of other CUG repeat containing transcripts. The expanded transcripts accumulate as a nuclear focus and alter the regulation and normal functions of the repeat binding proteins. They may form hairpin structures sequestering proteins and modifying the splicing of their target gene (Jasinska *et al.,* 2003).
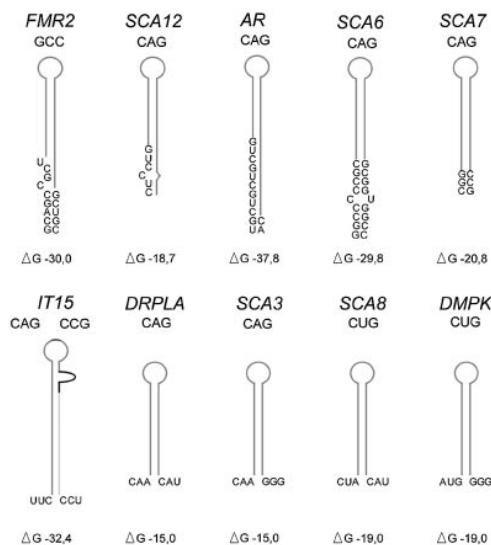
Figure 1.1 Schematic rapresentation of RNA structure modules predicted for trinucleotide repeats and their nearest flanking sequences from 10 triplet expansion related transcripts. Repeated sequences are marked with a grey line. The secondary structures were predicted and energy values calculated using the M-fold program version 3.0 (Jasinska *et al.,* 2003).

These observations prompted to address the issue of whether CAG repeats present in transcripts from several mutant genes associated with hereditary neurodegenerative diseases may make a

contribution to the pathogenesis. It was thus shown (Figure 1.1) that the structures formed by the repeats and their natural flanking sequences in the spinocerebellar ataxia (SCA) type 3 and type 6, and dentatorubral-palidoluysian atrophy (DRPLA) transcripts have different molecular architectures which may have functional and pathological relevance (Michlewski *et al.*, 2005).

In particular, the genetic transcripts responsible for SCA3, SCA6 and DRPLA form secondary hairpin structures, and there is a correlation between the pathological threshold of repeats and the nature of the sequences flanking the triplet expansion that form the hairpin in the corresponding transcript (Michlewski *et al.*, 2005). Furthermore, hairpin structures, formed by expanded CAG repeats in the transcript, cause a frameshift from polyQ to polyA that are toxic at the cellular level (Gaspar *et al.*, 2001).

1.3 Polyglutamine (polyQ) diseases

Research in the past decade discovered a new class of inherited, autosomal dominant neurodegenerative diseases, the polyQ expansion diseases (Table 1.1). The increase in size of the repeat over generations within families and the resulting increasing severity and/or an earlier onset of the disorder, is referred to as anticipation, and the mutation as dynamic (Richards and Sutherland, 1997). PolyQ diseases are all progressive, ultimately fatal disorders, whose onset is typically in adulthood, and progress over 10 to 30 years. The clinical features and pattern of neuronal degeneration differ among the diseases, yet

increasing evidence suggests that polyQ diseases share important pathogenic features. In particular, abnormal protein conformations promoted by polyQ expansions seem to be central to pathogenesis (Paulson, 1999). PolyQ diseases also share important features with a growing group of neurodegenerative disorders, including Alzheimer's disease and many other dementias, in which abnormal protein folding and aggregation are also implicated. The hallmark of all of these pathologies is the typical aggregation state of the proteins involved, which appear as amyloid structures, characterized by fibrillar appearance under electron microscopy, Congo red staining and birefringence, and cross-β-structure. Their localisation may be either intra- or extracellular (or both) (Sipe and Cohen, 2000). The basic features of the polyQ disease are outlined below.
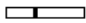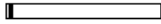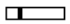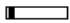
Spinal and bulbar muscular atrophy (Kennedy's disease). First described by Kennedy *et al.* in 1968, the genetic basis was identified in 1991 when La Spada *et al.* mapped the gene to the proximal long arm of the X-chromosome (Xq11–12), a region encoding the androgen receptor (AR). The causative mutation was identified as a CAG repeat expansion encoding a polyQ expansion within the translated AR protein. The AR, a member of the steroid receptor superfamily, is a ligand-dependent nuclear transcription factor that plays the central role in masculinization of the male fetus, development of male secondary sexual characteristics and maintenance of spermatogenesis. The molecular basis of Kennedy's disease is an expansion of the polyQ region. This region is polymorphic within the normal population,

6

numbering between 10 and 36 repeats, whereas in Kennedy's disease this repeat region is expanded to number between 40 and 62. Expansion of this region to beyond 40 repeats places this protein in the pathogenic range. Individuals with higher numbers of repeats generally tend to develop symptoms at an earlier age (Greenland and Zajac, 2004). The expansions do not affect hormone binding as the polyQ tract is far from the hormone-binding domain, yet their expansion results in the hormonal activation (Zoghbi *et al.,* 2000). Kennedy's disease is characterized by motor-neuron loss in the spinal cord and brain stem and is associated with a less extensive loss of sensory neurons and chronic denervation atrophy in the skeletal muscles (Tanaka *et al*., 1999).

Dentatorubral pallidoluysian atrophy (DRPLA) is an autosomal dominant neurodegenerative disorder characterized clinically by myoclonus, epileptic seizures, cerebellar ataxia, choreoathetotic movements, personality change and dementia. The basic clinical features depend on the age of onset. The dentate nucleus of the cerebellum is the most severely affected site followed by the pallidum. Recently, the causative gene of DRPLA was assigned to the short arm of chromosome 12, and the underlying abnormality was identified as an expansion of a CAG repeat within its codifying region. The function of the gene product atrophin 1, has not yet been determined. Among the CAG repeat diseases, DRPLA exhibits a most prominent instability in the number of CAG repeats; they expand significantly in following generations. Furthermore, DRPLA shows a

strong ethnic predilection for Asian, particularly Japanese populations (Zoghbi *et al.,* 2000). Atrophin 1 is a cytoplasmic protein that has 1185 amino acids, and does not show any homology to other known protein. In the normal allele the glutamine repeats are between 6 and 36, in the abnormal allele they are in the range 49-84 (Zoghbi *et al.*, 2000). It has

Table 1.1 Basic molecular properties of proteins responsible of polyQ diseases.

Disease	Protein	CAG (n) normal	CAG (n) expanded	Relative dimension of the protein	Localiza-tion	Main character i-stics	Brain region
SBMA	Androgen receptor	9-36	38-62		Nucleus e cytoplasm		Basal lamina
DRLPA	Atrophin-1	6-36	49-84		Cytoplasm		Cerebellar and cerebral cortex
HD	Huntingtin	6-34	36-121		Cytoplasm	Intermediate alleles: 29-35 rep.	Striatum and cerebral cortex
SCA1	Ataxin-1	6-44	39-82		Nucleus	Interruption of 1-4 CAT in normal alleles	Purkinje cells and dentatus nucleus
SCA2	Ataxin-2	15-31	36-63		Cytoplasm	Interruption of 1-2 CAA in normal alleles	Purkinje cells
SCA3	Ataxin-3	12-40	55-84		Cytoplasm		Cerebellar neurons and spinal marrow
SCA6	Ataxin-6	4-18	21-33		cellular membrane		Purkinje, olive cells and dentatus nucleus
SCA7	Ataxin-7	4-35	37-306		Nucleus	Alleles with 28-35 rep.	Macula and cerebellar cortex

been demonstrated a statistically significant negative correlation between the size of the CAG repeat in the DRPLA gene and the age of onset of the disease: the longer the CAG repeat length, the earlier the age of onset. This anticipation is more pronounced when the disease is paternally transmitted. Instability of the CAG repeat is considered to result from "slippage", especially in paternal transmission, i.e. during spermatogenesis. Concerning the correlation between the numbers of CAG repeats and disease phenotype, clinical features are strongly influenced by the age of onset of DRPLA (Hashida *et al.*, 2001).

Huntington's disease (HD) is a late onset inherited neurodegenerative disorder that manifests with personality changes, motor impairment, and cognitive decline. The disease progresses to death over a period of 15-20 years, and there is no effective treatment. The HD mutation is a CAG repeat expansion that results in an abnormally long tract of glutamines in the HD protein huntingtin. The physiological range of CAG repeat is 6- 35, whereas alleles carrying at least 40 repeats are fully penetrant and cause HD within a normal life span, while alleles in the range 36-39 confer an increasing risk of developing HD. There is an inverse relationship between the age of onset of HD and the CAG repeat size, with alleles of 60 repeats and above invariably causing a juvenile onset (Tsang *et al.*, 2006). Huntingtin is made by a single polypeptide chain consisting of 3141 amino acids, with a molecular mass of 348 kDa. In neuronal cells, pathogenic variants of huntingtin give rise to intranuclear inclusions (NIL; neuronal intranuclear inclusions), so it has been assumed that

such inclusions are responsible for the observed neurodegeneration. According to this model, a polyQ stretch beyond the critical threshold provokes a conformational alteration of the protein. During the aggregation process other proteins, notably ubiquitin, are sequestered. This phenomenon is toxic to the cell, altering cellular metabolism (Zoghbi *et al.,* 2000). Although the function of huntingtin has been long completely unknown, it was recently proposed that it might be involved in the embryonic neurogenesis (Bates *et al.,* 1998) and in the transcription of the gene coding for a neurotrophic factor that plays a key role for the survival of the cells in the striate tissue, i.e., the brain-derived neurotrophic factor (BDNF). The neuron restrictive silencer element (NRSE) is the target of wildtype huntingtin activity on BDNF promoter II. Wild-type huntingtin inhibits the silencing activity of NRSE, increasing transcription of BDNF. This effect occurs through cytoplasmic sequestering of repressor element- 1 transcription factor/neuron restrictive silencer factor (REST/NRSF), the transcription factor that binds to NRSE. In contrast, aberrant accumulation of REST/NRSF in the nucleus is present in Huntington's disease. Consistently, loss of expression of NRSE controlled neuronal genes is shown in cells, mice and human brain with Huntington's disease. Thus, wild-type huntingtin acts in the cytoplasm of neurons to regulate the availability of REST/NRSF to its nuclear NRSE-binding site and that this control is lost in the pathology of Huntington's disease (Zuccato *et al.*, 2003).

The autosomal dominant spinocerebellar ataxias (SCAs) represent a clinical and genetically heterogeneous grouping of debilitating and often fatal neurodegenerative diseases characterized by a generalized incoordination of gait, speech and limb movements. Extracerebellar deterioration also occurs in most patients, presenting as variable nuclear or supranuclear ophthalmoparesis, slow saccades, pyramidal or extrapyramidal symptoms, neuropathy, or decreased vibration sense. Typically, the onset of symptoms occurs between the ages of 30 and 40, and symptoms progress slowly. Anticipation may be observed (Jardim *et al.,* 2001).

Spinocerebellar ataxia type 1 (SCA1) is one subtype of the hereditary ataxias. The SCA1 gene which maps to the short arm of human chromosome 6 was identified using a positional cloning approach (Orr *et al.,* 1993; Zoghbi *et al.,* 1995). The age at onset usually ranges between 20 and 60 years; thereafter the disease progressively worsens, leading to death in 10–20 years. Normal SCA1 alleles contain an uninterrupted (CAG)n repeat when they carry less than 21 units. Instead, the repeat is interrupted by one to three CAT encoding for histidine when there are more than 21 triplets. The interruptions (CAT, CATCAGCAT, and CATCAGCATCAGCAT) are localized approximately in the middle of the (CAG)n stretch. The trinucleotide stretch in the expanded alleles is always made up by an uninterrupted (CAG)n repeat. The majority of normal alleles range from 18 to 38 repeats, while expanded alleles range from 39 to 82 repeats. At the protein level, ataxin-1, the SCA1 gene product, is found

predominantly in the nucleus of neurons and in the cytoplasm of peripheral tissues. Despite the wide expression pattern of ataxin-1, a selective degeneration of cerebellar Purkinje cells and brainstem neurons can be found in SCA1 (Calabresi *et al.,* 2001).

Spinocerebellar ataxia type 2 (SCA2). Ataxin-2 – the protein responsible for this disease - has 1312 residues (including 22 glutamines of the polyQ stretch) and a molecular mass of 140 kDa. The SCA2 gene has been mapped to the chromosome 12q24.1 (Albrecht *et al.,* 2004). The number of triplets from the wild-type gene is between 15 and 31. Ataxin-2 proves to be pathogenic when the number of repetitive triplets is between 36 and 63. The protein is located predominantly in the Golgi apparatus (Albrecht *et al.,* 2004). In SCA2, mutant ataxin-2 causes neurodegeneration primarily in Purkinje neurons and selected neurons in the brain stem, resulting in a progressive ataxia and death. As in other polyQ diseases, SCA2 becomes more severe and has an earlier age of onset with increasing length of the polyQ repeat.

Ataxin-3 (AT3) is the responsible protein for **spinocerebellar ataxia type 3** (SCA3), is the subject of this thesis, and will be thoroughly described below.

The gene involved in **spinocerebellar ataxia type 6** (SCA6) encodes the subunit α from the voltage-dependent calcium channels (Durr *et al.,* 1996). In his normal form, this gene has 4 to 18 consecutive CAG repeats, whereas in the pathogenic form the number of triplets is between 21 and 33. Thus, the pathogenic threshold for this

ataxia is much lower than for the other polyQ diseases. The repeats are substantially stable, so an increase in size is rarely observed in the successive generations (Zoghbi *et al.,* 2000).

Spinocerebellar ataxia type 7 (SCA7). The protein involved has the polyQ repeat close to the N-terminal end. The encoding gene does not have any interruption in the consecutive CAG triplets, unlike the case of ataxin-1 and 2. ataxin-7 has a molecular mass in the range 130-180 kDa, depending on the polyQ size. In pathogenic forms, the size polyQs is in the range 37- 306, in normal forms 4-35 (Zoghbi *et al.,* 2000). In Table 1.2, the most prominent features of proteins responsible for polyQ diseases are presented.

1.4 Relationship between genotype and phenotype

The comparison of genotype (CAG repeat length) and consequent phenotype (age of onset and disease manifestation) as a structure–function assessment has been particularly informative in the polyQ disorders, because in each case a single type of mutation, varying only in severity, accounts for all individuals suffering from the disorder. An important finding shared by the polyQ disorders is that the age of the patient at neurological onset decreases with increased polyQ length (Gusella and Mac Donald, 2000).

Each disorder shows a characteristic threshold for the polyQ size below which no clinical symptom is observed. Above the threshold, the progressive decrease in onset age with polyQ length (Figure 1.2) shows

a somewhat different profile in each disorder, indicating that the increased severity due to each extra glutamine residue depends on the protein context. These curves imply that in this class of inherited neurodegenerative disease, there is a common trigger of pathogenesis, the polyQ segment, which has different consequences depending on the protein in which it is contained.

Most patients with polyQ diseases are heterozygous for the mutant allele, but in some cases homozygotes have been described, with two mutant alleles and no normal allele. The age of onset for homozygous individuals is primarily determined by the length of the polyQ tract encoded by the longest mutant allele.

The above genotype–phenotype correlations lead to the formulation of five criteria for he mechanism triggering pathogenesis (Gusella and Mac Donald, 2000):

1. a threshold polyQ length below which the pathogenic mechanism is not triggered within the average human lifespan;

2. increasing severity of the disease with increasing polyQ length;

3. dominance of the mutant over the wild-type allele;

4. a greater effect of polyQ length than allele dosage on the pathogenic mechanism;

5. cellular specificity that varies with protein context.
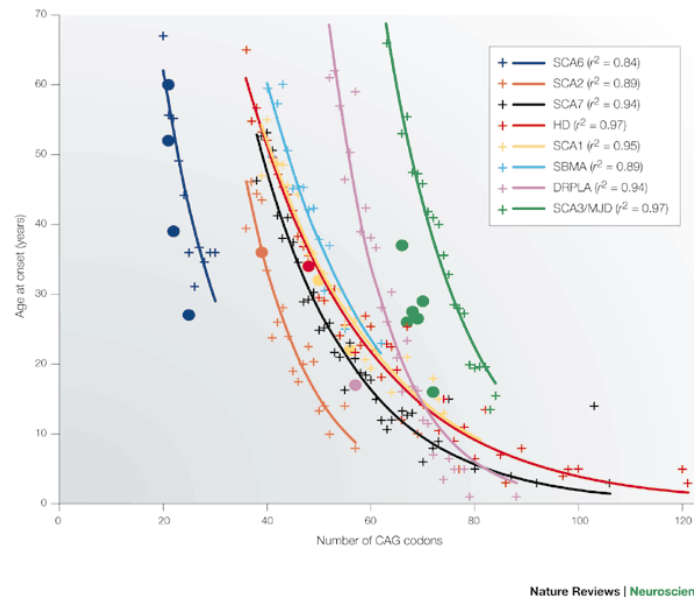
Figure 1.2 Relationship between the age of disease onset and length of CAG repeats (Gusella and Mac Donald, 2000)

1.5 Possible functions of the normal polyQ tract

The possible functions of normal polyQ tracts are far from being understood. Long glutamine repeats occur in various proteins, prominently in transcription factors, such as, for instance, the homeobox proteins in *Drosophila*. Their possible functions have been investigated in two homologous proteins encoded by the gene Abdominal B in *Drosophila* (Perutz *et al.*, 1994). They both have a DNA-binding segment in the C-terminal domain. However, one variant also has an extra N-terminal, 224 residues long domain rich in glutamine. Its deletion did not reduce the affinity for DNA, but halved its transcriptional activity. Conversely, splicing a distant part of the

glutamine-rich domain to an otherwise inactive C-terminal domain restored transcriptional activity, which showed that the glutamine-rich domain did serve a necessary function, but without a hint as to its possible mechanism (Perutz *et al.*, 1994).

Almost nothing is know regarding the function of the glutamine repeats in the proteins responsible for polyQ diseases, but some clues have emerged from studies of the human transcription factor Sp1. This is a trans activator of gene expression that binds to GC-rich regions in the promoters of several cellular and viral genes, including that of simian virus SV40. The C-terminal fragment of Sp1 is a single chain of 696 residues with a glutamine-rich segment between residues 260 and 391, and with 3 zinc fingers beyond residue 540. An *in vivo* translation assay was designed to study the function of the glutamine-rich segment. A C-terminal fragment of Sp1 containing the zinc fingers was transcriptionally inactive but became activated after a fragment containing residues 369-391 had been spliced onto it. This had the sequence PGNQVSWQTLQLQNLQVQNPQAQ; it contained 8 glutamines, 3 asparagines, a serine, and a threonine; these are all residues with polar side chains capable of forming hydrogen bonds with complementary polar side chains in neighbouring β-strands (Perutz *et al*., 1994 and literature therein). Alternatively, the inactive C-terminal fragment could be activated by splicing to it the glutamine-rich segment of the Antennapedia protein of *Drosophila*. In this in vivo assay, authors next contructed a reporter plasmid with a single GC box close to the initiation site of transcription, and six GC boxes 1.7 kb

16

downstream. Binding of Sp1 to this distantly placed GC boxes stimulated the weak activation induced by the binding of Sp1 to the close GC box. A similar stimulation was produced by the addition of a truncated form of Sp1 without the zinc fingers but in which had been included the glutamine-rich segment. These experiments demonstrated that interaction between the glutamine-rich segments of Sp1 molecules bound to widely separated DNA segments enhanced transcription (Perutz *et al.*, 1994).

On the other hand, no functions has so far been found for a stretch of 38 consecutive glutamines in the human TATA box-binding factor TFIID, but its conservation in mouse argues in favor of its fulfilling an essential function (Perutz *et al.*, 1994).

It remains to be explained why longs repeats occurring in human proteins, such as AT3, are much shorter in the closely related murine counterpart, where only 5-6 consecutive glutamines are found.

1.6   Structural properties of the polyQ stretch

Although the aggregation process of polyQ containing proteins *in vivo* may be mediated by interactions with other proteins or cellular components, *in vitro* experiments clearly indicate that aggregation is self-driven and not triggered by the presence of other partners (Scherzinger *et al.*, 1999).

These observations suggest that the aggregation process may be initiated by a conformational change induced by an expanded polyQ stretch (Masino *et al.,* 2001). In particular, a property of the glutamine

tract, when present in a short protein fragment, is to promote self-aggregation, with a conversion to an insoluble β– sheet amyloid structure. Molecular modeling showed that β-strand made of polyQ can be assembled into sheets or barrels by hydrogen bonds between their main-chain and side-chain amides forming the so called "polar zippers". These zippers are responsible for the formation of proteic aggregates (Perutz *et al.*, 1994).

Along with molecular modeling studies, a few experimental works have been carried out in order to characterize the structural features of polyQ stretches in solution. PolyQ peptides are difficult to characterize since they are mostly insoluble in water. So, in 1994 Perutz studied the Asp2-Gln15-Lys2 peptide. CD, electron and x-ray diffraction data indicated that it forms hydrogen-bonded hairpins and aggregates to yield tightly packed β-sheets. Thus, the experimental studies supported the polar zipper model and the hypothesis that the polyQ stretches form multimeric aggregates that are not covalently bonded (Perutz *et al.*, 1994). Altschuler group, instead, studied a peptide composed by 17 glutamines flanked by two α-helices. This peptide does not aggregate in solution and its characterization showed that the polyQ stretch is in a random coil conformation (Altschuler *et al.*, 1997). Similar results were obtained by Masino *et al.* studying AT3 (Masino *et al.*, 2003).

CD spectra of AT3/Q27 and AT3/Q78 have shown that the latter, unlike the former, underwent loss of α-helix and gain of β-sheet, which destabilised the protein structure. The longer is the polyQ tract, the

more evident is this phenomenon (Bevivino *et al.*, 2001). By Fourier transform infrared spectroscopy (FTIR) it was proven possibile to detect fibril formation by AT3/Q78 as an increase of the peak at at 1625 cm-1, resulting from the appearance of parallel β-structure (Bevivino *et al.*, 2001). One important difference between parallel and anti-parallel conformations lies in the hydrogen-bonding pattern adopted by the glutamine side chains: in the parallel model, each side chain hydrogen-bonds to two other side chains, one from each of the two adjoining strands; whereas in the anti-parallel model, each side chain hydrogen-bonds to only one side chain. Hence, in the parallel model, the strands are stabilized by continuos chains of side-chain-side-chain hydrogen-bonds, and the hydrogen-bonding capacity of both the carbonyl oxygen and the amide nitrogen of each side chain is satisfied. In contrast, in the anti-parallel model, adjoining strands are joined by pairwise hydrogen bonds, so for a given side chain, either the oxygen or the nitrogen participates in a hydrogen bond, but not both. Thus, parallel polyQ β- sheet may be more energetically favourable that the antiparallel ones (Bevivino *et al.*, 2001). In particular, at least two types of anti-parallel structures are possible: extended structures (in which the entire polyQ region of one molecule forms a single strand that associates with strands from adjacent molecules), and hairpin structures (in which the polyQ region forms one or more anti-parallel β-hairpins, which can then associate with hairpins from neighboring molecules) (Bevivino *et al.*, 2001).

19

Liu *et al.* (2001) have suggested that amyloid-fibril formation by proteins might, in many cases, reflect domain swapping. When the interactions between a peripheral domain and the core domain of a protein are weakened, the peripheral domain can be released from the central core and bind to the core of another protein molecule. Furthermore, successive domain-swapping events lead to oligomer formation (Bevivino *et al.*, 2001).

Some years ago, Perutz *et al.* have proposed a more refined model of fiber formation by polyQ proteins. This envisages a cylindric β-sheet, 31 Å in diameter, composed by a filament helically wound around the fiber axis and enclosing a central cavity, There are 20 residues per turn and the minimum length is 40 residues (two turns). Turns are stabilized by hydrogen bonds between main chain and side chain. The structure may act as a nucleation core for bigger aggregates (Perutz *et al.*, 2002).

1.7 Mechanism of polyQ aggregation

A still largely unaddressed issue regarding polyQ diseases is the mechanism by which the expansions give rise to aggregates and provoke the onset of the relevant diseases. Many experiments *in vitro* showed that polyQ tracts tend to aggregate spontaneously. Also, it was found that the rate aggregation was directly correlated with both protein concentration and size of the polyQ tract (Ross *et al.,* 2003). However, *in vivo*, such phenomenon might be enhanced or affected by other proteins or cellular components. It is assumed, in any case, that a

prerequisite for the aggregation is a conformational change caused by the intrinsic property of the polyQ tract (Masino *et al.*, 2001).

It has been proposed that fibril formation generally occurs by a mechanism of nucleated polymerization. This mechanism is characterized by the rate-limiting formation of an oligomeric nucleus from monomers that have undergone a (transient) conformational change followed by rapid recruitment of further monomers or oligomers into highly ordered fibrils. A model of how such a mechanism may apply to polyQ fibrils is shown in Figure 1.3 (Sakahira *et al.*, 2002).
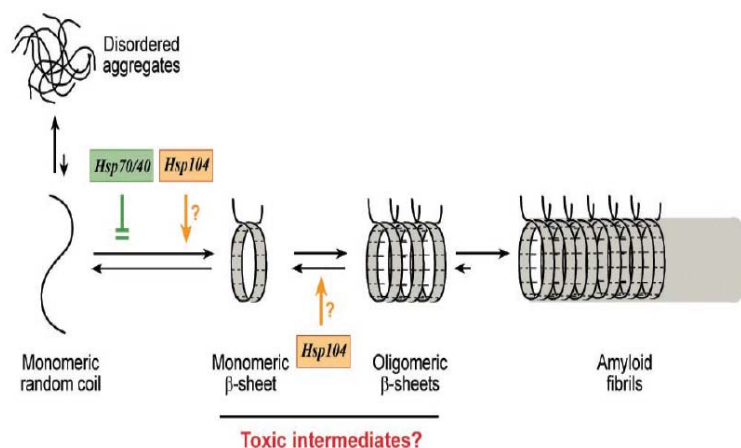
Figure 1.3 Hypothetical model for the pathway of polyQ aggregation and its modulation by molecular chaperones.

In this model, the first step in the aggregation process has been proposed to be the repeat length dependent conformational change of polyQ monomers from random coil to a parallel, helical β-sheet. This structural conversion then results in the formation of ordered polyQ oligomers that could function as nuclei for the rapid polymerization of

21

amyloid-like fibrils. Either the initial conversion or the subsequent oligomerization may be the rate-limiting step in polyQ fibrillogenesis, dependent on protein concentration. The intramolecular formation of β-sheet structure is likely to be rate-limiting only at high concentrations of polyQ protein, as reported for the Sup35 protein. In the case of huntingtin exon 1, the proteolytic cleavage of the polyQ-containing segment from a non aggregating precursor construct *in vitro* initiates aggregation, presumably by relieving steric restrictions and facilitating both intramolecular conversions and formation of oligomeric nuclei. Thus, after cleavage, the concentration-dependent formation of soluble polyQ oligomers is likely to be rate-limiting in the aggregation of this protein. Indeed, both full-length huntingtin (350 kDa) and the SCA3 protein (ataxin-3, 42 kDa) are cleaved by as-yet-unidentified proteases *in vivo*. This results in production of polyQ-containing fragments (Sakahira *et al.*, 2002).

1.8 *Molecular mechanisms of the PolyQ diseases*

The widely accepted mechanism of the polyQ disease involves proteins with expanded polyQ tracts as key players in etiology. The proteins with polyQ expansions interfere with transcription, form nuclear aggregates and give rise to death of specific neuronal cells by apoptosis (Michlewski *et al.*, 2004).

The polyQ tract itself seems to be the source of toxicity: transgenic mice expressing either intact protein with an expanded

poly-Q tract or a truncated protein containing the polyQ expansion develop neurological phenotypes and neuropathology reminiscent of the human diseases. Transgenic mice expressing protein with a normal polyQ tract (or null mice lacking the relevant protein function) do not develop the disease phenotype (Hickey and Chesselet, 2003). Although the primary sites of neuropathology vary depending on the type of disease, and the function of most of polyQ-carrying proteins remains unknown, this gain-of-function mechanism predominates and all the diseases are progressive. The longer the repeat tract, the more severe is the disease and the earlier its onset. In HD, as in most of the other triplet repeat diseases, the mutant proteins form nuclear aggregates that have resisted the most strenuous biochemical efforts to solubilize them. Even truncated proteins with an expanded polyQ tract
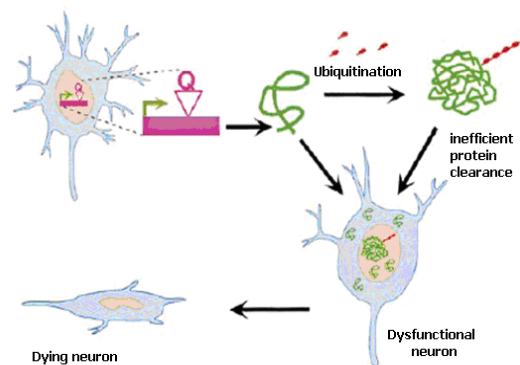
Figure 1.4 A model of polyQ-induced neurodegeneration. Expression of a mutant peptide with expanded polyQ tract leads to neuronal degeneration and eventual death. Note that both aggregated and solitary proteins induce neuronal dysfunction that precedes death (Orr *et al.,* 2000).

23

form these aggregates; indeed, truncated proteins seem to be even more toxic than the full-length proteins. It is important to note that symptoms arise from neuronal dysfunction long before neuronal death becomes significant. Although apoptosis plays a role in some neurological diseases, data from both humans and animal models indicate that neurodegeneration is process prevented by different mechanisms, that therefore culminates in cell death only after a prolonged period of visible disease (Orr *et al.,* 2000).

Amyloid diseases are all characterized by the accumulation of protein either outside the cell (e.g., amyloid plaques in AD) or inside (e.g., nuclear inclusions and cytoplasmic aggregates). As regards polyQ disorders, although intracellular aggregates are a common feature, it is questioned whether they are directly responsible for the pathological symptoms. Rather, they are currently regarded as a neuron's efforts to cope with the mutant protein. The expanded polyQ tract could make the protein resistant to degradation by altering its native structure. *In vitro* studies actually show that ataxin-1 with an expanded polyQ tract is less efficiently degraded than its wild-type counterpart, although are both ubiquitinated. The colocalization *in vivo* of various chaperones, ubiquitin, and components of the proteasome with the aggregated proteins further supports this model. Besides the polyQ diseases, α-synuclein with the A53T mutation is associated with familial PD and has a 50% longer half-life than its wild type counterpart. Oligomerization or fibril formation, promoted by the mutations in the respective proteins with resulting protein

accumulation, demonstrated that the disease-causing mutations in α-synuclein accelerate the oligomerization of the protein. Whether the mutated proteins gradually compromise the function of the proteasome remains to be seen (Orr *et al., 2000*).

The importance of the ubiquitin–proteasome pathway (UPP) in neuronal degeneration has been recently highlighted. Indeed, several neurodegenerative disorders are caused by mutations in genes that play a role in the UPP (Figure 1.4) (Orr *et al., 2000*).

1.8.1 Roles of nuclear inclusions in polyQ diseases

The two basic characteristics of neurodegenerative pathologies are late onset and selective vulnerability of some cellular types. Symptoms of the polyQ disease normally do not appear until adulthood, although the expanded protein is being expressed since the birth. This delay suggests a slow, progressive accumulation of toxic products and damaging of several cellular processes, which eventually result in cell death (Paulson, 1999). Moreover, the presence of the polyQ tract expanded could favour protein misfolding, which in turn might make the polyQ-carrying protein more prone to proteolytic attack. This is relevant to the pathogenesis, as fragments carrying polyQ tracts are believed to be much more toxic than the whole protein (Paulson, 1999).

There is evidence that the nucleus is a more favourable environment for protein aggregation. In particular, fragments form inclusions preferentially in the nucleus, rather than in the cytoplasm.

Probably, this is because the nucleus can less efficiently promote protein degradation, refolding or rescue aggregated proteins. It might also be that proteins attain a higher local concentration in subnuclear compartments (Paulson, 1999). The formation of nuclear inclusions (NI) has been observed in most polyQ diseases, and seems therefore to play a key role in their onset. Relevant to pathogenesis is also the observation that that several proteins, either carrying normal polyQ tracts, such as transcription factors, or even devoid of any such tract, are recruited in NI. In particular the "green fluorescent protein" (GFP) containing a polyQ tract coexpressed with a form of expanded ataxin-3 was found in the inclusions (Evert *et al.*, 2000).

Many immunohistochemical studies have demonstrated that the nuclear inclusions contain components of the proteasome complex and molecular chaperones. However it has been suggested that aggregation is associated with, but not necessarily responsible for the pathogenesis. Aggregation would be a protective mechanism aimed at sequestering precipitated proteins. According to this view, the really toxic elements would be the protofibrils, which arise in the early stages of the aggregation process (Zoghbi *et al.,* 2000).

1.8.2 Role of proteolysis in polyQ diseases

Proteins encoded by genes involved in polyQ pathologies are expressed ubiquitously. They do not share structural or functional features and every pathology involves different subpopulations of neural cells (Tarlac and Storey, 2003). The onset of the different polyQ

diseases might be accounted for by a conformational change of the polyQ tract, with resultant loss of normal interactions. Limited proteolysis, with release of small, polyQ containing fragment is believed to play a major role in pathogenesis by different mechanisms (Tarlac and Storey, 2003; Figure 1.5).
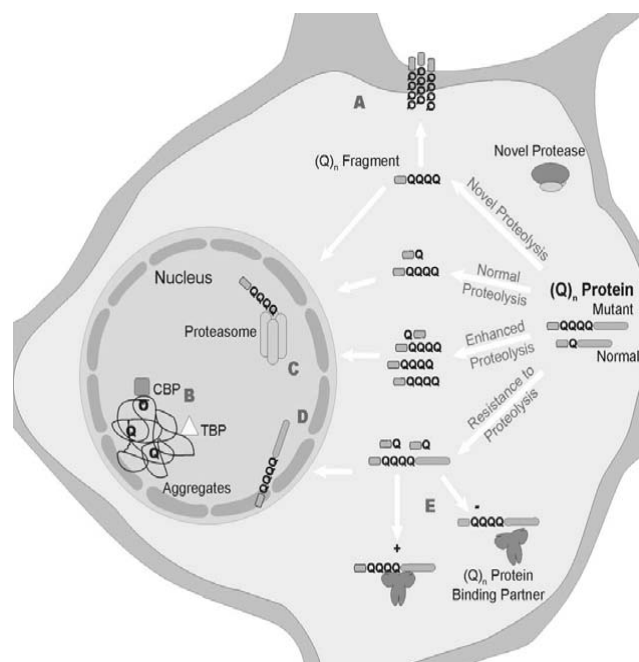
Figure 1.5 Possible outcomes of proteolysis of expanded polyQ proteins (Tarlac and Storey, 2003). Whether proteolysis of expanded proteins is unaffected, enhanced, reduced or the result of novel proteolysis, there are several possible toxic outcomes for the cell. Proteolysis of the expanded protein resulting in production of an expanded toxic fragment may cause several deleterious effects to the cell. First, the expanded toxic fragment may form cationic channels in the membranes **(A).** The expanded fragment may enter the nucleus where it can form macroaggregates that can recruit other containing proteins such as TBP, chaperons and components of the Proteasome **(B).** Another possibility is that the initial expanded cleavage fragment could be resistant to further proteolysis by the Proteasome **(C).** If the expanded protein is resistant to proteolysis, toxicity could be caused by disruption of the nuclear matrix by the full-length protein **(D),** or by an alteration of normal protein partner interaction **(E).**

27

Recently, Haacke *et al.* discovered that AT3 is a sensitive substrate of calcium-dependent calpain proteases. As a matter of fact AT3 fragmentation is inhibited by the calcium chelator EGTA, by the calpain inhibitor ALLN, the cysteine protease inhibitors E-64 and leupeptin, and by the proteasome inhibitor MG132 that also inhibits calpains, whereas caspase inhibitors are without effect. The sequence motifs that are recognized by calpain II are identified by microsequencing and are located in the disordered domain, mainly between residues 182 and 290 (Haacke *et al.*, 2007). This is of particular interest because cleavage of polyQ expanded AT3 in this region is known to produce highly aggregation-prone fragments of 32 kDa that coinitiate the aggregation process and recruit full-length AT3 into coaggregates. A variety of chronic neurodegenerative conditions, including amyotrophic lateral sclerosis, Parkinson disease and Alzheimer disease are accompained by altered levels of calpains and/or its inhibitor calpastatin. This observation would suggest that calpains can act on polyQ proteins early in diseases and without being strongly activated as a result of an apoptotic program (Haacke *et al.*, 2007).

1.9 Therapeutic perspectives

Although the precise molecular mechanisms which trigger neurodegenerative diseases is poorly understood, all these pathologies have in common the formation of intranuclear aggregates. In recent studies it was shown that the inhibition of the formation of aggregates leads to the inhibition of the disease (Sanchez *et al.*, 2003).

Having this in mind, one major goal of therapeutic approaches is to discover compounds capable to inhibit the formation of amyloid, non-toxic and preserving the cellular activity. This might be the key to prevent and treat this kind of pathologies.

1.10 Spinocerebellar ataxia type 3 (SCA3)

Spinocerebellar ataxia type 3 or Azorean disease is a dominant inherited disorder. It is named after the Azores, the group of nine Portuguese islands where the disease is prevalent. Many of the reported cases have been found in the direct descendants of William Machado, an Azorean native who immigrated to the New England area of the United States, and Atone Joseph, a Portuguese sailor from the island of Flores who came to California in 1845. Other name for Azorean disease is Machado-Joseph's disease (Gale Encyclopedia of Genetic Disorders, 2002). Main symptoms are incoordination (ataxia), which is usually the first and most consistent manifestation and usually shows itself in the patient's awkward gait. Other associated features include slurred speech (dysarthria) and abnormal eye movements (nystagmus), muscular rigidity, stiffness (especially of the knees), abnormal postures (dystonia), muscle atrophy, sensory loss in the legs, depressed reflexes, weight loss, sleeplessness, vertigo, preservation of intellectual function. One usually becomes bedridden and goes into a coma at the very end (Cummings and Zoghbi, 2000). Spinocerebellar ataxia type 3 is classified into three types depending on the age of onset and the specific symptoms (Gale Encyclopedia of Genetic Disorders, 2002):

29

Type I- the age of onset is usually before age 25 and the affected individuals experience extreme muscle stiffness and rigidity.

Type II- the age of onset is typically in the mid-30s, and progressive loss of muscle coordination (ataxia) occurs, resulting in the inability to walk.

Type III- the average age of onset is 40 or later, and the main symptoms are weakness and loss of sensation in the legs.

The symptoms of Machado-Joseph's disease (MJD) result from the loss of brain cells and the impairment of neurological connections in the brain and spinal cord. This impairment of the central nervous system is believed to be caused by the production of a pathogenic form of AT3 from a mutated gene. AT3 shares no homology with other proteins outside the polyQ tract and is expressed in the cytoplasm and nucleus of CNS neurons (Cummings and Zoghbi, 2000). Despite the wide distribution of AT3 in the brain, SCA3 neurodegeneration is mainly found in brainstem, basal ganglia, spinal cord and cerebellum (Chou *et al.,* 2005).

1.10.1   *Molecular and biochemical property of ataxin-3*

The gene responsible for spinocerebellar ataxia type 3 was mapped at chromosome 14q32.1. The encoded protein, AT3, has a molecular mass of about 42 kDa. Alternative splicing of MJD results in the production of different isoforms, which are expressed in various tissues and have been detected both in the nucleus and in the cytoplasm

(Costa *et al.*, 2004). The polyQ tract is close to the C-terminus (Table 1.1) and in non-pathogenic forms contains 12–41 glutamines, 62–84 in disease-causing forms (Mao *et al.*, 2005). The amino acid sequence of a human variant containing 26 glutamines is presented in figure 1.6.

```
MESIFHEKQEGSLCAQHCLNNLLQGEYFSPVELSSIAHQLDEEERMRMAEGGVTS
EDYRTFLQQPSGNMDDSGFFSIQVISNALKVWGLELILFNSPEYQRLRIDPINER
SFICNYKEHWFTVRKLGKQWFNLNSLLTGPRLISDTYLALFLAQLQQEGYSIFVV
KGDLPDCEADQLLQMIRVQQMHRPKLIGEELAQLKEQRVHKTDLERMLEANDGSG
MLDEDEEDLQRALALSRQEIDMEDEEADLRRAIQLSMQGSSRNISQDMTQTSGTN
LTSEELRKRREAYFEKQQQKQQQQQQQQQQQQQQQQQQQQQQQQQQRDLSGQSSH
PCERPATSSGALGSDLGKACSPFIMFATFTLYLT
```

Figure 1. 6 Amino acid sequence of human AT3.

Studies performed by far-UV circular dichroism (CD) showed that the protein is highly thermostable at least as far as the secondary structure is concerned, but the tertiary structure collapses above 50ºC. Thus, AT3 acquire a molten-globule-like structure at temperatures higher than 50ºC (Shehi *et al.*, 2003; Marchal *et al.*, 2003). A previous study showed that a pathological variant carrying 76 glutamines forms amyloid fibrils under physiological conditions, whereas a normal variant (Q26) is soluble (Bevivino and Loll, 2001). Further investigations performed on three different types of AT3 (Q26 human, Q36 and Q6 murine) showed that only the Q36 form underwent heat-induced protein denaturation and resultant amyloid formation (Shehi *et al.*, 2003).

1.10.2   Structure of AT3

First attempts to determine the 3D structure of AT3 were performed by molecular modeling and bioinformatics approaches, which predicted a structure consisting of a highly conserved compact N-terminal Josephin domain (residues 1-182) and a flexible C-terminal tail containing two or three potential ubiquitin-interacting motifs (UIM), depending on the splice variant. According to these studies, the N-terminal domain also carries the catalytic triad found in cysteine proteases, similar to that found in UBP- and UCH-type ubiquitin proteases. This lead to the suggestion that the protein can remove ubiquitin from polyubiquitinated proteins (Albrecht *et al.*, 2003; Scheel *et al.*, 2003).

Other features of the protein (depicted in Figure 1.7) are a highly conserved putative nuclear localization signal (NLS) upstream of the polyQ strech (amino acid 282-285), which follows a potential casein kinase II (CK-II) phosphorylation site (residues 277-280). Phosphorylation has been proposed to regulate the rate of the observed AT3 transport into the nucleus. Furthermore, a nuclear export signal (NES) following the Josephin domain (residues 174-183) as been also predicted (Albrecht *et al.*, 2003; Scheel *et al.*, 2003). Recently Antony *et al.* predicted *in silico* two new AT3 NES and performed a functional analysis of them. Only NES 77 and NES 141 induced the transport of their assay constructs into the cytoplasm. They could not find export activity of the other analysed sites including the NES 174, which was predicted previously (Albrecht *et al.*, 2004; Tait *et al.*, 1998). They analized also nuclear localization signal (NLS) and discovered that

NLS (273-286) has a detectable nuclear import activity. This signal, however, shows only weak activity in the full-length of AT3 possibly due to the presence of NES 77 and NES 141 that strongly exceed its activity.
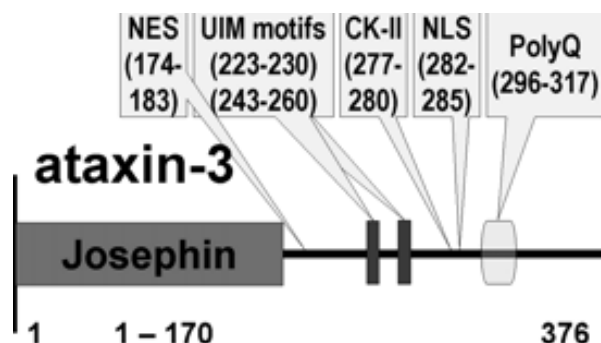
Figure 1.7 Protein architectures of AT3.

Based on CD and NMR investigations, Masino *et al.* proposed that the N-terminal domain is globular and rich in α-helices; instead, the C-terminal domain is flexible and not well structured, with glutamines exposed to the solvent (Masino *et al.*, 2003). More recently, Nicastro *et al.* (2005) determined the structure in solution of the Josephin domain by NMR spectroscopy (Figure 1.8 and 1.9). This showed that it is composed by 2 subdomains separated by a cleft.

• The N-terminal subdomain is composed of four α-helices (α1, residues 14-22; α2, 31-47; α3, 56- 62; α4, 78-85), of which α1 e α4 lie approximately within the plane of the β-sheet, while α2 and α3 form a

long "helical hairpin", which protrude from the core of the structure, that appear as a thumb-like extension.

• The C-terminal subdomain contains instead a 6-stranded antiparallel β-sheet, with a β1, β6, β2, β3, β4, β5 topology. β1 is connected to β2 by two short 3_{10} helices that flank and stabilize the conformation of the interconnecting loops. Strands β2-β5 are connected by short turns, whereas β5 is connected to β6 by a 12- aa-long α-helix (β5: residues Tyr 147-Glu 158) located on one side of the sheet. Overall, the surface is highly negatively charged with a large patch that clusters around the α2-α3 helical hairpin. At least 2 exposed hydrophobic patches are also visible on the surface of the Josephin structure, one being centered around Trp 87. The Josephin domain structure is relatively ridig as indicated by NMR relaxation experiments. An interesting feature is the helical hairpin formed by α2 and α3, comprising 2 antiparallel relatively well-defined helices. Although the hairpin is well attached to the rest of the structure by several salt bridges, hydrophobic

Figure 1.8 Tridimensional structure of the Josephin domain as determined in NMR spectroscopy
(*PDB ID code*: 1yzb). The structure is rendered using the pyMOL program.
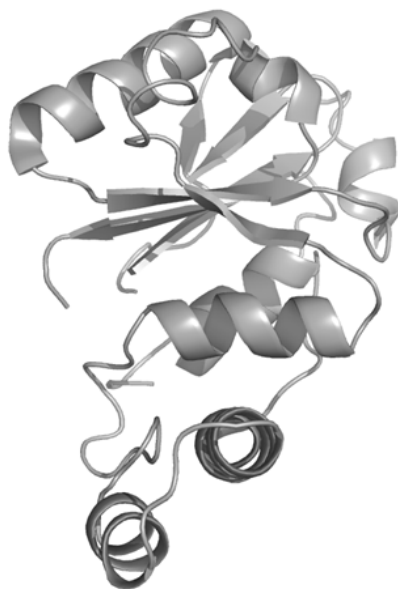
Figure 1.9 Tridimensional structure of the Josephin domain as determined in NMR spectroscopy (*PDB ID code*: 1yzb). With respect to figure 1.8, this different perspective highlights the relative postions of helices and β-sheet. The structure is rendered using the pyMOL program.

interactions and H-bonds, the relaxation parameters indicate that this region is overall distinctly more flexible than the rest of the protein. The exposed hairpin, therefore, appears to behave as an exposed waving hand, which could be available for interactions with other molecules. Because of its proximity to the active site, the hairpin could determine specificity and stabilize protease substrates and/or inhibitors. Excellent candidates for interacting with this region are the histones, because they would have the correct charge complementary to the highly negatively charged surface of the hairpin. An even more obvious molecular partner of Josephin is ubiquitin (Nicastro *et al.*, 2005).

1.10.3   Possible physiological roles of AT3

Comparing the AT3 sequence with UCH (Ubiquitin C-terminal hydrolase) and UBP (Ubiquitin specific protease) ubiquitin proteases, Scheel and coworkers observed that, although not all of the structural features of UCH and UBP proteases could be reliably mapped to the AT3 sequence, the catalytic residues could be identified with high confidence as those of a typical cysteine protease catalytic site (Figure 1.10): Cys 14, His 119 and Asn 134 (Scheel *et al.,* 2003). Cys 14 is the catalytic residue, while His 119 is the proton-donating residue. The third residue, which is Asp 134 in UCH proteins and Asn 134 in UBP and AT3 proteins (Scheel *et al.,* 2003), is responsible for the correct orientation of the imidazole ring of histidine. This further substantiates for AT3 a role as a deubiquitinating enzyme involved in the ubiquitin-proteasome pathway of protein degradation. *In vitro* studies demonstrate that recombinant AT3 is able to cut ubiquitin chains from artificial substrates (Burnett *et al.*, 2003).

Structural data collected by Nicastro *et al.*, (2005) also showed that the fold of the catalytically inactive AT3 (AT3 C14A), in which Cys 14 is substituted by alanine, causes accumulation of polyubiquitinated proteins. Then, AT3 functions as a DUB, binding ubiquitin chains through its UIMs and cleaving them through the Josephin domain, and it might be therefore involved in the ubiquitin-proteasome degradative pathway of several substrate proteins (Nicastro *et al.,* 2005).
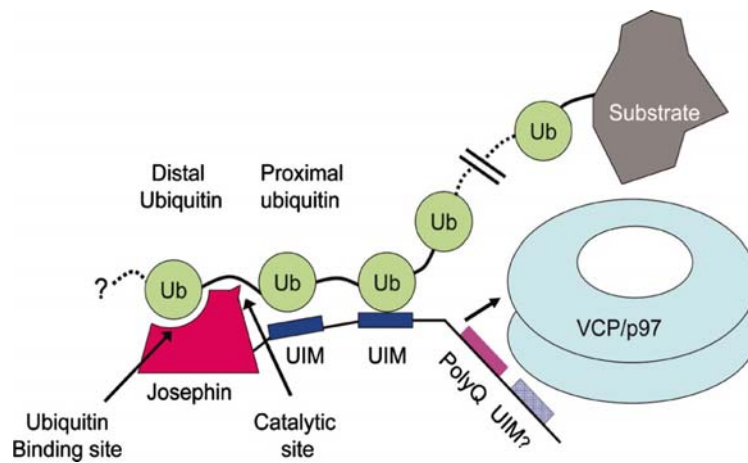
Figure 1.10 A possible mechanism by which AT3 participates in the ubiquitin-proteasome pathway (Mao *et al*., 2005). PolyUb chain must be long enough to bind UIM motifs and the Josephin domain. Dotted lines represent the variable length of poliubiquitin chains.

Ubiquitination is a dynamic post-translational modification that serves diverse cellular roles. Ubiquitin is covalently attached to a substrate protein through the formation of an isopeptide bond between the C-terminal glycine residue of ubiquitin and the ε-amino group of a lysine residue on the substrate by a cascate of enzymatic reactions. Successive conjugation of ubiquitin molecules to one of the seven internal lysine residues (K6, K11, K27, K29, K33, K48, and K63) within the preceding ubiquitin molecule results in formation of a polyubiquitin chain (Pickart and Fushman, 2004). K^{48}-linked polyubiquitination acts as the canonical signal for targeting the substrate to the proteasome for degradation. In contrast, K^{63}-linked polyubiquitination has recently been shown to have a proteasome-

independent role in the regulation of several cellular processes, including endocytosis, signal transduction, DNA repair, NFkB pathway, autophagy, lewy bodies and aggresome formation (Arnason and Ellison, 1994; Hofmann and Pickart, 1999; Deng *et al.*, 2000; Pickart and Fushman, 2004; Chen, 2005; Lim *et al.*, 2005; Tan *et al.*, 2007). Winborn and colleagues show that AT3 functions as ubiquitin chain-editing enzyme with preference for non-Lys^{48} linkages in mixed linkage chains. Both normal and expanded AT3 bind similarly to longer Lys^{48}- and Lys^{63}- linked ubiquitin chains yet preferentially cleaves Lys^{63}-linkages, especially in mixed linkage chains (Winborn *et al.*, 2008). These findings raise the possibility that AT3 functions in the cell to prevent the accumulation of very large and possibly aberrantly structured ubiquitin chains.

There are two different isoforms of AT3. Both contain UIM1 and UIM2 motifs and the polyQ domain, whereas only one contains also UIM3 at the C-terminus. The occurrence of these isoforms probably results from alternative splicing. Both variants are expressed in brain. The UIM is a short 15-residue sequence that allows ubiquitin binding and promotes ubiquitination. This motif is conserved in eukaryotes and is present in proteins involved in some cellular processes such as endocytosis, signal transduction and protein sorting; thus, AT3 might be also endowed with some of these activities. Recent studies on neuronal cells demonstrate that both isoforms of AT3 bind ubiquitinated substrates and that binding is abolished by mutations introduced into these UIM motifs (Berke *et al.*, 2005). Winborn *et al.*

demonstrated that the binding of ubiquitin chains by the UIMs determines ubiquitin cleavage-specificity. Mutating the UIMs reduces ubiquitin chain binding while unexpectedly expanding the range of linkages that can be cleaved. Thus, the UIMs of AT3 constitute selectively determinants that allow cleavage of Lys^{63}-linked ubiquitin while preventing cleavage of Lys^{48}-linked ubiquitin (Winborn *et al.,* 2008).

In their work Winborn *et al.* proposed a model in which the precise topology of ubiquitin chains bound by AT3 is critical for isopeptide bond cleavage (Figure 1.11). According to this model, binding of purely Lys^{48}-linked ubiquitin chains by the UIMs does not properly position the Lys^{48}-Gly^{76} isopeptide bond for access to the catalytic pocket of the Josephin domain. In contrast, when AT3 binds a chain containing adjacent Lys^{48}- and Lys^{63}- linkages, the Josephin domain is well positioned to attack the Lys^{63}-Gly^{76} bond. Chain positioning determined by binding through the UIMs dictates the catalytic specificity of AT3, as indicated by the loss of Lys^{63} linkage specificity when the UIMs are mutated (Winborn *et al.,* 2008).

Growing evidence implicates AT3 in protein quality control pathways. Recent work has demonstrated the interaction between AT3 and different cellular proteins involved in ubiquitin-proteasome pathway. One of these proteins is RAD23, which is involved in DNA repair (Doss-Pepe *et al*., 2003; Wang *et al*., 2000) and also shuttles ubiquitinated protein to proteasomes.
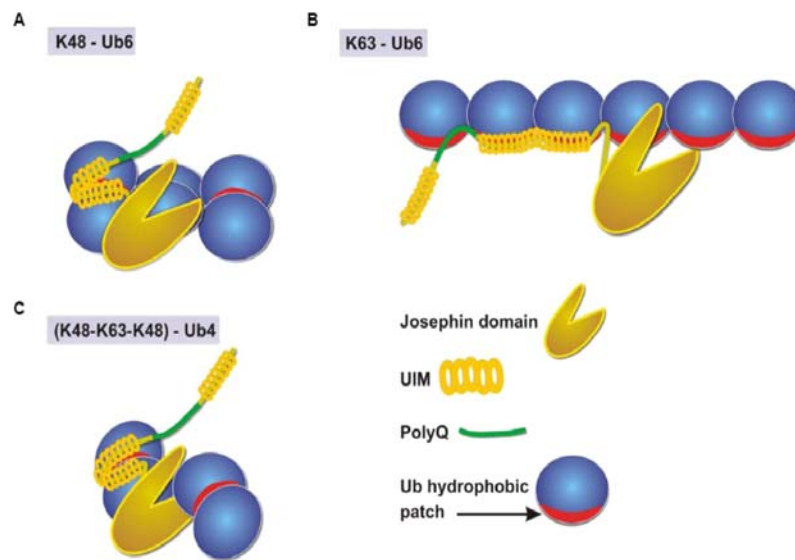
Figure 1.11 Model of AT3 ubiquitin chain binding and cleavage. Binding of a Lys[48]-linked ubiquitin chain (A) to the UIMs of AT3 positions it such that the cleavage by the catalytic Josephin domain is not favoured. In contrast, AT3 binding of Lys[63]-linked ubiquitin (B) permits proteolysis of long chains. AT3 binding of mixed linkage chains (C) favorably orients the catalytic region for proteolysis of Lys[63]-linkages (Winborn *et al.,* 2008).

In Doss-Pepe's model, AT3 is a protein transiently associated to the proteasome. A possible role would be the recognition of polyubiquitinated proteins handed over by the VCP/RAD23 system. The overall process would consist of three steps (Figure 1.10): 1) binding between polyubiquitinated proteins and RAD23 through its UBA domains (ubiquitin-associated domains), while VCP would bind AT3; 2) RAD23 binding to proteasome through its Ubl domain (ubiquitin like); 3) VCP transfer of ubiquitinated proteins from RAD23 to AT3. This would make it possible protein substrate degradation by the proteasome (Doss-Pepe *et al*., 2003).

VCP ("valosin containing protein") is a mammalian ATPase with a N-terminal domain followed by 2 highly conserved AAA domains required for ATP binding and hydrolysis (Boeddrich *et al.*, 2005). This protein is involved in different cellular events such as postmitotic fusion of Golgi membranes and endoplasmic reticulum (Kondo *et al.*, 1997), regulation of gene expression (Rape *et al.*, 2001), degradation of soluble and membrane proteins via the ubiquitin-proteasome system (Ye *et al.*, 2003). When VCP binds and hydrolizes ATP, it undergoes a rearrangement involving rotation of the AAA domains. Recent studies demonstrated that VCP might be involved in pathogenesis of triplet expansion diseases as it colocalizes with inclusion bodies associated with these diseases (Higashiyama *et al.*, 2002). An arginine-lysine rich motif present in the AT3 sequence allows the binding between AT3 and VCP, whereas the polyQ only promotes this event (Boeddrich *et al.*, 2005). Furthermore, it has been observed, both *in vivo* and *in vitro*, that, depending of its concentration, VCP can also modulate AT3 aggregation.

Interaction between AT3 and VCP seems to be also involved in the retrotranslocation of ERAD (endoplasmic reticulum-associated degradation) substrates (Figure 1.12). ERAD is a quality control system in the secretory pathway responsible for degrading misfolded proteins (Zhong and Pittman, 2006). Proteins targeted for ERAD are deglycosylated, ubiquitinated, extracted from the endoplasmic reticulum and degraded by the proteasome. For each step, different proteins are recruited and assembled around the substrate targeted for

degradation. The key protein essential for extracting substrates from the endoplasmic reticulum to the cytosol is VCP, that binds the integral membrane proteins of endoplasmic reticulum Derlin-1/2, SEL1L/Ubx2 and VIMP (VCP-interacting membrane protein). Mammalian orthologs of ubiquitin-ligase E3, Hrd1p/Hrd3p, are recruited to the complex by Derlin-1/2 and SEL1L/Ubx2 and are responsible for ubiquitinating the substrate. VCP recruits the heterodimer Ufd1-Np14, to form a subcomplex that is responsible for extracting the ubiquitinated substrate from the endoplasmic reticulum. In particular, Ufd1 binds directly to VCP, while Np14 interacts indirectly by binding to Ufd1. Both VCP and Ufd1 bind ubiquitin chains and their interaction synergistically enhances binding to the ubiquitinated substrate (Zhong and Pittman, 2006). AT3 participates in the process by binding VCP, thus decreasing its interaction with Ufd1 and polyubiquitin chains, which results in decreased retrotranslocation of substrates from the endoplasmic reticulum, and degradation of ERAD substrates. Mutating the active site or UIMs in AT3 does not alter binding to VCP and, hence, there are no effects on degradation activity. In contrast, AT3 with an expanded polyQ tract shows a much stronger interaction than normal AT3 with VCP; so it binds VCP more efficiently and this diminishes substrate degradation by ERAD (Zhong and Pittman, 2006). In a recent study Boeddrich *et al*. (2005) identified a region contiguous to the polyQ (residues 277-291) tract was identified as a binding site for VCP as supported by the effect of mutations in this region, which strongly decrease binding of AT3 to VCP. It is possible that the

42

expansion of the polyQ tract alters the conformation of the contiguous sequence that promotes the binding between VCP and AT3. An alternative possibility for the enhanced effect of pathological AT3 is that it forms aggregates and sequesters VCP or inhibits the proteasome, might contribute to the pathogenesis. The involvement of AT3 in the regulation of the ERAD system ensures additional cycles of protein folding, so it represents a good quality control for endoplasmic reticulum proteins by reducing the rate of the extraction process when the proteasome is overcrowded with substrate proteins.
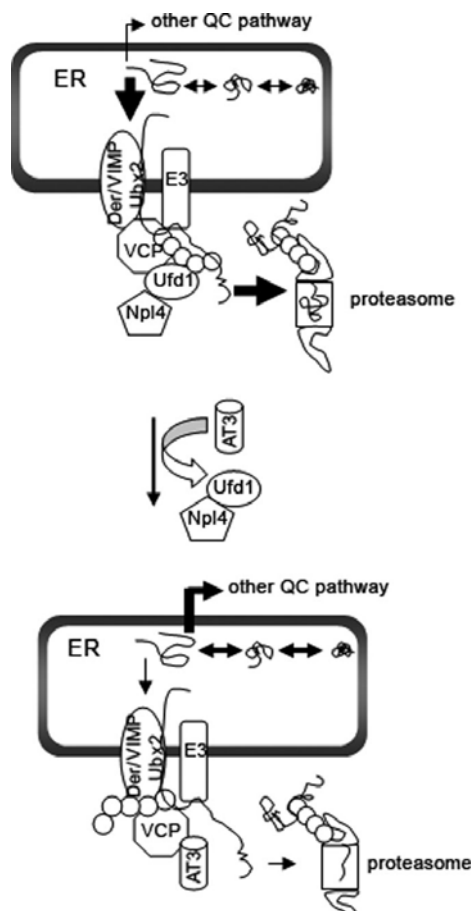
Figure 1.12 A Model for the regulation of the ERAD pathway by AT3 (Zhong and Pittman, 2006). *Upper panel*: the VCP/Ufd1-Npl4 complex associates with ER proteins including Derlin 1/2, VIMP, Ubx proteins and E3 ligase (E3). An ER protein that does not fold properly is ubiquitinated while still associated with the ER: this allows the VCP/Ufd1-Npl4 complex to bind to it. VCP then extracts the ubiquitinated protein from the ER and through a series of steps delivers the ubiquitinated protein to the proteasome for degradation, in the absence of AT3. *Lower panel*: AT3 compete with Ufd1 for binding to VCP; displacing Ufd1 from VCP impairs its binding to ubiquitinated ERAD substrates and slows down their extraction from the ER, which decreases delivery to the proteasome. In the presence of AT3, more proteins remain in the ER and may undergo additional cycles of folding or may be sorted into other quality control pathways.

43

Besides the ubiquitin-proteasome system, there are other pathways regulating protein homeostasis in the cells. Subcellular structures called aggresomes, are formed in response to undegradable (or slowly degraded) protein aggregates, when a cell's capacity to degrade misfolded proteins is exceeded (Johnston e*t al*., 1998). The aggresome is a pericentriolar membrane-free, cytoplasmatic inclusion containing misfolded, ubiquitinated proteins ensheathed in a cage of intermediate filaments (IF). It has been observed that overexpressing in cells mutant proteins that are not able to fold correctly, and exposing the proteasome to inhibitors, aggresomes form spontaneously, which shows that they represent a cellular response to stress situations resulting from the presence of misfolded proteins. Instead of arising at random sites within the cytoplasm, which would be predicted by a "seed" based model of inclusion body formation, aggresomes are formed specifically at the microtubule-organizing center (MTOC) by an ordered process requiring intact microtubules (MT) and accompanied by a dramatic reorganization of the IF cytoskeleton (Johnston *et al*., 1998; Garcìa-Mata, *et al.*, 1999; Burnett and Pittman, 2005). In particular, there is a redistribution of vimentin to form ring-like structures around pericentriolar aggresomes. Vimentin is a fibrous protein that is present in IF and it functions as support for cellular organelles. Hence, it is possible that this redistribution is a cellular attempt to prevent the dispersion of the aggresome content in cytoplasm (Johnston *et al*., 1998; Figure 1.13). Misfolded proteins are therefore eliminated from cells in different ways such as ubiquitin-

44

proteasome degradation and refolding of molecular chaperons system. When the activity of the proteasome is compromised or when it is not able to take up some more proteins to degrade, misfolded proteins are translocated to the perinuclear region and form aggresomes. In this way cell prevents the formation of toxic intracellular aggregates. It is possible that the aggresome formation provide a "staging ground" for the incorporation of protein aggregates into autophagic structures, possibly by facilitating interaction with endosomes and lysosomes, which are also delivered by MT to the same region of the cell (Matteoni and Kreis, 1987). Consistent with this notion, it has been frequently observed double-membrane vescicular structures in the immediate vicinity of the aggresome (Johnston *et al.*, 1998). Although aggresome formation seem to be important to cellular homeostasis, the knowledge of proteins responsible for recognition, processing and transport of misfolded proteins is very poor. Besides those of MT and IF, the only proteins known to be involved in this process are: Hsp 70 and Hsp 90 (Wigley *et al.*, 1999), ubiquitin (Johnston *et al.*, 1998, Burnett and Pittman, 2005), Dynein/Dynactin complex and histone deacetylase 6 associated with MT (HDAC6). In a recent work, it was shown that cellular AT3 regulates aggresome formation (Burnett, and Pittman, 2005). Using *in vivo* immunolocalization experiments they demonstrated that AT3 localizes to aggresomes and preaggresome particles and interacts with Dynein and HDAC6.

It is possible that AT3 binds ubiquitin chains of ubiquitinated proteins shielding them from the proteasome before they are

transported to MTOC to form aggresomes. Alternatively, AT3 may use its deubiquitinating activity to stabilize proteins involved in the trafficking and fast retrograde axonal transport. It is not well known if there is a relation between the regulation of the flow of ERAD substrates by AT3 and the formation of aggresomes. However, in the cell some proteins may have the function of monitoring and coordinating the different degradative pathways. The capacity of AT3 to regulate ERAD, aggresomes formation and to interact with VCP and RAD23, clearly suggests a regulative role of this protein in the cell.
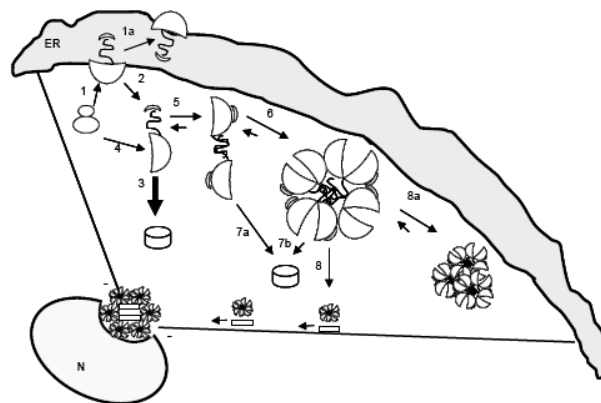
Figure 1.13 Model for aggresome formation (Johnston *et al*., 1998). Figures indicate the various steps in the aggresome biogenesis pathway. Membrane proteins are cotranslationally translocated to the membrane of the ER (1). Some molecules fold to adopt a maturation-competent conformation (1a). Others misfold and are dislocated from the ER membrane (2). Some proteins may escape the translocation machinery and be delivered directly to the cytoplasm (4). Dislocated, ubiquitinated, misfolded protein can either be rapidly degraded by cytosolic proteasome (3) or aggregate (5 and 6). Because aggregates are difficult to unfold, they are likely to be slowly degraded by the proteasome (7a e 7b). Misfolded, aggregated protein is transported to the MTOC by MT where it becomes entangled with collapsed IF (8). In the absence of MT, protein aggregates coalesce at dispersed sites throughout the cytoplasm (8a). N, nucleus; Ub_n, Ubiquitin conjugates; +, orientation of MT in the cell.

Among proteins regulated by oligo-ubiquitination there are some transcription factors whose loss may represent one possible pathogenic mechanism of polyQ diseases. Indeed, some proteins with expanded polyQ may interact with transcription factors such as TATAbox binding protein, CREB-binding protein, Sp1, p53 and NFkB, sequestering them in nuclear aggregates (Goswami *et al.*, 2006). NFkB is a transcription factor that plays an important role in control of cellular survival, in apoptosis, whose activation represents a feature of neurodegenerative diseases. NFkB downregulation, due to sequestration of the protein into aggregates, is involved in cell death mediated by polyQ proteins (Goswami *et al.*, 2006). Furthermore, it has been demonstrated that AT3 interacts with two of the major histone acetyltransferases and with proteins associated with them: cAMP response element-binding protein ("CREB-binding protein" o CBP) and p300 (Li *et al.*, 2002). CBP and p300 are transcriptional coactivators and have a very important role in transcription and are regulated by polyQ proteins that associate with them. Transcriptional activation of the two proteins is mediated by many cofactors as CRE ("cAMP repressor element") and CREB ("CRE-binding protein"). CREB, that is linked to CRE enhancer, is phosphorylated in response to cAMP. This causes the recruitment of CBP and p300 and transcriptional activation of cAMP responsive genes. It is possible that polyQ proteins share the important role to modulate transcription.

Some studies demonstrate that the N-terminal domain of AT3 binds DNA, inhibits acetylation of histones and represses transcription
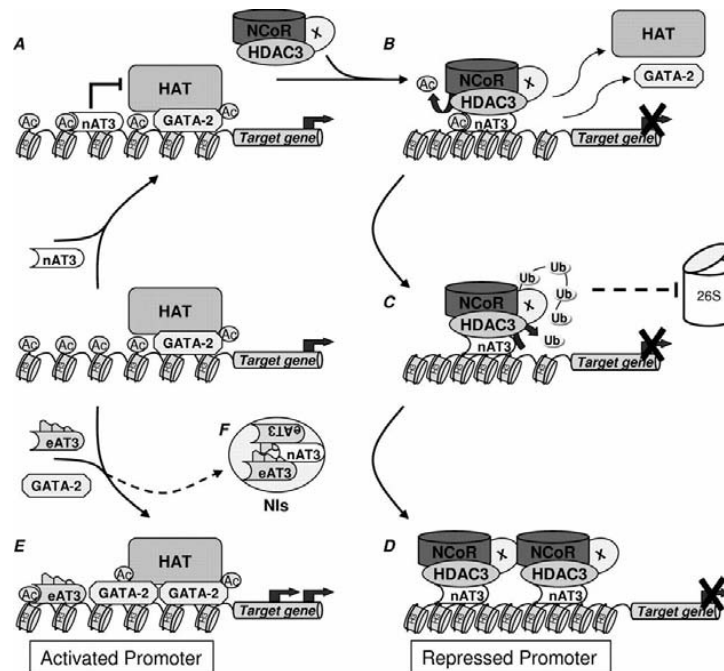
Figure 1.14 Model of AT3 transcriptional regulatory role, including known properties of AT3 (Evert *et al.,* 2006). **A**, Non-expanded AT3 (nAT3) targets chromatin via either histone and/or direct binding of specific DNA sequences and inhibits HAT activity. **B**, AT3 recruits the corepressors HDAC3, Ncor and possibly other required repressor proteins, resulting in a repressor complex actively deacetylating core histones of the promoter. This repressor complex may serve as well to deacetylate and release the activating transcription factor GATA-2. **C**, AT3 then may stabilize the repressor complex via deubiquitination (Ub) of a yet unknown repressor component (X) and inhibition of its proteasomal degradation by the 26S proteasome. **D**, A repressed, hypoacetylated chromatin conformation is established via formation of several AT3- HDAC3-Ncor-containing repressor complexes along the promoter. **E**, Altered chromatin binding of expanded AT3 (eAT3) fails to recruit and form histone-deacetylating repressor complexes. The promoter remains hyperacetylated and allows increased binding of GATA-2 to its target regions, mediating enhanced transcriptional activation of the promoter. **F**, In addition, expanded AT3 additionally may promote transcription via depletion of AT3 normal repressing activity by aggregation into NIs.

mediated by CBP and p300. It has been observed that the binding of AT3 with these coactivators causes a decrease in the acetylation of

histones and a subsequent *in vitro* inhibition of transcription. In a recent work it has been demonstrated that AT3 is able to bind specific sites on the promoter of the gene *mmp-2* (metalloproteinase-2) and interact with HDAC3 and NcoR corepressors, causing deacetylation of histones and decrement of binding between GATA-2 transcriptional factor and its promoter. Expanded AT3, instead, is able to activate gene espression as polyQ alters binding properties of AT3 to DNA, so corepressors are not recruited, DNA is acetylated and becomes transcriptionally active and accessible to GATA-2 (Figure 1.14) (Evert *et al*., 2006).

1.10.4   *Possible aggregation mechanisms of AT3*

Knowledge regarding the aggregation mechanism of AT3 is still largely incomplete. Only recently a new model of fibril formation was proposed (Ellisdon *et al.* 2006; Figure 1.15). AT3 undergoes a two-stage aggregation. By comparing the aggregation pathway of normal (15Q) and pathological (64Q) AT3, it was observed that both variants are able to aggregate but they form inclusions with different characteristics. Non-expanded AT3 formed aggregates through a nucleation-dependent process, which was monitored by ThT fluorescence emission. AT3/Q64 showed an increased rate of aggregation. The first step of aggregation was indistinguishable from that of the shorter variant. However, only AT3/Q64 underwent a second step, which is characterized by the formation of large SDS-insoluble aggregates. These aggregates are highly stable (Ellisdon *et al.,* 2006). Based on these findings, they proposed a two stage model

for AT3 aggregation, which takes into account both protein context and polyQ expansion. The first stage involves a conformational change and self-association in regions other than the poly-Q tract, that results in the formation of SDS-soluble fibrils. The early aggregates formed during this first stage by all variants resemble the morphologies of pre-fibrillar aggregates implicated in the toxicity of numerous neurodegenerative diseases (Ellisdon *et al.,* 2006). However, only pathological protein is able to form stable, long, mature fibers. The first step is therefore dependent on the particular protein context of the Josephin domain, whereas the second requires an expanded polyQ tract. In a further paper the same authors also demonstrated that, after the nucleation step, the fibril elongation proceeded by a mechanism of monomer addition (Ellisdon *et al.*, 2007).

Fibril formation is also associated with loss of α-helix and increase in β-sheets, as shown by CD spectra of AT3/Q27 and AT3/Q78 (Bevivino *et al.*, 2001). In these experiments it was also observed that the α → β transition was more pronounced in the expanded form. Fourier transform infrared spectroscopy (FT-IR) showed that the fibrils formed by AT/Q78 displayed an increase in the signal at 1625 cm-1, indicating appearance of parallel β-structure (Bevivino *et al.*, 2001). Recently, evidence was also provided that some metal ions can also play a role in modulating the biophysical behavior of native AT3. Results obtained by recording ANS and ThT fluorescence clearly show that, at neutral pH, the

misfolding/aggregation process of AT3/Q6, AT3/Q26 and AT3/Q36 variants was substantially unaffected (Q6) or even inhibited (Q26, Q36) by Mn^{2+} and Cu^{2+}, whereas Zn^{2+} and Al^{3+} stimulated the conversion of native AT3s into altered, aggregation-prone conformations (Ricchielli *et al.*, 2007). Furthermore, this study
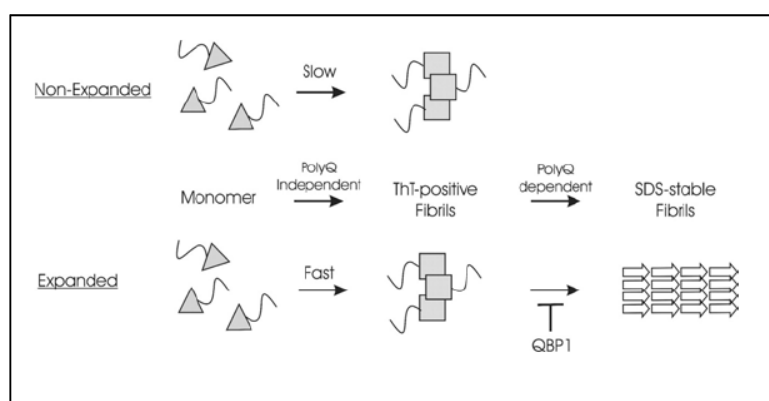
Figure 1.15 Proposed model for AT3 aggregation. A schematic representation of the two-stage aggregation pathway of AT3. The non polyQ region of AT3, including Josephin domain and the two ubiquitin-interacting motifs are represented as a triangle with the C-terminal polyQ tract as a tail. All variants are able to aggregate into ThT-positive aggregates. This first stage of aggregation occurs faster in expanded AT3 but appears not to be structurally dependent on the polyQ tract. During this stage of aggregation the conformation of the Josephin domain has been shown to be altered. Only expanded AT3 is capable of forming highly stable, SDS-resistant aggregates. This stage of aggregation is directly reliant on polyQ tract interactions.

evidenced that the extent and rate of aggregation was directly correlated to the polyQ length also in the presence of Zn^{2+} and Al^{3+} , and that the presence of the metals abbreviated the initial lag phase (Ricchielli *et al.*, 2007). The pathological mechanism of metal action is still unclear and diverse explanations have been proposed: metal ions may induce protein misfolding by altering the charge density of

the molecule; they may also cause cross-linking or bridging between two or more metal-binding groups, thus producing a protein structure that supports aggregation.

1.11 Aim of the work

Given the growing attention towards the possible loss of function as a major determinant of pathogenesis of polyQ diseases, in this work I will attempt to extend our knowledge on possible physiological roles of AT3. This will accomplished searching for further molecular interactors of this protein. We will try to identify, by advanced mass spectrometry techniques, molecules from mouse brain capable of binding to different AT3 variants and I will validate this findings with some *in vitro* and *ex vivo* experiments. Then I will try to elucidate what AT3 regions are involved in this interaction through SPR experiments using different truncated variants of AT3. Finally, in order to elucidate sorting mechanisms of misfolded proteins to aggresome or proteasome and roles of protein involved in this we performed by SPR a competition assay between AT3, tubulin and Lys[48]- or Lys[63]-polyubiquitin chain. These findings might help establish a correlation between aberrant phenotype and cellular mechanisms in which AT3 is involved.

2 Materials and methods

2.1 E. coli strains

2.1.1 E. coli strains used for cloning and expression of AT3 variants

XL-1 Blue: recA1 gyrA96 thi-1 hsdR17 supE44 relA1 lac [F' pro AB lacI^q Z ΔM15 Tn10(Tet^r)]. (Stratagene, La Jolla, CA) (Bullock *et al.*, 1987).

This strain is useful for cloning, propagation and maintenance of high copy number plasmids like pCRBlunt and pGEX-6P-1.

DH5α: F- mcrA Δ(mrr-hsdRMS-mcrBC) Φ80lacZ ΔM15 ΔlacX74 deoR recA1 araD139 Δ(ara-leu)7697 galU galK rpsL (Str^R) endA1 nupG (Invitrogen,

Paisley, England).

BL-21CodonPlus(DE3)-RIL: B F- ompT hsdS($r_B^-r_M^-$) dcm$^+$ Tet^r gal λ (DE3) endA Hte [argU ileY leuW (Cam^r)] (Jerpset *et al.*,1998).

This strain is used to express genes of pGEX-6P-1 plasmid. This strain carries the lambda DE3 lysogen, which expresses T7 RNA polymerase from the lacUV5 promoter by isopropyl-1-thio-s-D-galactopyranoside (IPTG) induction. When IPTG is present in the medium, T7 polymerase is transcripted and translated. This protein, therefore, allows the transcription of the gene under the control of T7 phage promoter. T7 RNA polymerase (100 kDa) consists of one polypeptide chain; it binds DNA very strongly and is five-fold faster

in the transcription then the normal *E. coli* RNA polymerase. Furthermore, the codons AGA/AGG, AUA and CUA are rarely used in *E. coli*. These codons are common in eukaryotes. Therefore, their presence in cloned genes affects protein accumulation and synthesis. These problems are usually solved by using site-directed mutagenesis to replace rare codons by genes encoding AGA/AGG, AUA and CUA tRNA.

SG13009: (Qiagen, Chatsworth, CA). This strain derives from *E. coli* K12 and has the phenotype Nal^s, Str^s, Rif^s, Thi^-, Lac^-, Ara^+, Gal^+, Mtl^-, F^-, $RecA^+$, Uvr^+, Lon^+. It contains the pREP4 plasmid that inhibits basal expression of recombinant protein. *E. coli* strains that harbor the $LacI^q$ mutation, such as XL-1 Blue, produce enough *lac* repressor to efficiently block transcription and are ideal for storing and propagating pQE plasmids. These strains can also be used as expression hosts for expressing non-toxic proteins, but they may be less efficient that SG13009 [$pREP4^+$]. pREP4 plasmid confer kanamycin resistance to the cell and constitutively expresses the *lac* repressor protein encoded by the *lacI* gene. Multiple copies of pREP4 are present in the host cell that ensure the production of high levels of the *lac* repressor protein which binds to the operator sequences and tightly regulates recombinant protein expression.

2.1.2 Mammalian cells used for cellular culture "ex vivo"

A COS-7 continuous cell line derived from CV-1 cell line was used. This is obtained from explants of monkey kidney and immortalized by infection of SV40 virus. It is a fibroblast line. These cells require 10% foetal bovine serum in the growth medium and grow adherent to glass and plastic surfaces subjected to "Tissue Culture" (TC) treatment.

Cells grow on 25-75 cm^3 flasks, on 100 mm Petri plates and on 22 mm square glass coverslips (in 30 mm multiwell plates), in an incubator at 37°C with 5% of CO_2 and 90% of humidity. Subconfluent cells are diluted using trypsin and, then, properly replated. When appropriate, cells are stored with complete medium containing 10% (v/v) dimethilsulfoxide (DMSO) in liquid nitrogen.

If necessary, before replating cells are counted using a Bürker chamber under microscope. To avoid contaminations, cell manipulation has been done under sterile using laminar flow hood Bio Hazard, P2 level.

Centrifuge: Beckman Coulter Avanti J-20 centrifuge with rotor JA10; Heraeus Biofuge 13 with 45° fixed angle rotor.

Trypsin: pbi-international, Trypsin-EDTA solution C, containing 0.05% of trypsin, EDTA 1:5000 and red phenol as pH indicator.

Incubator: Heraeus – electronic -, Mod. B 5060 EK/CO2.

Bio Hazard hood: Gelaire, Mod BSB-3A.

Phase contrast, Optical inverse Microscope: Zeiss, Mod. 47 12 02-9901.

2.2 Cloning and expression plasmids

pGEX-6P-1 (Amersham Bioscences UK Ltd. Little Chalfont, England)(Figure 2.1):

pGEX plasmid system allows cloning of exogenus genes or fragments of genes in "frame" with the sequence of the fusion protein glutathione-S-transferase (GST), derived from *Schistosoma japonicum*. GST (26 kDa) can be expressed in *E. coli* without misfolding, retaining its normal activity.
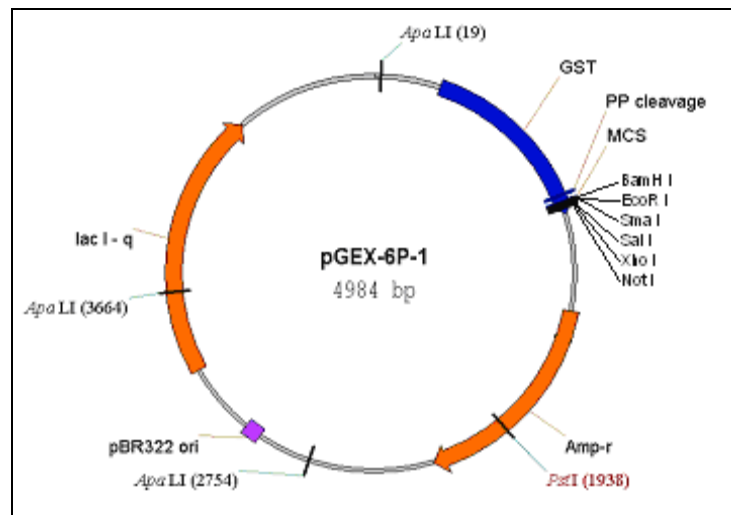
Figure 2.1 Map of the pGEX-6P-1 plasmid.

The plasmidic vector pGEX-6P-1 has the following features:

• Inducible *tac* promoter by IPTG.

• lacI^q gene, which allows the repression of the promoter when IPTG is not present in the medium.

• A polylinker site containing cleavage sites of six restriction enzymes.

• A cleavage site of PreScission protease, located between the GST-coding sequence and the polylinker site.

• β-lactamase gene, which is responsible for cell resistance to ampicillin (Amp).

AT3 genes are cloned between the restriction sites *BamHI* and *SmaI*. If IPTG is added to the medium, AT3 proteins are synthesized in fusion with GST.
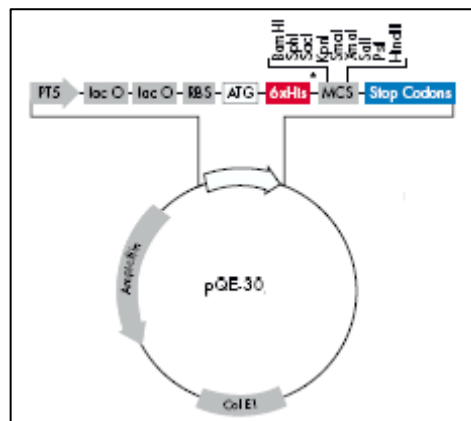
Figure 2.2 Map of the pQE30 plasmid.

pQE30 (Figure 2.2):

This vector allows cloning and expression of an exogenous gene "in frame" to the 6xHis tag. It contains the following elements:

•T5 promoter, an IPTG-inducible transcription-translation system.

• Two *lac* operator sequences.

• Ampicillin resistance gene.

• RBS, ribosome-binding sequence.

• 6xHis tag sequence.

57

• A polylinker containing nine restriction sites.

pcDNA3X(+HA) (Figure 2.3) :

All pcDNA vectors are designed for a rapid cloning of an exogenous gene; they contain a strong promoter which allows to obtain high levels of expression in mammalian cells.
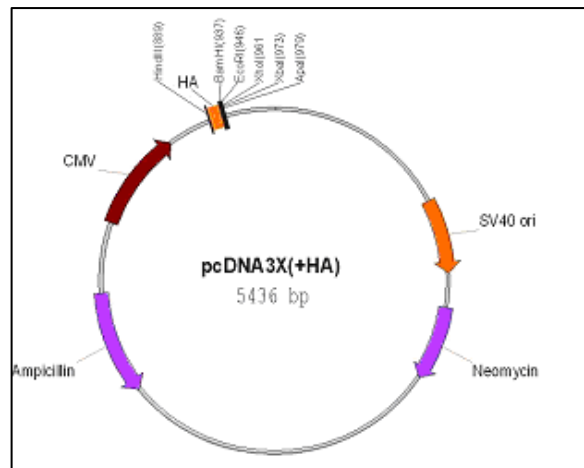
Figure 2.3 Map of the pcDNA3x(+HA) plasmid.

The pcDNA3x(+HA) vector has:

• A strong promoter CMV (cytomegalovirus) that permits a high-level expression in an exogenous mammalian cells.

• A polylinker containing various restriction sites.

• The polyadenylation signal BGH.

• One operator/promoter region and one ORF for Neomycin resistance for the selection of stable clones.

• The replication origin for the plasmid pUC.

• Ampicillin resistance gene.

2.3 Media

2.3.1 Medium for growth of E. coli strains

LB-glucose: (Sambrook *et al.*, 1989) this medium is used for growth of *E. coli* strains.

- Glucose 1 g/l
- Triptone/Peptone 10 g/l
- Yeast Extract 5 g/l
- NaCl 10 g/l
- Ampicillin 100 μg/ml
- Chloramphenicol 25 μg/ml
- Agar 15 g/l (only for plates)

2TY: this medium is used for growth of SG13009 *E. coli* strain.

- Triptone/Peptone 16 g/l
- Yeast Extract 10 g/l
- NaCl 5 g/l
- Ampicillin 100 μg/ml
- Kanamycin 25 μg/ml
- Agar 15 g/l (only for plates)

2.3.2 Medium for mammalian cells

The medium used to maintain in culture COS-7 cell lines is *Dulbecco's Modified Eagle Medium* (DMEM) with foetal bovine serum (FBS; 10% v/v), L-glutamine (4 mM), penicillin (100 U/ml) and streptomycine (100 μg/ml).

Dulbecco's Modified Eagle Medium (DMEM)	(mg/l)	L-Isoleucine	105.00
		L-Leucine	105.00
Inorganic Salts		L-Lysine HCl	146.00
$CaCl_2$(anhydrous)	200.00	L-Methionine	30.00
$Fe(NO_3)$ $9H_2O$	0.10	L-Phenylalanine	66.00
KCl	400.00	L-Serine	42.00
$MgSO_4$(anhydrous)	97.67	L-Threonine	95.00
NaCl	6400.00	L-Tryptophan	16.00
NaH_2PO_4 H_2O	125.00	L-Tyrosine 2Na 2H_2O	104.33
Other Components		L-Valine	94.00
D-Glucose	4500.00	**Vitamins**	
Red Phenol	15.00	D-Pantothenic acid, calcium salt	4.00
Amino acids		Coline Chloride	4.00
L-Arginine HCl	84.00	Folic Acid	4.00
L-Cysteine 2HCl	63.00	i-Inositol	7.20
L-Glutamine	584.00	Niacinamide	4.00
Glycine	30.00	Riboflavin	0.40
L-Histidine HCl H_2O	42.00	Thiamine HCl	4.00

L-Glutamine: pbi international, L-Glutamine Solution (200 mM, 29.2 g/l).

FBS: pbi international, Foetal Calf Serum filtered lot. 716810.

Penicillin and Streptomycine: pbi international, Pen-Strep Solution (Penicillin 10000 U/ml; Streptomycine 10 g/l).

2.4 Techniques for DNA analysis and manipulation

2.4.1 Site-directed mutagenesis

LEGEND

target site of mutation

parental DNA

mutagenic primer

DNA mutated

Step 1: Plasmid preparation

Step 2: PCR

Step 3: Parental DNA digestion
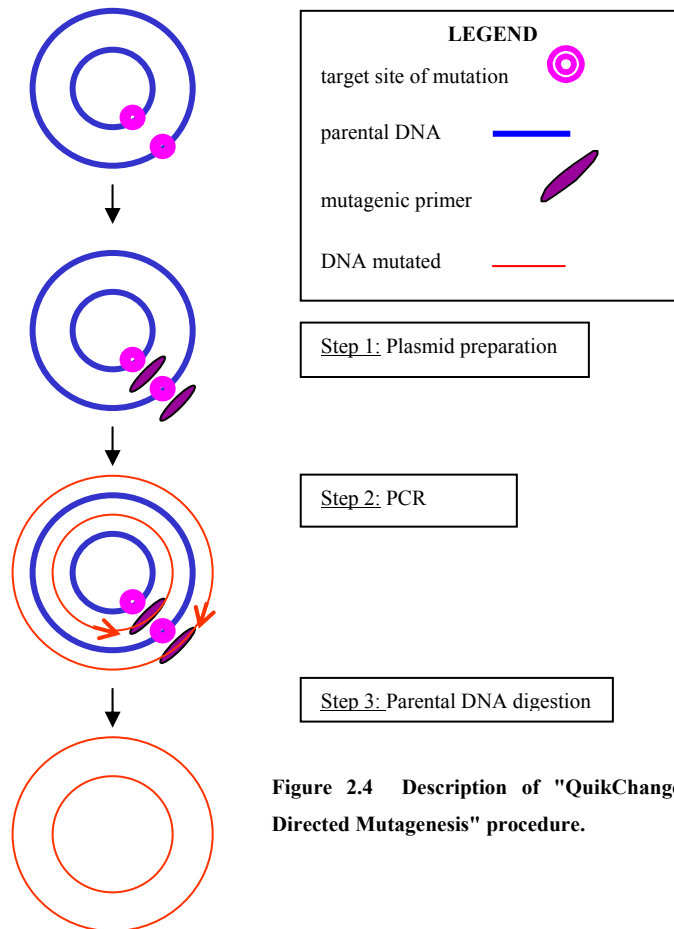
Figure 2.4   Description of "QuikChange Site-Directed Mutagenesis" procedure.

Site-directed mutagenesis experiments is used to insert point mutations and delete or insert single or multiple amino acids. Site-directed mutagenesis is performed using *PfuTurbo*TM high fidelity DNA polymerase. The QuickChange site-directed mutagenesis kit (Stratagene, La Jolla, CA) was used to insert or delete some restriction

sites in order to produce different AT3 truncated variants, using a normal site-directed mutagenesis protocol (Stratagene, La Jolla, CA) (Figure 2.4). PCR products were, then, digested with therestriction enzyme *Dpn I* (Roche, Milan, Italy) to remove parental DNA. DNA was then used to transform *E. coli* strains.

PRIMER DESIGN:

The mutagenic oligonucleotide primers for use in this protocol must be designed individually according to the desired mutation. The following considerations should be made for designing mutagenic primers:

- Both of the mutagenic primers must contain the desired mutation and anneal to the same sequence on opposite strands of the plasmid.

- Primers should be between 25 and 45 bases in length, with a melting temperature (*T*m) of ≥78°C.

- The desired mutation (deletion or insertion) should be in the middle of the primer with ~10–15 bases of correct sequence on both sides.

- The primers optimally should have a minimum GC content of 40% and should terminate in one or more G or C bases.

The following formula is commonly used for estimating the T_m of primers:

$$T_m = 81.5 + 0.41(\%GC) - 675/N - \% \text{ mismatch}$$

Where *N* is the primer length in bases and values for %GC and % mismatch are whole numbers.

PCR REACTION:

DNA template (10 ng/μl)	2 μl
dNTP mix (10mM)	1 μl
Primers (25 ng/μl)	5 μl
Pfu Ultra buffer 10X	5 μl
Molecular grade water	36 μl
PfuUltra DNA polimerase (2.5 U/μl)	1 μl

REACTION'S CONDITIONS:

Segment	Temperature	Time	Number of cycles
1	95°C	30 sec.	1
2	95°C	30 sec.	12-18
	55°C	1 min.	
	68°C	1min/kb plasmid lenght	

Adjust segment 2 of the cycling parameters in accordance with the type of mutation desired (see the following table):

Type of mutation desired	Number of cycles
Point mutation	12
Single amino acid change	16
Multiple amino acid deletions or insertions	18

PCR PRODUCTS DIGESTION

Add 1 μl of *Dpn I* (10 U/μl) to reaction mix and incubate at 37°C for 1 h in order to digest parental DNA.

PCR: Mastercycler gradient, eppAG 22331 (Hamburg).

Centrifuge: Eppendorf 5804 R, (Hamburg); Eppendorf 5415 (Hamburg).

Immersion thermostat: HAAKE F3 (Gebrüder HAAKE GmbH).

2.4.2 Purification of plasmidic DNA

Promega Mini Kit of Promega corporation (Madison, WI, USA) is used to purify small amounts of plasmid to transform *E. coli* strain.

PROTOCOL:

- Use a single, well-isolated colony from a fresh Luria-Bertani (LB) agar plate (containing antibiotic) to inoculate 5 ml of LB medium (containing the same antibiotic).

- Incubate overnight at 37°C in a shaking incubator.

- Harvest bacterial culture by centrifugation for 10 minutes at 4,000 rpm in a centrifuge and discard the supernatant.

- Add 250 μl of Cell Resuspension Solution and completely resuspend the cell pellet by pipetting.

- Add 250 μl of Cell Lysis Solution and mix by inverting the tube 4 times and incubate for less than 5 minutes.

- Add 10 µl of Alkaline Protease Solution and mix by inverting the tube 4 times. Incubate for 5 minutes at room temperature.

- Add 350 µl of Neutralization Solution and immediately mix by inverting the tube 4 times.

- Centrifuge the bacterial lysate at maximum speed (around $14,000 \times g$) in a microcentrifuge for 10 minutes at room temperature.

- Prepare plasmid DNA purification units by inserting one Spin Column into one 2 ml Collection Tube for each sample.

- Transfer the cleared lysate to the prepared Spin Column by decanting.

- Centrifuge the supernatant at maximum speed in a microcentrifuge for 1 minute at room temperature. Remove the Spin Column from the tube and discard the flowthrough from the Collection Tube.

- Add 750 µl of Column Wash Solution, previously diluted with 95% ethanol, to the Spin Column.

- Centrifuge at maximum speed in a microcentrifuge for 1 minute at room temperature. Remove the Spin Column from the tube and discard the flowthrough.

- Repeat the wash procedure using 250 µl of Column Wash Solution.

- Centrifuge at maximum speed in a microcentrifuge for 2 minutes at room temperature.

- Transfer the Spin Column to a new, sterile 1.5 ml microcentrifuge tube.

- Elute the plasmid DNA by adding 50 µl of Nuclease-Free Water to the Spin Column. Centrifuge at maximum speed for 1 minute at room temperature.

- After eluting the DNA discard the Spin Column and store the purified plasmid DNA at -20°C.

Midiprep kit of QIAGEN (Hilden, Germany) is used to obtain high amount of pure DNA to perfom site-directed mutagenesis and cloning DNA.

PROTOCOL:

- Pick a single colony from a freshly streaked selective plate and inoculate a culture of 100 ml LB medium containing the appropriate selective antibiotic.

- Incubate overnight at 37°C with vigorous shaking.

- Harvest the bacterial cells by centrifugation at 6000 x *g* for 15 min at 4°C.

- Resuspend the bacterial pellet in 4 ml Buffer P1.

- Add 4 ml Buffer P2, mix thoroughly by vigorously inverting the sealed
  tube 4–6 times, and incubate at room temperature (15–25°C)
  for 5 min.

- Add 4 ml of chilled Buffer P3, mix immediately and
  thoroughly by vigorously inverting 4–6 times, and incubate on ice for 15 min.

- Clarify the lysate by filtration.

- Equilibrate a QIAGEN-tip 100 by applying 4 ml of Buffer QBT, and allow the column to empty by gravity flow.

- Apply the cleared lysate to the QIAGEN-tip and allow it to enter the resin by gravity flow.

- Wash the QIAGEN-tip with 2 x 10 ml of Buffer QC.

- Elute DNA with 5 ml of Buffer QF.

- Precipitate DNA by adding 3.5 ml (0.7 volumes) of room-temperature isopropanol to the eluted DNA. Mix and centrifuge immediately at $\geq$15,000 x g for 30 min at 4°C. Carefully decant the supernatant.

- Wash DNA pellet with 2 ml of room-temperature 70% ethanol, and centrifuge at $\geq$15,000 x g for 10 min. Carefully decant the supernatant without disturbing the pellet.

- Air-dry the pellet for 5–10 min, and redissolve the DNA in 30 μl of molecular grade water.

Centrifuge: Eppendorf 5804 R, (Hamburg); Eppendorf 5415 (Hamburg).

2.4.3 Restriction enzyme digestion

The DNA is digested with restriction enzyme according to the method described by Sambrook *et al* (1989).

The enzymes (from Roche Diagnostics, Mannheim, Germany) are added with their respective buffers 10x concentrated. Enzymes and

buffers are stored at -20°C. Digestion is performed for 1 h and 30 min at 37°C and for 1 h and 30 min at 25°C, adding enzymes at the beginning of digestion. The enzymes used (approximately 1U/μg of DNA) are *BamHI* (recognition sequence: GGATCC) and *SmaI* (CCCGGG). After the incubation the digestion mixture was analyzed by electrophoresis.

Immersion thermostat: HAAKE F3 (Gebrüder HAAKE GmbH).

2.4.4 Extraction and purification of DNA fragments from agarose gel

High Pure PCR Product Purification Kit from Roche (Mannheim, Germany) is used to solubilize DNA fragments excised from agarose gel.

PROTOCOL:

- Cut desired DNA band from gel using an ethanol-cleaned scalpel.
- Place excised agarose gel slice in a sterile 1.5 ml microcentrifuge tube.
- Determine gel mass by first pre-weighting the tube, and then reweighting the tube with the excised gel slice.
- Add 300 μl Binding Buffer for every 100 mg agarose gel slice to the microcentrifuge tube.

- Dissolve agarose gel slice incubating the suspension for 10 min at 56°C. Vortex the tube briefly every 2 - 3 min during incubation.

- After the agarose gel slice is completely dissolved add 150 µl isopropanol for every 100 mg agarose gel slice to the tube and vortex thoroughly.

- Insert one High Pure Filter Tube into one Collection Tube and pipette the entire contents of the microcentrifuge tube into the upper reservoir of the Filter Tube.

- Centrifuge 30 - 60 s at maximum speed in a microcentrifuge at +15 to +25°C.

- Discard the flowthrough solution and add 500 µl Wash Buffer to the upper reservoir.

- Centrifuge 1 min at maximum speed and discard the flowthrough solution.

- Add 200 µl Wash Buffer and centrifuge 1 min at maximum speed.

- Discard the flowthrough solution and Collection Tube.

- Recombine Filter Tube with a clean 1.5 ml microcentrifuge tube and add 50 - 100 µl Elution Buffer to the upper reservoir of the Filter Tube.

- Centrifuge 1 min at maximum speed.The microcentrifuge tube now contains the purified DNA.

Immersion thermostat: HAAKE F3 (Gebrüder HAAKE GmbH).

Centrifuge: Eppendorf 5804 R, (Hamburg); Eppendorf 5415 (Hamburg).

2.4.5 Ligation of DNA fragments

DNA-ligase from T4 phage is used (Roche Diagnostics, Italy) at a concentration of 1 U/µl. Plasmidic vector and linear fragment, digested with the same restriction enzymes, are combined in the appropriate buffer (66 mM Tris-HCl, 5 mM $MgCl_2$, 5 mM DTT and 1 mM ATP, pH 7.5) with 1 µl of ligase in a final volume of 30 µl. A ratio between vector and insert of 1:5 is used for the ligation, as suggested by data sheet of ligase.

Samples are incubated overnight at 16°C and then precipitated (par. 2.4.6) before performing the transformation.

Immersion thermostat: HAAKE F3 (Gebrüder HAAKE GmbH).

2.4.6 DNA Precipitation

After ligation, DNA is precipitated and resuspended in distilled water to allow transformation of *E. coli* strains. The procedure is the following:

- Add ethanol (2:1) and Sodium Acetate pH 5.2 at a 0.1 M final concentration.
- Keep DNA at -20°C for 2h.
- Centrifuge DNA at 4°C 13000 x g for 30 min. Discard the supernatant.
- Wash DNA with 750 µl of cold 70% ethanol and then, centrifuge at 4°C, 13000 x g for 15 min.
- Air-dry the pellet for 10 min.

▪ Resuspend the pellet in 10 μl of sterile water.

Centrifuge: Eppendorf 5415 R, (Hamburg).

2.4.7 DNA electrophoresis

The most commonly used technique for DNA separation is horizontal electrophoresis in 0.5 to 2% agarose gels submerged in TAE buffer (TAE: solution stock 50 x: 242 g Tris base, 51.7 ml glacial CH_3COOH, 100 ml 0.5 M EDTA pH 8.0). The use of gels having different agarose concentration makes the resolution of a wide size range of DNA fragments possible. Different resolution ranges can be obtained with various concentrations of agarose.

Agarose was purchased from Sigma (Milan, Italy) in ultrapure form for molecular biology. DNA was revealed by addition of Ethidium Bromide (EtBr) to a final concentration of 0.5 μg/ml using UV excitation. To determine the sizes of the DNA "1 kb DNA Ladder" (Roche Diagnostics, Mannheim, Germany) was used. BBF-glycerol (6.2% BBF, 87% glicerol) in a 1:10 ratio with respect to the final volume, was added to the samples to prevent diffusion outside the wells and to visualize migration in the gel.

Electrophoresis was run at a constant voltage of 60 V.

Electrophoresis apparatus: Minnie Submarine Agarose Gel Unit Mod. HE 33–Hoefer (San Francisco, CA).

Power supplies: Electrophoresis Power Supply EPS 300 and EPS 1000 Pharmacia (Uppsala, Sweden); 2301 Macrodrive Power Supply – Pharmacia LKB (Uppsala, Sweden).

2.4.8 Cloning of AT3/Q24 truncated variant JDΔ, 291Δ and 323Δ

The procedure used to produce AT3/Q24 truncated variants and to clone them to pGEX-6P-1 is:

- Purify plasmid pGEX-6P-1/AT3/Q24 using MIDI prep kit (par. 2.4.2).

- Mutate the restriction site of *SmaI* in the multiple cloning site of pGEX-6P-1 using "Site-Directed Mutagenesis" (par. 2.4.1) in a *AvaI* restriction site.

- Insert a restriction site for *BamHI* at the codons 181-182 (JDΔ truncated variant) or a restriction site for *SmaI* at the codons 292-293 or 324-325 (respectively 291Δ and 323Δ truncated variant) using "Site-Directed Mutagenesis" (par. 2.4.1).

- Excise the AT3/Q24 gene from the plasmid, cutting with *BamHI* and *SmaI* restriction enzymes (1 h and 30 min at 25°C with *SmaI* and 1 h and 30 min at 37°C with *BamHI*).

- Load the digestion mixture onto agarose gel and after electrophoresis excise the bands.

- Solubilize gel bands as described in par. 2.4.4.

- Ligate (par. 2.4.5) pGEX-6P-1 and the linear fragment of AT3/Q24 obtained by the digestion with the same restriction enzymes.

72

▪ Precipitate the ligation mixture before transfomation in *E. coli*.

2.4.9 Cloning of AT3/Q6/296Δ

The procedure used to produce AT3/Q6/296Δ and to clone them to pGEX-6P-1 is:

▪ Purify plasmid pGEX-6P-1/AT3/Q6 using MIDI prep kit (par. 2.4.2).

▪ Mutate the restriction site of *SmaI* in the multiple cloning site of pGEX-6P-1 using "Site-Directed Mutagenesis" (par. 2.4.1) in a *AvaI* restriction site.

▪ Insert a restriction site for *SmaI* at the codons 297-298 using "Site-Directed Mutagenesis" (par. 2.4.1).

▪ Excise the AT3/Q6 gene from the plasmid, cutting with *BamHI* and *SmaI* restriction enzymes (1 h and 30 min at 25°C with *SmaI* and 1 h and 30 min at 37°C with *BamHI*).

▪ Load the digestion mixture onto agarose gel and after electrophoresis excise the bands.

▪ Solubilize gel bands as described in par. 2.4.4.

▪ Ligate (par. 2.4.5) pGEX-6P-1 and the linear fragment of AT3/Q6 obtained by the digestion with the same restriction enzymes.

▪ Precipitate the ligation mixture before transfomation in *E. coli*.

2.4.10   Cloning of AT3/Q24 truncated variant 224Δ, 244Δ, 331Δ, 343Δ and 35Δ

It is performed a PCR reaction using oligos 5'-phosphorilated. An high fidelity polymerase supplied from Stratagene is used to amplify the plasmid DNA in order to produce AT3/Q24 trunceted variant 224, 244, 331, 343 and 358.

The PCR products was incubated 1 h at 37°C with DpnI and so metilated DNA was digested.

Then this mixture was used to transform *E. coli* XL-1 blue supercompetent cells.

2.4.11   Production of plasmids pGEX/AT3/Q24/359-363mouse and pGEX/AT3/Q24/363-367mouse

The procedure used to produce pGEX/AT3/Q24/359-363 mouse and pGEX/AT3/Q24/363-367 mouse:

- Purify plasmid pGEX/AT3/Q24 using MIDI prep kit (par. 2.4.2).

- Substitute respectively this aminoacids with the mouse ones using "Site-Directed Mutagenesis" (par. 2.4.1).

2.4.12 Competentation of E. coli for transformation with CaCl$_2$ and RbCl

This technique uses CaCl$_2$ and RbCl (Kushner, 1978).

- Pick a single colony from a freshly streaked selective plate and inoculate a culture of 5 ml LB medium containing appropriate antibiotics.

- Incubate overnight at 37°C under vigorous shaking.

- Add 2 ml of the cell culture to 100 ml of LB-medium containing appropriate antibiotics and incubate at 37° C under shaking until the Abs$_{600}$ is 0.5-0.7.

- Centrifuge 5 ml of cell culture at 4000 x g for 15 min at 4°C.

- Resuspend the pellet in 2,5 ml of sterile MOPS I solution (10 mM MOPS (acido 3-[N-morfolino]propansulfonico), pH 7.0, 10 mM RbCl).

- Centrifuge cells at 4000 x g for 15 min at 4°C and resuspend pellet in 2,5 ml of sterile MOPS II solution (0.1 M MOPS, pH 6.5, 50 mM CaCl$_2$, 10 mM RbCl).

- Incubate in ice for 15 min.

- Centrifuge cells at 4000 x g for 15 min at 4°C and finally resuspend the pellet in 500 μl of sterile MOPS II solution.

Centrifuge: Eppendorf 5804 R, (Hamburg).

2.4.13   Transformation of E. coli with CaCl₂ and RbCl

Transformation is a technique that allows DNA to enter *E. coli* cells. Cells are transformed with pGEX-6P- 1 plasmids as follows:

- Add 10 ng of circular DNA at aliquot of competent cells.

- Incubate the cells in ice for 30 min.

- Keep cells at 42°C for 30 seconds and, once more, in ice for 2 min (heat shock).

- Add 0.9 ml of medium and place cells at 37°C for 1 h.

- Centrifuge cells at 4000 x g for 15 min at 4°C.

- Resusped the pellet with 200 µl of LB medium.

- Plate cells on agar plates containing the appropriate antibiotic at 1/10 and 9/10 diluitions.

- Incubate overnight at 37°C.

- The following day some colonies grow on the plate.

Centrifuge: Eppendorf 5804 R, (Hamburg).

Immersion thermostat: HAAKE F3 (Gebrüder HAAKE GmbH).

2.4.14   Competentation of E. coli for transformation with electroporation

- Pick a single colony from a freshly streaked selective plate and inoculate into a culture of 5 ml LB medium containing appropriate antibiotics.

- Incubate overnight at 37°C under vigorous shaking.

- Add 2 ml of the cell culture to 200 ml of LB-medium containing appropriate antibiotics and incubate at 37° C under shaking until the Abs_{600} is 0.5-0.7.
- Keep cells in ice for 15-20 min.
- Centrifuge cells at 4000 x g for 15 min at 4°C.
- Resuspend the pellet in 200 ml of sterile 10% glycerol solution.
- Centrifuge cells at 4000 x g for 15 min at 4°C.
- Resuspend the pellet in 100 ml of sterile 10% glycerol solution.
- Centrifuge cells at 4000 x g for 15 min at 4°C.
- Resuspend the pellet in 4 ml of sterile 10% glycerol solution.
- Centrifuge cells at 4000 x g for 15 min at 4°C.
- Resuspend the pellet in 400 μl of sterile 10% glycerol solution.
- Store cells in aliquots at -80°C for at last 6 months.

Centrifuge: Eppendorf 5804 R,(Hamburg).

2.4.15   Transformation of E. coli by electroporation

- Thaw in ice an aliquot of the competent cells for each transformation.
- Put the electroporation chambers in ice.
- Pipet 5-10 μl of each ligation mixture into the cells suspension and mix gently. Incubate in ice for 10 min.
- Transfer cells into the electroporation chamber.

- Set the electroporation apparatus to 750 V and apply an electrical discharge.

- Add 1 ml of sterile medium and leave cells at 37°C for 1 h.

- Centrifuge at 4000 x g for 15 min at 4°C.

- Discard the supernatant.

- Resusped cells in 200 µl of LB medium.

- Plate on LB plate with appropriate antibiotics at 1/10 and 9/10 diluitions.

- Incubate overnight at 37°C.

- The following day some colonies grow on the plate.

Electroporator: Bio-Rad model 1000/500 power supply; electroporator: elettroporator Co_Co.

Centrifuge: Eppendorf 5804 R,(Hamburg).

2.5 Expression and purification of AT3 variants

2.5.1 Growth conditions of BL21(DE3) CodonPlus expressing GST/AT3/Q24/182Δ, 224Δ, 244Δ, 291Δ, 323Δ, 331Δ, 343Δ, 358Δ, JDΔ and GST/AT3/Q6/291Δ, 296Δ

E. coli cellular growth is performed as follow:

- Pick a single colony from a freshly streaked selective plate.

- Pre-inoculate into a 100-ml LB culture containing ampicillin (100 µg/ml), chloramphenicol (25 µg/ml).

- Incubate overnight at 37°C under vigorous shaking.

78

- Add ampicillin (100 μg/ml), chloramphenicol (25 μg/ml) and 100 ml of pre culture into 4 l of sterile LB-medium.

- Incubate cells under shaking at 37°C until they reach Abs_{600} 0.8. Induction is effected by adding IPTG to a final 50 μM concentration.

- After 3 h at 37°C the cells are collected by centrifugation at 4000 x g for 15 min at 4°C.

- Resuspend the pellet using PBS buffer (2.7 mM KCl, 10 mM Na_2HPO_4, 1.8 mM KH_2PO_4, pH 7.2, 150 mM NaCl) and centrifuged once more at 4000 x g for 15 min at 4°C.

- Cells are frozen at -20°C.

Centrifuge: Beckman Coulter Avanti J-20 centrifuge, rotor JA-10.

2.5.2 Purification of AT3/Q24/182Δ, 224Δ, 244Δ, 291Δ, 323Δ, 331Δ and AT3/Q6/291Δ, 296Δ

The procedure is reported on "GST Gene Fusion System, third Edition, revision 2" (Amersham Biosciences UK Ltd., Little Chalfont, England).

PREPARATION OF CRUDE EXTRACT:

- Thaw the pellet and resuspend it in 50 ml of Lysis buffer (2.7 mM KCl, 10 mM Na_2HPO_4, 1.8 mM KH_2PO_4, pH 7.2, 150 mM NaCl, 0.5 mM PMSF [phenyl-methyl-sulfonyl-fluoride], 5 mM DTT [Dithiotreitol], 100 mM $MgCl_2$, 1 mg/ml lysozime).

- Incubated under shaking at 4°C for 1 h.

- Incubate cells at -80°C for 30 min and thaw them as quickly as possible.
- Add DNase I (0.2 mg/grams of cells) and 1% Triton final concentration.
- Incubate cells at room temperature for 30 min under shaking.
- Centrifugate at 39000 x g for 30 min at 4°C.
- Save the supernatant that it consitutes the crude extract.

Centrifuge: Beckman Coulter Avanti J-20 centrifuge, rotor JA-20.

AFFINITY CHROMATOGRAPHY:

Glutathione Sepharose 4B (Amersham Biosciences UK Ltd., Little

Chalfont, England) is the resin used to purify proteins in fusion with GST (glutathione S-transferase).

- Crude extract is incubated with the resin (2 ml of bed volume: 10 grams of cells) for 40 min at 4°C under shaking.
- Load the crude extract incubated with resin onto the column.
- Wash the column with 10 bed volumes of PBS buffer (2.7 mM KCl, 10 mM Na_2HPO_4, 1.8 mM KH_2PO_4, pH 7.2, 150 mM NaCl).
- Equilibrate the column with 10 bed volumes of Cleavage buffer (50 mM TrisHCl, pH 7.0, 150 mM NaCl, 1 Mm EDTA, 1 mM DTT).
- Resuspend the resin and AT3 with 1 bed volume of Cleavage buffer.

- Cleave AT3 from the fusion partner in a batch procedure by incubating Prescission Protease (10 U/μl) (Amersham Biosciences UK Ltd., Little Chalfont, England) with the resin at 4°C overnight under shaking. The amount of PreScission Protease added is 40 μl per bed volume of resin.

- The following day elute 5 fractions, each of 2 ml. Fractions are analyzed by SDS-PAGE and Western Blot.

2.5.3 Purification of GST/AT3/Q24/343Δ, 358Δ, JDΔ

The procedure is reported on "GST Gene Fusion System, third Edition, revision 2" (Amersham Biosciences UK Ltd., Little Chalfont, England).

PREPARATION OF CRUDE EXTRACT:

- Thaw the pellet and resuspend it in 50 ml of Lysis buffer (2.7 mM KCl, 10 mM Na_2HPO_4, 1.8 mM KH_2PO_4, pH 7.2 150 mM NaCl, 0.5 mM PMSF [phenyl-methyl-sulfonyl-fluoride], 5 mM DTT [Dithiotreitol], 100 mM $MgCl_2$, 1 mg/ml lysozime).

- Incubated under shaking at 4°C for 1 h.

- Incubate cells at -80°C for 30 min and thaw them as quickly as possible.

- Add DNase I (0.2 mg/grams of cells) and 1% Triton final concentration.

- Incubate cells at room temperature for 30 min under shaking.

- Centrifugate at 39000 x g for 30 min at 4°C.

- Save the supernatant that it consitutes the crude extract.

Centrifuge: Beckman Coulter Avanti J-20 centrifuge, rotor JA-20.

AFFINITY CHROMATOGRAPHY:

Glutathione Sepharose 4B (Amersham Biosciences UK Ltd., Little

Chalfont, England) is the resin used to purify proteins in fusion with GST (glutathione S-transferase).

- Crude extract is incubated with the resin (2 ml of bed volume: 10 grams of cells) for 40 min at 4°C under shaking.
- Load the crude extract incubated with resin onto the column.
- Wash the column with 30 bed volumes of Wash buffer (2.7 mM KCl, 10 mM Na_2HPO_4, 1.8 mM KH_2PO_4, pH 7.2, 250 mM NaCl).
- Elute 5 fractions, each of 2 ml with Eluition buffer (50 mM TrisHCl, pH 8.0, 10 mM Gluthatione reduced). Fractions are analyzed by SDS-PAGE and Western Blot.

2.5.4 Growth conditions of E. coli SG13009 expressing His/AT3/Q24

E. coli cellular growth and purification of AT3/Q24 is made as follow:

- Pick a single colony from a freshly streaked selective plate and inoculate a culture of 100 ml 2TY medium containing ampicillin (100 μg/ml), kanamycin (25 μg/ml).

- Incubate overnight at 37°C with vigorous shaking.

- Add ampicillin (100 μg/ml), kanamycin (25 μg/ml) and 100 ml of preculture in 4 l of sterile 2TY medium.

- Incubate cells under shaking at 37°C until they reach Abs_{600} 0.6. Induction is performed with IPTG 1 mM for 3 h at 30°C.

- Collect cells by centrifugation at 4000 x g for 15 min at 4°C.

- Wash the pellet with PBS buffer (50 mM Na_2HPO_4, 50 mM NaH_2PO_4, 300 mM NaCl, pH 8.0).

- Centrifuged once more at 4000 x g for 15 min at 4°C.

- Resuspend the pellet in 50 ml of Lysis buffer (PBS buffer with 10 mM imidazole, 0.1% Triton, 10% Glycerol, protease inhibitors [Roche Diagnostics, Mannheim, Germany; 1 pill / 50 ml solution]).

- Store overnight at -20°C.

Centrifuge: Beckman Coulter Avanti J-20 centrifuge, rotor JA-10.

2.5.5 Purification of His/AT3/Q24
<u>PREPARATION OF THE CRUDE EXTRACT:</u>

- Thaw the frozen pellet.
- Add 1.4 mM lysozime and 0.5 mM PMSF.
- Incubate the solution in ice for 30 min.

- Sonicate the solution by 3 cycles of 30 sec. sonication with and 2 min. intervals in ice.
- Centrifuge the solution at 53000 x g for 1 h at 4°C.
- Filter the crude extract using 0.45 μm cut-off filters.
- Incubate crude extract with p-aminobenzamidine agarose resin (Sigma ALDRICH, Milan, Italy) (1 ml per 4 l of culture) for 2 h at 4°C under shaking. This resin binds proteases present in the solution, which could degrade the protein of interest.

Centrifuge: Sorvall Discovery 90 SE, HITACHI, Connecticut, USA.

Sonifier: Branson sonifier 250, Branson ultrasonic corporation, Danburg, CT.

ION EXCHANGE CHROMATOGRAPHY:

Nichel-NTA agarose (Qiagen, Milan, Italy) (2 ml of the bed volume for 4 l of culture) allows purification of histidine-tagged proteins.

- Incubate the crude extract with Nichel-NTA resin for 2 h at 4°C under shaking. Load the crude extract onto the column.
- Wash the column with 5 bed volumes of Wash buffer (50 mM Na_2HPO_4, 50 mM NaH_2PO_4, 300 mM NaCl, pH 8.0, 20 mM imidazole, 0.1% Triton, 10% Glycerol, protease inhibitors [Roche Diagnostics, Mannheim, Germany; 1 pill / 50 ml solution]).
- Elute proteins in 5 fractions of 2 ml with Elution Buffer (50 mM Na_2HPO_4, 50 mM NaH_2PO_4, 300 mM NaCl, pH 8.0, 500

mM imidazole, 0.1% Triton, 10% Glycerol, protease inhibitors [Roche Diagnostics, Mannheim, Germany; 1 pill / 50 ml solution]). Fractions are subsequently analyzed by SDS-PAGE and Western Blot and stored at -20°C.

2.6 Protein assay

Protein content was determined using the Bradford method (1976) (Rockford, IL). The Bradford assay is based on Comassie brilliant blue G-250 (CBBG) that specifically binds to protein at arginine, tryptophan, tyrosine, histidine and phenylalanine residues. CBBG binds to these residues in the anionic form, which has an absorbance maximum at 595 nm. The assay is monitored at 595 nm in a spectrophotometer, and determines the CBBG-protein complex. Bovine plasma immunoglobulin was used as standard protein.

Spectrophotometers: Uvikon   Spectrophotometer   930   (Kontron Instruments); Uvidec-V-550 UV / VIS.

2.7   SDS-PAGE

SDS-PAGE was carried out according to King and Laemmli (1971), in a Mighty Small apparatus (Hoefer Scientific Instruments, San Francisco, CA) using a 12% running gel and a 4% stacking gel.

	12% Running gel	4% Stacking gel
Acrylamide 40%/Bis 37,5:1(Ambion, Austin, TX)	3 ml	600 μl
1,5 M Tris/HCl, pH 8.8, 0.4% SDS	3 ml	/
0.5 M Tris/HCl, pH 6.8, 0.4% SDS	/	1.875 μl
Water (distilled)	3.9 ml	2.775 ml
Peroxydisulphate (100 mg/ml)	87.6 μl	30 μl
TEMED	6 μl	10 μl

Running buffer (1 l, pH 8.3) is composed as follow:

• Tris/HCl   15.1 g

• Glycine   94 g

• SDS 10%   50 ml

Sample Buffer 5X:

•Tris/HCl 0.5 M, pH 6.8   2.5 ml

• SDS 10%   1.0 ml

• Glycerol   1.0 ml

• 2-mercaptoethanol   250 μl

• Water (distilled)   250 μl

Samples are prepared adding 0.2 volumes of sample buffer and 0.1 volumes of BBF-glycerol. Then, samples are heated for 5 min at 100°C allowing protein denaturation and loaded onto gel wells.

86

Separation is performed at constant current (20 mA per gel) until BBF reaches the end of the running gel. Gels are stained as described below or used for Western Blot.

Electrophoresis apparatus: Mighty Small II SE 250 Hoefer Scientific Instruments (San Francisco, CA).

Power supply: Electrophoresis Power Supply EPS 300 and EPS 1000; Macrodrive Power Supply –LKB (Pharmacia, Uppsala, Sweden).

2.8 Coomassie staining

We used the Gel-Code® staining that is based on Coomassie Blue R-250. This dye binds non-specifically to virtually all proteins in an approximately stoichiometric fashion. The gel is first washed 3 times, for 10 minutes each, in water and then incubated for 1 h in Gel-Code Blue Stain Reagent (Pierce, Rockford, IL). Finally, it is washed in water to reduce the background.

2.9 Western blot

2.9.1 Blotting proteins from gel to Immobilon®-P filter

Proteins are transferred from SDS gels to Immobilon®-P filters (Millipore, Bedford, MA) as follows.

Before the end of SDS-PAGE, Immobilon®-P filter is soaked, first in methanol, then in CAPS (10 mM 3- [cyclohexylamino]-1-propansulfonic acid 10 mM, 10% HCOOH, pH 11) under shaking for at least 10 min. Then, it is laid onto the gel, taking care to remove any

bubble between them. Gel and filter are placed between sheets of Whatman paper® 3MM pre-soaked in CAPS, and two rigid plastic supports ("sandwich"). This sandwich is then placed into the electrophoretic chamber with the filter facing the anode.

The proteins, negatively charged because of the high pH, migrate towards the anode, and are absorbed by the filter. Blot transfer is done at constant current (400 mA) for 2 h.

Power supply: Electrophoresis Power Supply EPS 300 and EPS 1000; Macrodrive Power Supply –LKB (Pharmacia, Uppsala, Sweden).

2.9.2 Immunodetection System (ECL)

After transfer of proteins from the gel to the PVDF membranes, this is saturated at 4°C overnight with blocking solution (5% skim milk in PBS buffer 2.7 mM KCl, 10 mM Na_2HPO_4, 1.8 mM KH_2PO_4, pH 7.2, 150 mM NaCl). The next day the filter is incubated with primary anti-AT3-Z46 antibodies at 1:5000 dilution in blocking solution, for 1 h at room temperature under shaking. After incubation in primary antibody, membranes were rinsed 3 timesin 0.1% Tween in PBS buffer for 10 min each. Then, it is subsequently incubated for 1 h in secondary antibody (1:5000 horseradish peroxidase-goat anti-rabbit antibodies dilution in 5% skim milk, 0.3% Tween, in PBS buffer) at room temperature. At the end, membranes were rinsed 3 times in 0.3% Tween in PBS buffer for 10 min each.

For tubulin detection, membranes were incubated in PBS buffer, 5% skim milk and 0.1% Tween with anti-α-tubulin at a 1:5000 diluition for 1 h at 25°C and subsequently for 1 h at 25°C with secondary antibody (1:3000 anti-mouse antibody from Calbiochem, Darmstadt, Germany) in PBS buffer, 1% skim milk and 0.1% Tween.

For neuronal nuclei (NeuN) detection, membrane was incubated for 1 h at 25°C with anti-neuronal nuclei monoclonal antibodies (Chemicon, CA, USA) at 1:2000 diluition in blocking solution and subsequently overnight at 4°C with secondary antibodies (1:3000 anti-mouse sntibody from Calbiochem, Darmstadt, Germany) in PBS buffer, 1% skim milk and 0.1% Tween.

Immunoreactive bands were revealed using the "ECL Western Blotting detection System" (GE Healthcare, Life sciences, Little Chalfont, England). This is based on a luminol-HRP-chemiluminescence reaction. The chemiluminescence light emission can be recorded by a short exposure to blue-light sensitive autoradiography films. The solution test contains H_2O_2, luminol and a "chemical enhancer". Peroxidase catalyzes the following reaction:

$$2\ H_2O_2 \rightarrow 2\ H_2O + O_2$$
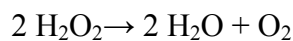
The oxygen released oxidizes the luminol, with subsequent light emission. This effect is stronger because of the presence of "chemical enhancer". The light impresses the autoradiography film during the exposure for a variable time depending on the light intensity (generally from 30 sec to 30 min).

The immunodecorated filter is dipped for 1 min in the "ECL Western Blotting detection System" solution, fresh prepared each time. The filter is dried and autoradiographed in a cassette, using a HYPERfilm slab (GE Healthcare, Life Sciences, Little Chalfont, England), which is then developed.

2.10 Immunofluorescence and confocal analysis

COS-7 cells were plated onto coverslips (2.5 x 10^4 cells/coverslip) and grown for 24 h in Dulbecco's Modified Eagle Medium containing 10% foetal bovine serum, 100 U/ml penicillin, 100 μg/ml streptomycin and 4 mM glutamine. Cells were transfected overnight with FuGENE6 (Roche Diagnostics, Mannheim, Germany), according to the manufacturer's instruction. 24 h after the transfection, cells were fixed for 5 min in 100% methanol at -20°C and quenched for 30 min with 50 mM NH_4Cl in PBS. Permeabilization was carried out incubating the cells in the presence of 0.3% (w/v) saponin in PBS (7 min for 3 times).

Cells were then double-stained with anti-*c-myc* rabbit and anti-α-tubulin mouse monoclonal antibodies (1:50 and 1:4000, respectively). Both antibodies were from Sigma (Sigma, St. Louis, MO, USA). After extensive washes, cells were incubated with donkey anti-rabbit Cy3 conjugated and donkey anti-mouse CY2 conjugated antibodies (1:400 and 1:200, respectively). Both antibodies were from Jackson ImmunoResearch laboratories (West Grove, PA, USA).

Incubations and washes were carried out at room temperature in PBS, 0.3% (w/v) saponin.

Confocal microscopy was carried out using Leica Mod. TCS-SP2 (Leica Microsystem, Wetzlar, Germany). Image processing was performed with Leica Confocal Software (LCS.EXE) and Adobe Photoshop Software. Double-staining microfluorometry analysis was performed using Multicolor analysis software (Leica, France) running on the TCS (Leica) confocal microscope. In the cytofluorogram, the pixel to pixel correlation between two channels (red and green for tubulin and AT3 colocalization, or red and blue for nucleus and nuclear inclusions of AT3/Q72 colocalization) could be obtained; colocalized or closely related areas could be selected (yellow cloud) and quantified. The selected cytofluorogram was superimposed in white onto the merged images of this same area.

Confocal microscopy: Leica Mod. TCS-SP2, Leica Microsystem, Wetzlar, Germany..

2.11 Pull-down experiments of GST/AT3/Q24/182Δ, GST/AT3/Q6/291Δ, GST/AT3/Q24 proteins using rat brain soluble extracts

2.11.1 BL21(DE3) codon plus E. coli growth conditions

- Pick a single colony from a freshly streaked selective plate and inoculate a culture of 25 ml LB medium containing ampicillin (100 μg/ml) and chloramphenicol (25 μg/ml).

- Incubate overnight at 37°C under vigorous shaking.

- Add ampicillin (100 μg/ml), chloramphenicol (25 μg/ml) and 6.25 ml of preculture in 250 ml of sterile LB medium.

- Incubate cells under shaking at 37°C untill they reach Abs_{600}= 0.8. Induction is effected by adding IPTG to a final 50 μM concentration.

- After 2 h at 37°C the cells are collected by centrifugation at 4000 x g for 15 min at 4°C.

- The pellet is resuspended using PBS buffer (2.7 mM KCl, 10 mM Na_2HPO_4, 1.8 mM KH_2PO_4, pH 7.2, 150 mM NaCl) and centrifuged once more at 4000 x g for 15 min at 4°C.

- Cells are frozen at -20°C.

Centrifuge: Beckman Coulter Avanti J-20 centrifuge, rotor JA-10.

2.11.2   Binding of AT3 variants to Glutathione Sepharose 4B Columns

- The crude extract, obtained as described in par 2.5.2, is incubated with 500 μl of Glutathione Sepharose 4B, for 40 minutes, under vigorous shaking.

- Crude extract and the resin is loaded onto a column and washed with 10 bed volumes of PBS buffer (2.7 mM KCl, 10 mM Na_2HPO_4, 1.8 mM KH_2PO_4, pH 7.2, 150 mM NaCl).

- Then crude extract and the resin is incubated with 2 mg of soluble rat brain extracts for 40 min at room temperature.

- The column is washed once more with 10 bed volumes of PBS buffer.

- The column is equilibrated with 10 bed volumes of cold Cleavage Buffer (50 mM TrisHCl, pH 7.0, 150 mM NaCl, 1 mM EDTA, 1 mM DTT).

- Finally AT3 and bound proteins are eluted with Prescission Protease as described in par. 2. 5. 2 .

2.11.3   Preparation of soluble rat brain extracts

Soluble rat brain extracts were produced by Potter-homogenizing 1 g fresh tissue in 6 ml of PBS buffer (50 mM TrisHCl, pH 7.0, 150 mM NaCl, 1 mM EDTA, 1 mM DTT) plus protease inhibitors (Roche Diagnostics, Mannheim, Germany, 1 tablet/50 ml solution). Subsequently the sample was centrifuged at 50000 x g for 15 minutes at 4°C and the pellet discarded. Protein concentration of

the supernatants was determined by Bradford assay (par. 2. 6) and adjusted to 1 mg/ml.

Centrifuge: Sorvall Discovery 90 SE, HITACHI, Connecticut, USA.

2.12 Multidimensional PROTEIN IDENTIFICATION TECHNIQUE (MudPIT)

2.12.1   Trypsin digestion

Sequencing grade modified trypsin (Promega, Madison, WI, USA) was added to 25 μl of different AT3 samples at an enzyme/substrate ratio of about 1:50 in 200 mM ammonium bicarbonate, pH 8.9. After an overnigt incubation at 37°C, 1 μl of trypsin (0.1 μg/μl) is added again to the solution and samples are incubated for 3 h at 37°C. Digestion is stopped by adjusting the pH to 2.0 with the addition of formic acid.

Immersion thermostat: HAAKE F3 (Gebrüder HAAKE GmbH).

2.12.2   LC-MS and LC-MS/MS Analysis of enzymatic digestion

Trypsin-digested samples were analyzed by means of two-dimensional micro liquid chromatography coupled to ion trap mass spectrometer (2DC-MS/MS, also referred to as Multidimensional Protein Identification Technology, MudPIT), using the Proteome X system (Thermo Electron Corporation, San josè, CA, USA) for data

handling. Briefly 10 μl of the digested peptide mixtures (about 1.9 μg) were fist loaded onto a strong cation exchange column (Biobasic-SCX column, 0.32 i. d. x100 mm, 5 μm, Termo Electron Corporation, Bellefonte, PA, USA) and then eluted stepwise by applying a five step ammonium chloride concentration gradient (0, 100, 200, 400, 600 mM). Each salt step eluate was directly loaded onto a reversed-phase C_{18} column (Biobasic-18, 0.18 i. d. x100 mm, 5 μm, Termo Electron Corporation, Bellefonte, PA, USA) and separeted with acetonitrile gradient (eluent A, 0.1% formic acid in water; eluent B, 0.1% formic acid in acetonitrile); the gradient profile was 5% eluent B for 1 min followed by 5-65% eluent B within 30 min. The peptides eluted from the C_{18} column were directly analyzed with an ion trap $LCQ_{Deca}XP$ Mass spectrometer (Termo Electron Corporation, San Josè, CA, USA), equipped with a metal needle (10 μm i. d.). The electrospray source was given 3.2 kV of applied voltage and 15 arbitrary units of sheath gas flow, while the heated capillary was held at 160°C and capillary voltage at 67 V. Spectra of eluting peptides were acquired in positive ion mode and in a data-dependent fashion by fist acquiring a full MS scan in the range 300/1500 *m/z,* followed by a MS/MS scan of the most intense ion of the previous full MS scan. MS/MS scans were acquired using an activation time of 30 ms and 35% normalized collision energy. Once sampled, each MS/MS precursor mass was excluded from further tandem mass experiments for three min using a dynamic exclusion instrument method.

2.12.3   Mass spectrometry data handling

Computer analysis of MS/MS spectra was performed using the version 3.2 Bioworks, based on SEQUEST algorithm (University of Washington, licensed to ThermoFinnigan Corp., San Josè, CA, USA).

The experimental MS/MS spectra were correlated to tryptic peptide sequences by comparison with the teoretical mass spectra obtained by *in silico* digestion of the *Rattus norvegicus* protein database, downloaded December 2007 from the National Center for Biotechnology Information (NCBI) website (www.ncbi.nlm.nih.gov). This allowed the identification of peptide sequences and related proteins.

As the confidence of protein identification, particularly when using data from a single peptide, depends on stringency applied for the identification of the peptide sequence and peptide matching, a high stringency was guaranteed as follows. The chosen minimum values of Xcorr were greater than 1.5, 2.0 and 2.5 for single, double and triple charge ions, respectively. The peptide mass search tolerance was set to 1.0 Dalton, while this parameter was usually set to 2 or 3 Dalton; precurson ion tolerance was set to 1.400 amu, threshold to 1000, Group scan to 1, Minimum group count to 1 ang Minimum ions count to 15. The stringency applied was optimal because we considered an additional confidence parameter, Δcn (normalized correlation), which in our case was better than 0.1, when it is considered already optimal at >0.07.

Moreover, searches were done with tryptic specificity, allowing two missed cleavages and a tolerance on the mass measurement of 2.00 amu for peptide and 1.00 amu for MS/MS ions.

Finally, to assign a final score to proteins, the SEQUEST output data were filtered setting peptide/protein probability to 10^{-2} and consensus score higher than 10. The output data obtained from SEQUEST software were treated with the Multidimensional Algorithm Protein Map (MAProMA) in-house algorithm for comparison of the protein lists and evaluation of relative abundances (Mauri *et al.*, 2005).

2.13 AT3 immunoprecipitation from rat brain soluble extracts

Soluble rat brain extracts were produced by Potter-homogenizing 250 mg fresh tissue in 1 ml 20 mM TrisHCl, pH 8. 2, 150 mM NaCl, 1 mM EDTA, 5 mM $MgCl_2$, 1% Triton X-100, EDTA-free protease inhibitors (Roche Diagnostics, Mannheim, Germany, 1 tablet/50 ml solution).

Homogenates were then ultracentrifuged at 100,000 x g for 30 min at 4°C, and the pellet discarded. Supernatants were used for immunoprecipitation experiments.

Briefly, either anti-AT3 Z46 polyclonal antibodies or anti-α-tubulin monoclonal antibodies (Sigma, St. Louis, MO, USA) were cross-linked to 50 μl Dynabeads Protein G (Invitrogen) according to the manifacturer's protocol. Cross-linked beads were incubated for 1 h

at 25°C with 1 mg protein aliquots of supernatants and washed three times with 1 ml of PBS buffer (2.7 mM KCl, 10 mM Na_2HPO_4, 1.8 mM KH_2PO_4, pH 7.2, 150 mM NaCl).

As negative controls, non-cross-linked Dynabeads Protein G or cross-linked Dynabeads Protein G not incubated with the extract were used.

Bound protein was eluted boiling the beads for 10 minutes in SDS-PAGE application buffer. Extracted protein was analyzed by SDS-PAGE (par. 2.7) and immunoblotting (par.2.9) using either anti-AT3 or anti-α-tubulin antibodies.

Centrifuge: Sorvall Discovery 90 SE, HITACHI, Connecticut, USA.

2.14 Determination of quantitative binding parameters by surface plasmon resonance

A BIACORE X system (Uppsala, Sweden) was used to analyze molecular interactions by means of surface plasmon resonance (SPR)(Malmqvist, 1999).

Tubulin purified from bovine brain (Cytoskeleton Inc., Denver. CO. USA) or hisAT3/Q24 purified from *E. coli* (par. 2.5.5) was covalently linked to a carboxymethylated dextran surface, CM5 sensor chip, by using amine-coupling chemistry (Johnsson *et al.*, 1991). A surface density of 4800 resonance units (RU) was generated for tubulin by using 14 μl of a 0.1 μg/μl protein in 10 mM sodium acetate buffer, pH 4.3. A surface density of 3400 resonance units (RU) was

generated for ataxin by using 25 μl of a 5 μM protein in 10 mM sodium acetate buffer, pH 4.2. Solutions of the analyte were injected over the surface at 25°C with a flow rate of 10 μl/min in running buffer (10 mM HEPES, pH 7.4, 150 mM NaCl, 3 mM EDTA containing 0.005% (v/v) Surfactant P20). After injection, analyte solutions were replaced by running buffer at a continuous flow rate of 10 μl/min. Surface regeneration was accomplished by injecting 50 mM NaOH (10 μl/min; 0.5-minute contact time). All analyte solutions were run simultaneously over a control flow cell containing a blank surface (with no immobilized protein) at 25°C. Each sensorgram (time course of the SPR signal) was subtracted for the response observed in the control flow cell and normalized to a baseline of 0 RU. Different concentrations of the analyte were passed for 3 min over the sensor chip with immobilized ligand (30 μl injections at a flow rate of 10 μl /min).

The interaction rate constants were calculated by using the BIA evaluation 4.1 SPR kinetic software (BIAcore).

BIACORE biosensor: BIACORE X 100, Uppsala, Sweden.

3 Results

3.1 α- and β-tubulins are major interactors of AT3, as shown by MudPIT

Previous investigations showed that AT3 behaves as a multifunctional protein, in that it is capable of interacting with different proteins, both in the nucleus and the cytosol (Evert *et al.*, 2006; Mao *et al.,* 2005; Doss-Pepe *et al.,* 2003). This prompted us to search for further interactors by taking advantage of MudPIT technology. The experimental design consisted of: a) producing different AT3 variants in fusion with GST, with a Prescission Protease cleavage site in between, b) binding the different constructs to Glutathione Sepharose 4B, c) pouring the resin onto columns, d) loading soluble rat brain extracts onto the columns and washing to abolish non-specific binding, e) eluting AT3 and bound protein by PreScission Protease treatment, and f) identifying the bound protein species by tryptic digestion and subsequent MudPIT analysis of the resulting peptides.

To also spot the AT3 regions interacting with molecular partners, we used different AT3 variants, i.e., GST/AT3/182Δ (human; truncated at the residue 182 and consisting of the sole Josephin domain (JD)); GST/AT3/291Δ (murine; truncated at the residue 291 and devoid of polyQ); GST/AT3/Q6 (full-length murine, carrying 6 consecutive glutamines); GST/AT3/Q24 (full-length human, carrying 24 consecutive glutamines) and GST as a control. AT3 variants carrying expanded polyQ stretches could not be

employed in such assays, due to their extreme propensity to aggregate that prevented us from obtaining reproducible results. Several interacting proteins were detected. However, few significant MudPIT scores could be assigned, as reported in Table 3.1. They are a quantitative estimate of the relative protein abundance in different preparations, as shown in previous reports (Regonesi *et al*., 2006; Mauri and Dehò, 2008). In particular, a significant score could be assigned to α- and β-tubulins, which were consistently found in the list of the proteins identified.

In control experiments, performed with GST alone, keratins were the only significant interactors (data not shown). As representative results, sequence coverage and number of identified peptides of rat brain proteins interacting with AT3/291Δ are reported in Table 3.2.

MudPIT scores indicate that the JD in isolation can bind both α- and β-tubulins, although to a lower extent compared to full-length AT3/Q24, which suggests that the interacting surface encompasses the JD. Also noteworthy is AT3 binding to the cytoskeletal microtubule-associated protein 2 (MAP2) and β-actin. Furthermore, worth mentioning is the interaction of AT3/291Δ and AT3Q6, with VCP (Table 3.1) but not of the JD alone. This points to an absolute requirement of a tract in the C-terminal domain for such interaction, in keeping with previous reports (Boeddrich *et al.*, 2006).

Table 3.1 MudPIT identification and scores of rat brain proteins interacting with different AT3 constructs. GST/AT3 fusion proteins were bound to a Glutathione Sepharose 4B column. Protein was eluted from Glutathione Sepharose 4B by batch treatment with PreScission Protease and subjected to MudPIT analysis. Only keratins were found to interact with GST alone. Each column reports the mean value from two independent pull-down experiments, performed with different brain extracts.

GI Number	Protein description	AT3/182Δ	AT3/291Δ	AT3Q6	AT3Q24	Molecular mass (Da)
11067443	ataxin 3	55	125	105	55	40445.9
92930	tubulin beta chain 15	34	25	20	69	49936.7
223556	tubulin alpha	20	25	30	60	50241.4
547890	MAP2_RAT Microtubule-associated protein 2 (MAP 2)	0	20	0	0	202408.4
40018568	protein for MGC:73008 - tubulin beta C2	10	10	10	25	49800.7
34880797	similar to gamma actin-like protein	10	10	10	10	46471.9
1871639	Mature alpha chain of major histocompatibility complex class I antigen	0	10	10	0	39024.2
51556267	ciliary neurotrophic factor receptor	10	10	10	0	40822.1
17865351	valosin-containing protein	0	10	10	0	89348.3
34856664	similar to actin, alpha, cardiac	0	10	0	0	57683.6
34881719	similar to Elongation factor 1-alpha 1 (EF-1-alpha-1)	0	10	0	0	41224.4
539969	lysozyme homolog AT-2, bone - rat (fragments)	0	10	0	0	3164.3
2119326	alpha-smooth muscle actin - rat (fragment)	0	10	0	0	3541.8
34875163	similar to sacsin	0	10	0	0	456489.4

Table 3.2 MudPIT identification, sequence coverage and number of identified peptides of rat brain proteins interacting with AT3/291Δ. GST/AT3 fusion protein was bound to a Glutathione Sepharose 4B column. Protein was eluted from Glutathione Sepharose 4B by batch treatment with PreScission Protease and subjected to MudPIT analysis. Only keratins were found to interact with GST alone. Other experimental details are reported in the legend to Table 3.1.

GI Number	Protein description	Molecular mass (Da)	Sequence coverage (%)	Number of identified peptides
11067443	ataxin 3	40445.9	35.8	13
92930	tubulin beta chain 15	49936.7	16.4	4
223556	tubulin alpha	50241.4	17.7	4
547890	MAP2_RAT Microtubule-associated protein 2 (MAP 2)	202408.4	3.4	2
40018568	protein for MGC:73008 - tubulin beta C2	49800.7	7.2	1
34880797	similar to gamma actin-like protein	46471.9	3.8	1
1871639	Mature alpha chain of major histocompatibility complex class I antigen	39024.2	4.1	1
51556267	ciliary neurotrophic factor receptor	40822.1	6.7	1
17865351	valosin-containing protein	89348.3	2.1	1
34856664	similar to actin, alpha, cardiac	57683.6	3.1	1
34881719	similar to Elongation factor 1-alpha 1 (EF-1-alpha-1)	41224.4	6.3	1
539969	lysozyme homolog AT-2, bone - rat (fragments)	3164.3	42.9	1
2119326	alpha-smooth muscle actin - rat (fragment)	3541.8	28.2	1
34875163	similar to sacsin	456489.4	0.7	1

3.2 AT3 from rat brain coimmunoprecipitates with tubulin

To further validate the hypothesis that AT3 binds to α- and β-tubulins, we performed coimmunoprecipitation experiments. We cross-linked either anti-AT3 or anti-α-tubulin antibodies to magnetic Dynabeads G. Then, we incubated them with soluble rat brain extracts. Bound protein was subjected to Western blot using both anti-AT3 and anti-α-tubulin antibodies. Immunodecoration demonstrated the presence of both AT3 and tubulin in the immunoprecipitates, thus confirming MudPIT findings concerning interaction of AT3 with tubulin (Figure 3.1).
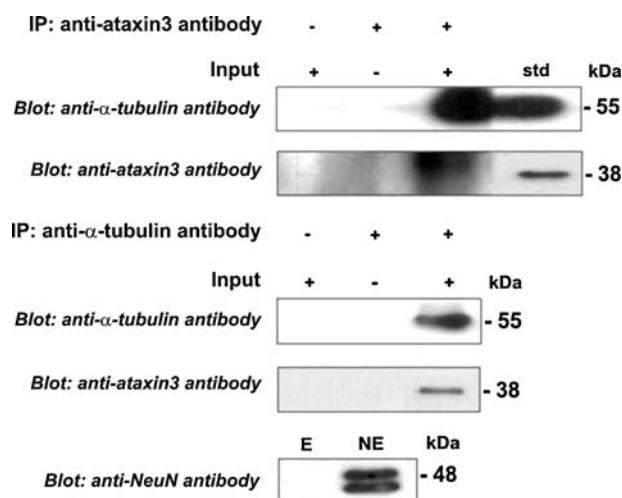

Figure 3.1 Coimmunoprecipitation of AT3 and tubulin. Immunoprecipitations (IP) were performed using either anti-AT3 or anti-α-tubulin antibody cross-linked to 50 μl Dynabeads Protein G. Beads were incubated for 1 h at 25 °C with 1-mg protein aliquots of cytoplasmic rat brain extracts (Input) and washed three times with 1 ml of PBS. As negative controls, non-cross-linked beads or cross-linked beads not incubated with the extract were used. Bound protein was then eluted in SDS-PAGE application buffer, electrophoresed and immunoblotted (Blot) using either anti-AT3 or anti-α-tubulin antibodies. 0.5 μg of

pure dimeric tubulin or of AT3 (std) were run in parallel and revealed by the respective antibodies. Aliquots of soluble (E) and nuclear (NE) extracts (50 μg protein each) were immunodecorated with anti-neuronal nuclei monoclonal (NeuN) antibodies, which showed the absence of nuclear contamination in soluble extracts. Molecular masses (kDa) of the proteins were estimated using suitable protein standards.

3.3 AT3 colocalizes with tubulin in situ

In order to investigate whether AT3 can bind tubulin in the context of a mammalian cell, we performed colocalization experiments using confocal microscopy on COS-7 cultured cells overexpressing AT3/Q6 or AT3/Q72 variants that carry a *c-myc* epitope at the C-terminus. Murine AT3/Q6 was chosen instead of human AT3/Q26 in order to prevent any possible polyQ-mediated protein aggregation, due to high AT3 intracellular concentration in transfected cells. Indeed, we showed that an AT3 variant harboring a polyQ in the physiological range is prone to aggregation when its concentration is sufficiently high (Marchal *et al*., 2003). On the other hand, murine and human AT3 are closely related to each other and in our MudPIT experiments both interacted with α- and β-tubulins.

COS-7 cells seeded on square glass coverslips were fixed and immunolabeled 24 h after transfection. Confocal microscopy localization of AT3 and tubulin on transfected cells was performed by primary mouse anti-α-tubulin and rabbit anti-*c-myc* antibodies, and secondary anti-mouse IgG-CY2-conjugated and anti-rabbit IgG-CY3-conjugated antibodies, which reveal α-tubulin (Figure 3.2a, a′) and AT3 (Figure 3.2b, b′), respectively. Overlays of a, b, and a′, b′ are shown in panels c and c′. To assess colocalization, a cytofluorogram

was plotted for each image, and an equivalent region of the scatter plot was selected in both graphs (Figure 3.2d, d′). When image points selected for colocalization (region of interest, ROI) in the cytofluorogram were highlighted in white in the original image, levels of punctuate colocalization between tubulin and AT3 were detected (e, e′). Panel f shows that nuclear inclusions of AT3/Q72 actually colocalize with the nucleus. Furthermore, tubulin and AT3-related emissions clearly showed a partial overlay of the two proteins. Also, immunolabeled tubulin colocalizing with AT3 displayed the filamentous morphology that is typical of microtubules, as shown in several previous reports (Nagayama and Matsumoto, 2008; Rathinasamy and Panda, 2008; Harries *et al.*, 2009). This provides evidence that AT3 also interacts with assembled microtubules, besides tubulin subunits. In contrast, AT3/Q72, when aggregated, did not colocalize with tubulin. Quite likely, aggregation prevented it from interacting with microtubules.
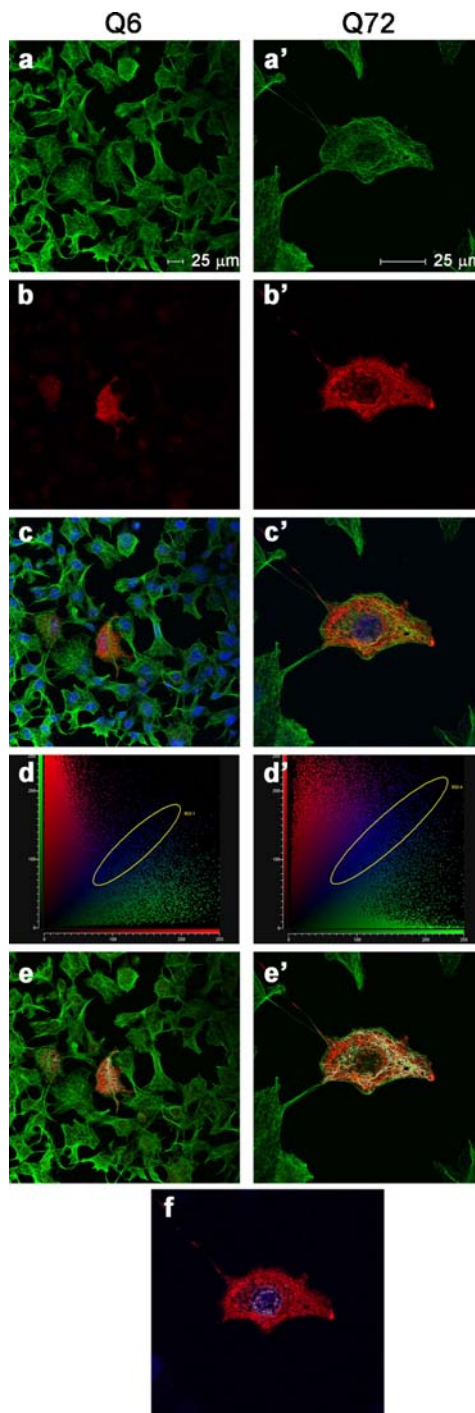
Figure 3.2. Subcellular colocalization of either AT3/Q6 or AT3/Q72, with tubulin. Green light emission results from CY2 fluorofore conjugated to secondary anti-mouse IgG antibody, which detects α-tubulin (a, a′); red light emission results from CY3 fluorofore conjugated to secondary anti-rabbit IgG antibody, which detects the two AT3 variants (b, b′). Overlays of a, b, and a′, b′ are shown in panels c and c′. A 2D cytofluorogram is plotted for each double-stained image (d, d′) in which the region of interaction between the red channel (*y*-axis) and the green channel (*x*-axis) is displayed in blue (area of colocalization). The set of value pairs selected in the area of colocalization (ROI) are highlighted in white in the original image (e, e′). In panel f, colocalization between nucleus and nuclear inclusion of AT3/Q72 is shown. Scale bars: 25 μm.

106

3.4 SPR provides evidence of tight AT3/Q24-tubulin interaction

SPR was used to describe the real time association and dissociation of AT3/Q24 to tubulin dimer that was coupled directly to the sensor chip. The binding and release of AT3 to and from this chip was monitored. The kinetics of binding were reproducible in the different experiments. Figure 3.3 depicts a typical sensorgram obtained by using five concentrations in the range from 100 to 1000 nM. Simultaneous fitting of sensorgrams with BIA evaluation software allowed the estimation by Langmuir 1:1 binding model of the association and dissociation rate constants, k_{on} and k_{off} for the binding to tubulin, which were $1.77 \times 10^4 \, M^{-1} \, s^{-1}$ and $9.2 \times 10^{-4} \, s^{-1}$, respectively, yielding a calculated K_D of $5.2 \times 10^{-8} \, M$. The plot of K_{obs} for each given AT3 concentration vs. conc. was linear ($R^2 = 1$), typical for a 1:1 model (data not shown). The Scatchard plot, obtained using the R_{eq} for each given AT3 concentration, is shown in panel B and a K_D of $7.5 \times 10^{-8} \, M$ was calculated from the slope of the plot. The similarity of the K_D values, obtained from the two different methods (Schuck and Minton, 1996) support the consistency of the obtained kinetic and thermodynamic parameters.
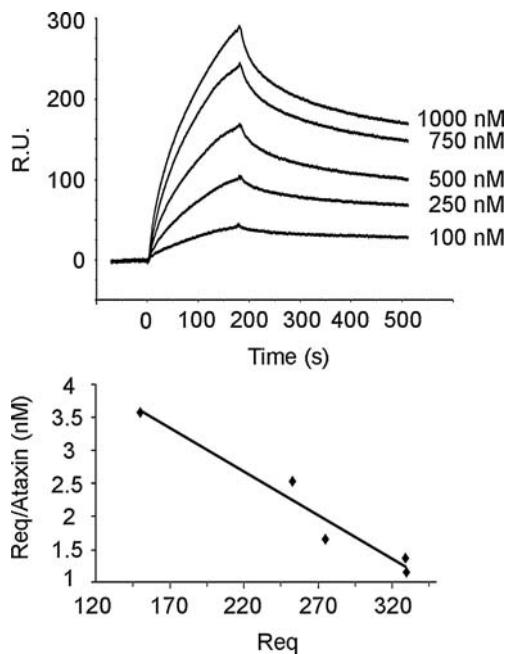
Figure 3.3 Association/dissociation kinetics for the binding between tubulin and AT3/Q24. (A) Tubulin was immobilized on the sensor chip and the indicated concentrations of AT3/Q24 were flowed onto the chip surface. (B) The R_{eq} value obtained for each given protein concentration was used to generate the Scatchard plot.

3.5 SPR experiments on AT3 truncated forms shed light on the mode of interaction with tubulin
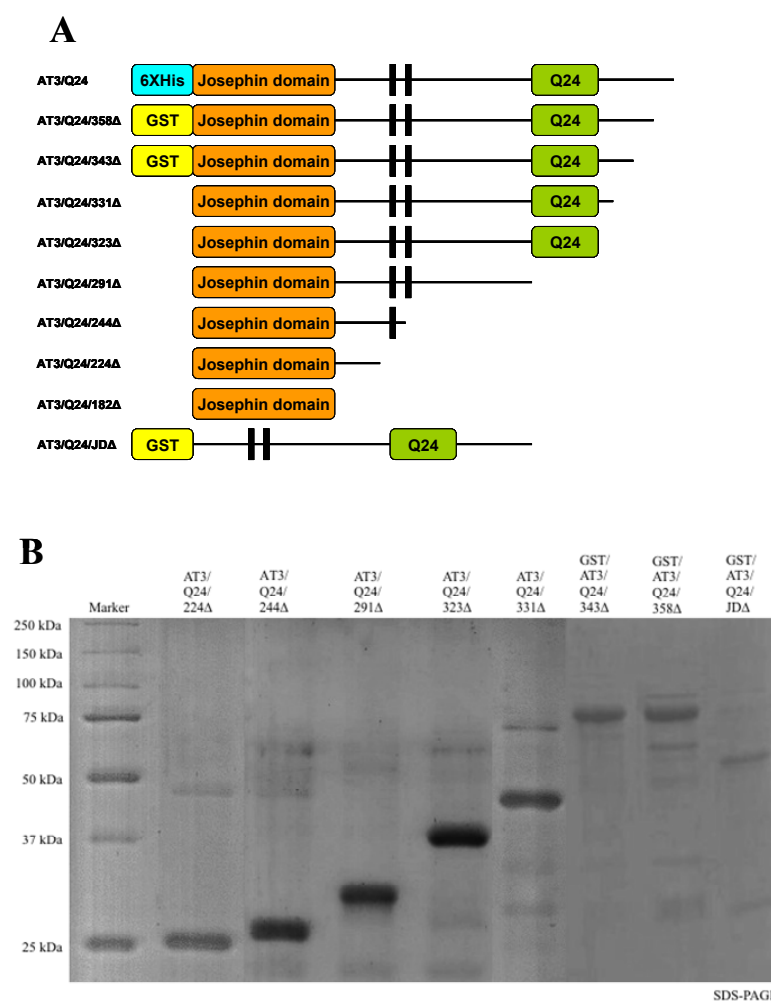

Figure 3.4 Panel A: schematic representation of AT3/Q24 and truncated forms. The vertical bars represent the UIMs. **Panel B: SDS-PAGE of AT3/Q24 and its mutants.** Lane 1: molecular weight markers Precision Plus Unstained (BIORAD). 4 μg of purified protein were loaded onto each lane (lanes 2-9).

In order to characterize the regions involved in the binding with tubulin α/β dimer we produced several truncated forms of human AT3/Q24 or murine AT3/Q6. We produced the N-terminal His-tagged wild-type protein and different truncated forms, in fusion with GST at the N-terminus (Figure 3.4 and 3.5). The mutants AT3/Q24/358Δ, AT3/Q24/343Δ and AT3/Q24/JDΔ (the sole C-terminal disordered domain, lacking the JD), were also purified in fusion with the GST tag in order to avoid aspecific degradation. Instead, the other truncated variants were eluted either by digestion with PreScission protease (GST), or by imidazole (His tag).
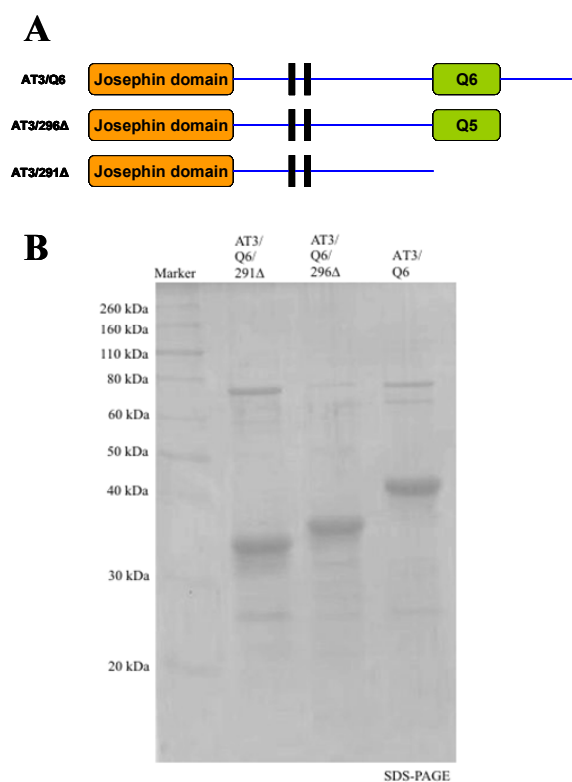
A

B

SDS-PAGE

Figure 3.5 Panel A: schematic representation of AT3/Q6 and truncated forms. The vertiacl bars represent the UIMs. **Panel B: SDS-PAGE of AT3/Q6 and its mutants.** Lane 1: molecular weight markers Precision Plus Unstained (BIORAD). 4 μg of protein purified on Gluthatione Sepharose resin were loaded onto each lane (lanes 2-4).
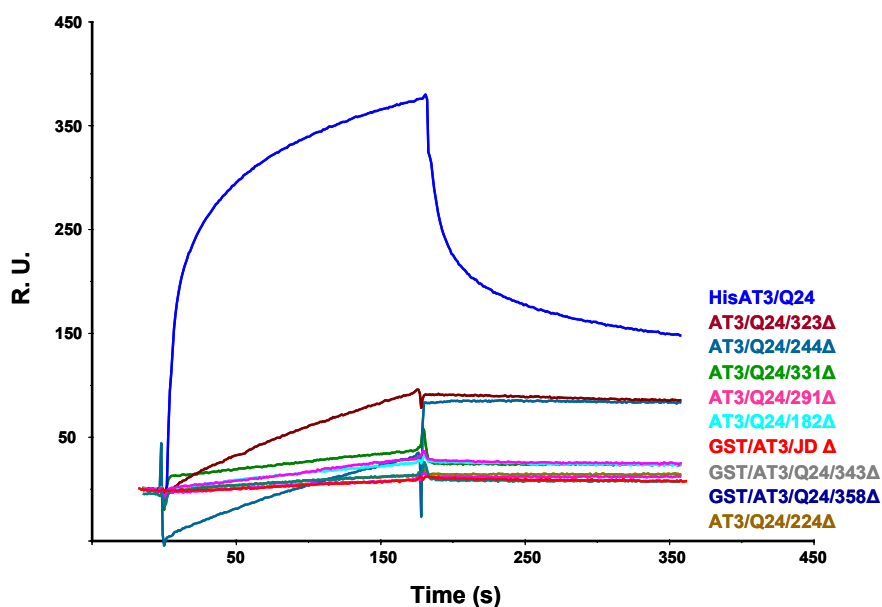
Figure 3. 6 Association/dissociation kinetics for the binding between tubulin and AT3/Q24 mutants. Tubulin was immobilized on the sensor chip and 5 μM of AT3/Q24 and each mutant were flowed onto the chip surface.

In order to characterize regions involved in the interaction AT3/tubulin, tubulin α/β dimers were coupled directly to a CM5 chip and used to evaluate by SPR the real-time association and dissociation of AT3/Q24 and AT3/Q6 truncated mutants. The binding and release of AT3 mutants to and from this chip was monitored. The kinetics of binding were reproducible in the different experiments. Figures 3.6 and 3.7 depict a typical sensorgram obtained using 5 μM protein. Only for AT3/Q24/323Δ, AT3/Q24/291Δ, AT3/Q6, AT3/Q6/296Δ and AT3/Q6/291Δ could we determine a K_D value using Langmuir 1:1 model fitting of simultaneous sensorgrams at different concentrations with BIA evaluation software (Table 3.3). GST protein was used as a a negative control (data not shown).
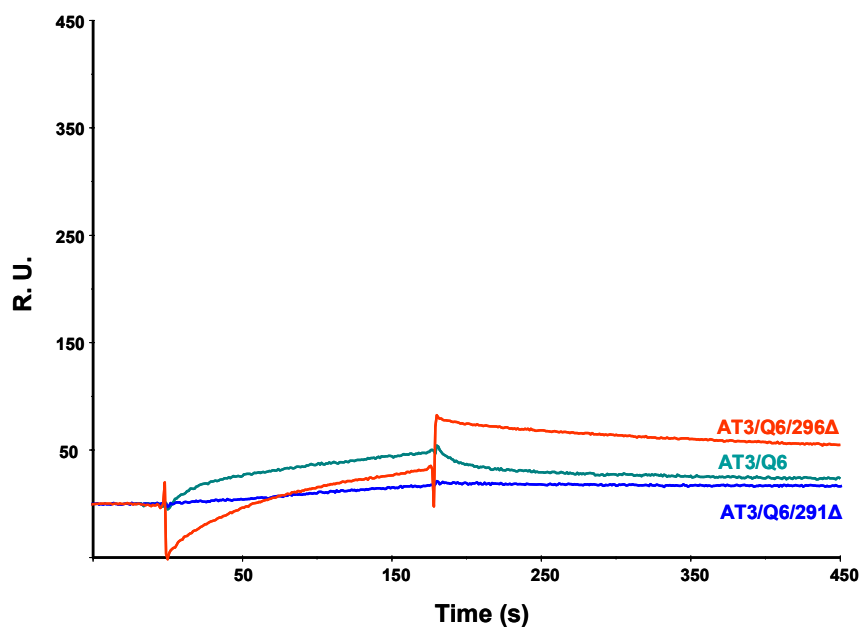
111

Figure 3. 7 Association/dissociation kinetics for the binding between tubulin and AT3/Q6. Tubulin was immobilized on the sensor chip and the 5 μM of AT3/Q6 and each mutant were flowed onto the chip surface.

These results suggest that in human AT3/Q24 three regions are involved in tubulin binding: one in the JD, (site 1), the second between residues 244 and 323 (site 2) and the third in a short stretch at the C-terminus (site 3). The JD seems to be necessary but not sufficient to fulfil this interaction. In fact, at least the binding site between residues 244 and 323 (site 2) is required for the association/dissociation kinetics to be quantifiable, whereas site 3 further increases the affinity. Moreover, in murine variants there are apparently only the binding sites 1 and 2 This hypothesis is substantiated by the low homology between human and mouse in the

C-terminal region and by the comparison of the K_D values of murine full-length and truncated AT3/Q6/296Δ forms.

Rather intriguing is the observation that mutants 331Δ, 343Δ and 358Δ did not display any detectable interaction with tubulin. This might be rationalized if one assumes that the stretches at the C-terminus of these truncated variants affect conformation and binding capacity of the site 2. On the other hand, the findings confirm that the short site 3 is located at the very end of the AT3 chain.

Table 3.3 Dissociation constant of different AT3 truncated variants determined by BIA evaluation software.

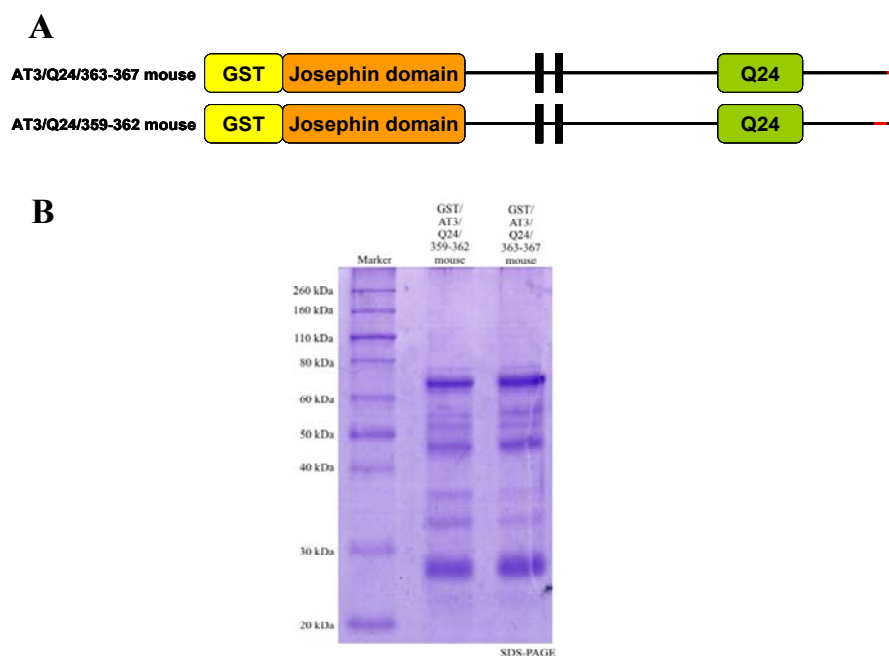|	K_D (M)
AT3/Q24/182Δ	b. d.[a]
AT3/Q24/224Δ	b. d.[a]
AT3/Q24/244Δ	b. d.[a]
AT3/Q24/291Δ	1.06×10^{-6}
AT3/Q24/323Δ	3.16×10^{-6}
AT3/Q24/331Δ	b. d.[a]
GST/AT3/Q24/343Δ	b. d.[a]
GST/AT3/Q24/358Δ	b. d.[a]
GST/AT3/Q24/JDΔ	b. d.[a]
AT3/Q6	6.37×10^{-6}
AT3/Q6/291Δ	4.19×10^{-6}
AT3/Q6/296Δ	1.09×10^{-7}

[a]: below detection

A

B

Figure 3.8 Panel A: schematic representation of AT3/Q24 substituted mutants. Panel B: SDS-PAGE of AT3/Q24/359-362 mouse and AT3/Q24/363-367 mouse. Lane 1: molecular weight markers Precision Plus Unstained (BIORAD). 4 µg of purified protein were loaded onto each lane (lanes 2, 3).

Furthermore, in order to assess the role of the stretch 358-368 downstream of the polyQ in human AT3, we produced by site-directed mutagenesis two chimeric human AT3/Q24 variants (figure 3.8), wherein the tracts 359-362 or 363-367 were replaced by the murine counterparts.

The real time association and dissociation of GST/AT3/Q24/359-362mouse and GST/AT3/Q24/363-367mouse was evaluated by SPR using a sensor chip CM5 coupled directly to tubulin α/β dimers. GST was used as a negative control (data not shown). Figure 3.9 shows a sensorgram obtained using 5 µM protein. Samples

tested do not exhibited a detectable association/dissociation kinetic, which prevented us from calculating the K_D. On the other hand, this result highlights the crucial role of the human 359-367 region in bringing about a strong interaction with tubulin.
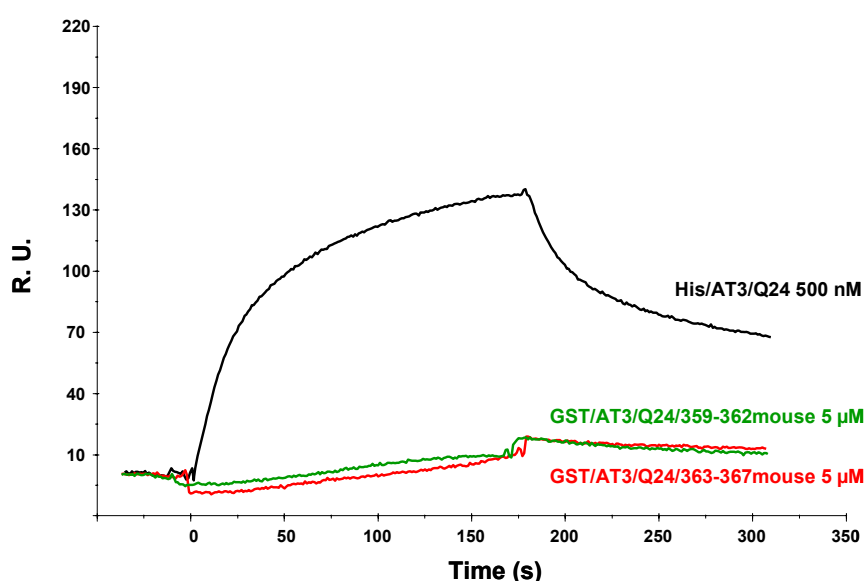
Figure 3.9 Association/dissociation kinetics for the binding between tubulin and AT3/Q24 truncated variants. Tubulin was immobilized on the sensor chip and 5 μM AT3/Q24/359-362mouse or AT3/Q24/363-367mouse were flowed onto the chip surface. 500 nM of AT3/Q24 were used as a positive control.

3.6 Tubulin and Lys^{48}-linked ubiquitin (but not Lys^{63}-linked) bind to AT3 in a mutually exclusive fashion

It has been shown that AT3 has the catalytic triad of Cys proteases and functions as a deubiquitinating enzyme, binding ubiquitin chains through its UIMs and cleaving them through the JD (Nicastro *et al.,* 2005). Ubiquitination is a dynamic post-translational

115

modification that serves diverse cellular roles: K^{48}-linked polyubiquitination acts as signal for proteasome degradation, whereas K^{63}-linked polyubiquitination has been recently demonstrated to act as a signal for endocytosis, autophagy, or aggresome formation (Pickart and Fushman, 2004; Chen, 2005; Lim *et al.*, 2005; Tan *et al.,* 2007). Recent work shows that both normal and expanded AT3 bind similarly to longer Lys^{48}- and Lys^{63}-linked ubiquitin chains, yet it preferentially cleaves Lys^{63}-linkages, especially in mixed linkage chains (Winborn *et al.,* 2008).

In order to elucidate the sorting mechanisms of misfolded proteins to aggresome or proteasome and the roles of the proteins involved, we performed by SPR a competition assay between AT3, tubulin and Lys^{48}- or $Lys^{63\text{-}}$polyubiquitin chain.

Tubulin α/β dimer coupled directly to sensor chip CM5 was used to evaluate the real-time association and dissociation of AT3/Q24 preincubated with either $4Ub^{K48}$ or $polyUb^{K63}$. The binding and release of AT3/Q24 to and from this chip was monitored. The kinetics of binding were reproducible in different experiments. Figure 3.10 depicts a sensorgram obtained by using a mixture of 500 nM AT3/Q24 and 5 μM $4Ub^{K48}$, or of 500 nM AT3/Q24 and 5 μM $polyUb^{K63}$. 500 nM AT3/Q24 was used as a positive control. Although these results do not allow a reliable assessment of the affinities, however they show that AT3 binds Lys^{63}-polyubiquitin without any displacement by tubulin, whereas Lys^{48}-polyubiquitin and tubulin binding are mutually exclusive. These data suggest therefore an

involvement of AT3 in sorting polyubiquitinated substrates to either aggresome or proteasome.
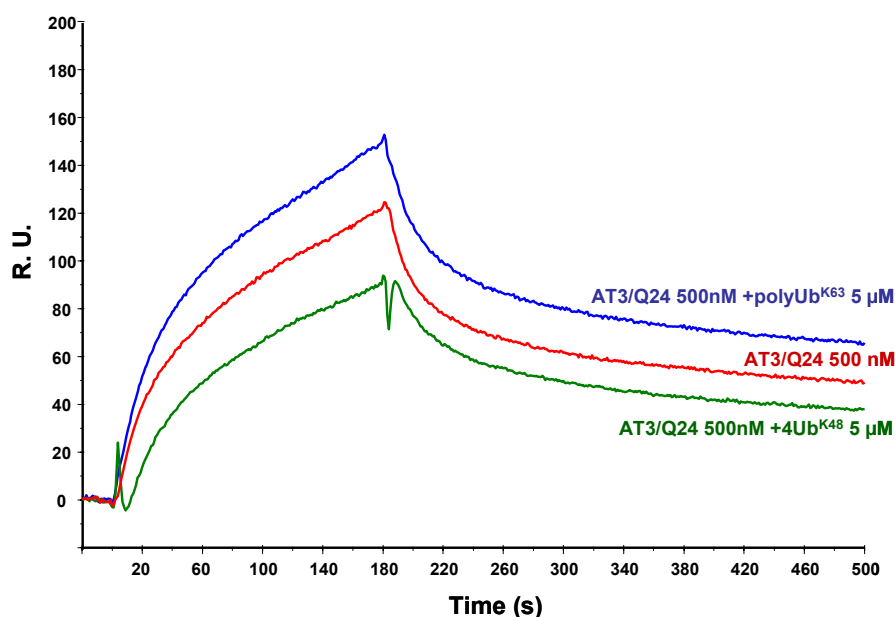
Figure 3.10 Competition assay between tubulin, ataxin-3 and 4Ub^{K48} or polyUb^{K63}. Tubulin was immobilized on the sensor chip and 500 nM of AT3/Q24 were incubated with 4Ub^{K48} or polyUb^{K63} and then were flowed onto the chip surface. 500 nM of AT3/Q24 were used as positive control.

3.7 SPR provides evidence of tight AT3/Q24-polyUb^{K63} interaction

SPR was used to describe the real time association and dissociation of polyUb^{K63} to AT3/Q24 that was coupled directly to the sensor chip. The binding and release of polyUb^{K63} to and from this chip was monitored. The kinetics of binding were reproducible in the different experiments. Figure 3.11 depicts a typical sensorgram obtained by using five concentrations in the range from 1 to 20 µM.

Simultaneous fitting of sensorgrams with BIA evaluation software allowed the estimation by Langmuir 1:1 binding model of the association and dissociation rate constants, k_{on} and k_{off} for the binding to AT3/Q24, which were $2.38 \times 10^3 \, M^{-1} \, s^{-1}$ and $5.23 \times 10^{-4} \, s^{-1}$, respectively, yielding a calculated K_D of 2.19×10^{-7} M. However the best fitting was obtained using a heterogenous ligand binding model that yielded different affinity values for each component of polyUb^{K63}. This may be due to the heterogeneity of the polyUb sample that actually contains a mixture of polyUb spanning from two to seven residues, and/or to different binding sites on the AT3 molecule. This latter assumption is substantiated by recent reports showing that AT3 can bind ubiquitin through both UIMs and the JD (Nicastro *et al.*, 2009).
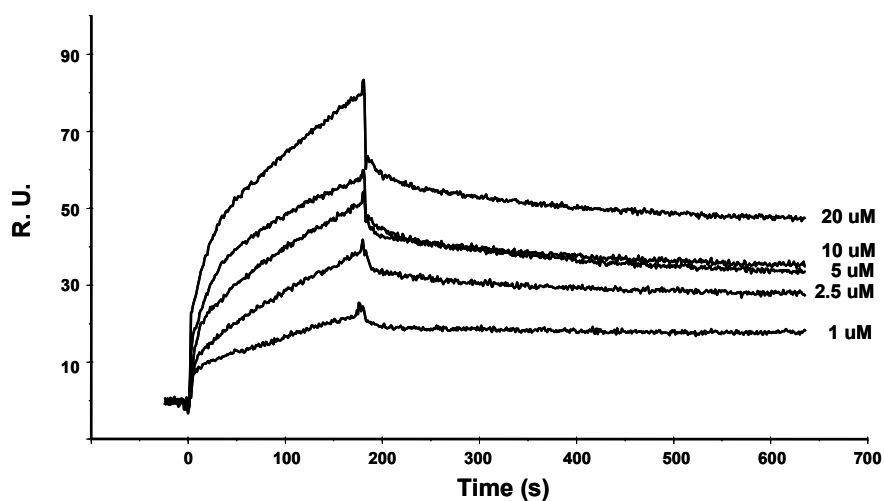

Figure 3.11 Association/dissociation kinetics for the binding between AT3/Q24 and polyUb^{K63}. AT3/Q24 was immobilized on the sensor chip and the indicated concentrations of polyUb^{K63} were flowed onto the chip surface.

3.8 SPR provides evidence of thight interaction of HDAC6 with tubulin and AT3

Previous work suggests that HDAC6, along with AT3, colocalizes with preaggresome particles and microtubules (Burnett and Pittman, 2005). This suggests an involvement of also HDAC6 in transporting aggregated protein to aggresomes. This prompted us to investigate the interaction of HDAC6 with both AT3 and tubulin. We used SPR first to describe the real time association and dissociation of HDAC6 to AT3/Q24 that was coupled directly to the sensor chip. The binding and release of HDAC6 to and from this chip was monitored. The kinetics of binding were reproducible in different experiments. Figure 3.12 depicts a typical sensorgram obtained by using four concentrations in the range from 50 to 1000 nM. Simultaneous fitting of sensorgrams with BIA evaluation software allowed the estimation by Langmuir 1:1 binding model of the association and dissociation rate constants, k_{on} and k_{off} for the binding to AT3/Q24, which were $2.9 \times 10^4 \, \mathrm{M}^{-1} \, \mathrm{s}^{-1}$ and $1.32 \times 10^{-3} \, \mathrm{s}^{-1}$, respectively, yielding a calculated K_D of $4.47 \times 10^{-8} \, \mathrm{M}$, in good agreement with previous reports (Burnett and Pittman, 2005). The plot of K_{obs} for each given AT3 concentration vs. conc. was linear ($R^2 = 1$), typical for a 1:1 model (data not shown). Based on the slope of the Scatchard plot, obtained using the R_{eq} for each given AT3 concentration, we calculated a K_D of $4.46 \times 10^{-8} \, \mathrm{M}$. The similarity of
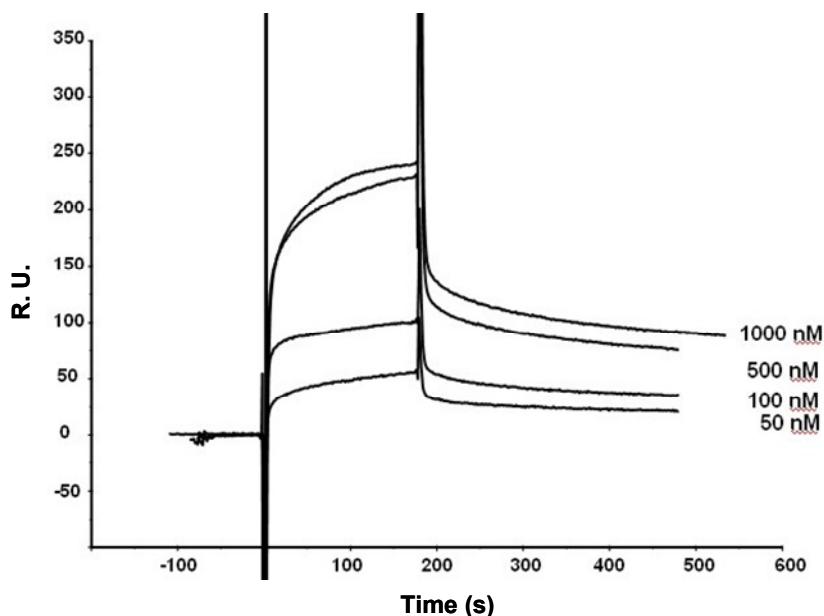
Figure 3.12 Association/dissociation kinetics for the binding between AT3/Q24 and HDAC6. AT3/Q24 was immobilized on the sensor chip and the indicated concentrations of HDAC6 were flowed onto the chip surface.

the K_D values, obtained from the two different methods (Schuck and Minton, 1996) support the consistency of the obtained kinetic and thermodynamic parameters.

We subsequently quantified by SPR the affinity between tubulin and HDAC6 . Tubulin α/β dimer was coupled directly to the sensor chip and the binding and release of HDAC6 to and from this chip was monitored in order to evaluate association and dissociation kinetics. The kinetics of binding were reproducible in the different experiments. Figure 3.13 depicts a typical sensorgram obtained by using four concentrations in the range from 25 to 200 nM. Simultaneous fitting of sensorgrams with BIA evaluation software allowed the estimation by Langmuir 1:1 binding model of a calculated

120

K_D of 2.36×10^{-8} M. The plot of K_{obs} for each given HDAC6 concentration vs. conc. was linear ($R^2 = 1$), typical for a 1:1 model (data not shown).
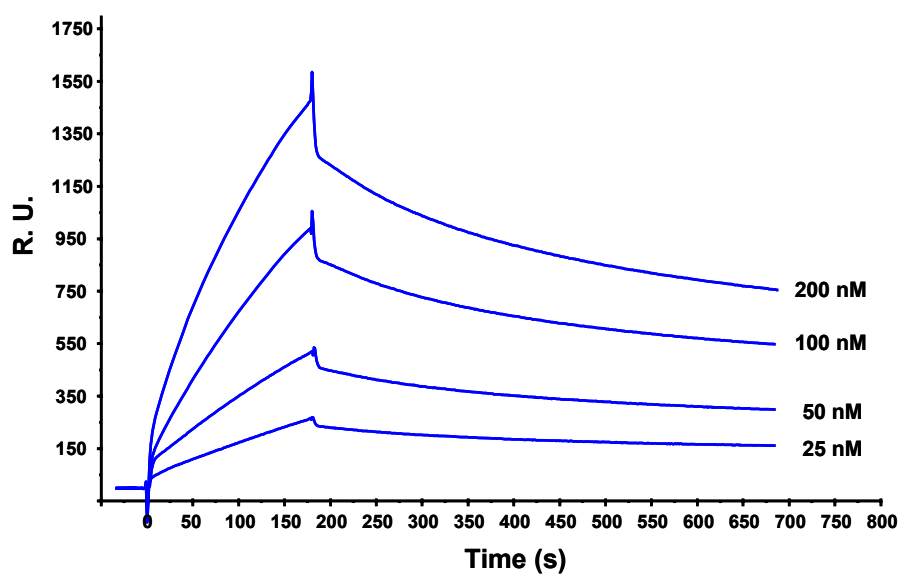

Figure 3. 13 Association/dissociation kinetics for the binding between tubulin and HDAC6.
Tubulin α/β dimer was immobilized on the sensor chip and the indicated concentrations of HDAC6 were flowed onto the chip surface.

4 Discussion

This work was undertaken to provide further insight into AT3's physiological roles. Previous reports showed that this is a multifunctional molecule, as it acts as both a ubiquitin-hydrolase/ubiquitin-binding protein (Donaldson *et al.*, 2003; Mao *et al.*, 2005), and a transcriptional repressor (Li *et al.*, 2002; Goswami *et al.*, 2006). Also, several recent works show that AT3 carries out its normal function on protein surveillance pathways. AT3 interacts with RAD23, which shuttles ubiquitinated protein to proteasomes, and with VCP that seems to be involved in the degradation pathway ubiquitin-proteasome dependent and in the retrotranslation of ERAD substrates (Doss-Pepe *et al.*,2003; Boeddrich *et al.*, 2006; Zhong and Pittman, 2006).

This prompted us to search for possible additional interactors from cytoplasmic extracts. To this end, we took advantage of MudPIT, a mass spectrometry-based proteomic approach (Gygi *et al.*, 1999; Wolters and Washburn, 2001) that made it possible to identify rat brain cytoplasmic proteins interacting with different AT3 variants in pull-down experiments. Thus, we found that α- and β-tubulins bound to all of the constructs assayed, whose size ranges from the JD in isolation to the full-length AT3. Also worth mentioning is that MudPIT experiments lead to the identification of some molecular partners related to, or involved in functions assigned to AT3. In particular, we identified MAP2 among the interacting proteins, which

is associated with the microtubules, and VCP, which is involved in the proteasome-mediated protein degradation, and whose interaction with AT3 was already reported in previous studies (Doss-Pepe *et al.*, 2003). Interestingly, we found that VCP binds to AT3/291Δ or longer constructs, but not to the JD. This implies that the disordered C-terminal domain is required for the interaction, a finding well in agreement with a previous report (Boeddrich *et al.*, 2006). We could not find any obvious explanation to justify the failure to identify ubiquitin among the interacting proteins. However, it should be pointed out that on the one hand AT3 affinity towards tubulin is about tenfold higher than that towards ubiquitin, as shown comparing our data with those of a previous work (Chai *et al.*, 2004); on the other hand, these authors preincubated the cells with proteasome inhibitors to detect AT3/ubiquitin interaction, which suggests that under normal conditions the amount of bound ubiquitin is scanty.

The hypothesis of a direct interaction of AT3 with tubulin suggested by these results was confirmed by both coimmunoprecipitation from brain extracts, and colocalization of AT3/Q6 with microtubules, achieved by overexpression of the protein in COS-7 cultured cells, and subsequent immunofluorescence analysis. COS-7 cells are a widely used cellular model, in which physiological sorting of overexpressed proteins can be reliably reproduced. We have previously used COS-7 cells in subcellular localization studies of different forms of AT3 (Pozzi *et al.*, 2008), and data obtained were well in accordance with those obtained in SHSY-

5Y human neuronal cells (data not shown). Despite the high affinity towards tubulin, colocalization of AT3/Q6 with microtubules was only partial. Plausibly, this may be accounted for by the diverse physiological roles of AT3, which require different interactors. In particular, it is expected that a significant fraction of the protein be generally associated with the proteasome (Doss-Pepe *et al.*, 2003). In turn, microtubules interact with a wealth of proteins that regulate their functions (Valiron *et al.*, 2001). When aggregated, AT3/Q72 did not colocalize at all and was probably associated with mitochondria, as suggested by a previous report (Pozzi *et al.*, 2008). Possibly, aggregation itself prevents the expanded AT3 from interacting with microtubules, which also might play a role in the Machado–Joseph disease.

Besides the aforementioned results, further and strong experimental support to the idea that the interaction detected does play a physiological role was provided by the high-affinity binding between AT3 and tubulin dimer, as substantiated by a dissociation constant of about 50–70 nM, which we determined by surface plasmon resonance. Actually, according to the PINT (Protein–Protein Interactions Thermodynamic) database (Kumar and Gromiha, 2007) such a figure is close to, and somewhat above the most populated range, i.e., 10^{-6} to 10^{-7} M. These results clearly point to a direct interaction between the two molecules rather than one mediated by other molecular partners.

124

Of course, our results raise the issue of what physiological role the interaction here detected plays. Previous work showed that AT3 is involved in aggresome-mediated protein degradation (Burnett and Pittman, 2005). Aggresomes are perinuclear proteinaceous aggregates, close to the microtubule-organizing center (MTOC), to which misfolded protein is sorted via microtubules under conditions where proteasomes are overloaded or their function compromised (García-Mata et al., 1999). Misfolded protein accumulated in aggresomes then undergoes lysosomal degradation (García-Mata et al., 2002). AT3 also works as a deubiquitinating enzyme via its cysteine protease catalytic triad located in the JD domain, and binds ubiquitin chains through its UIMs in the disordered tract (Nicastro, G. *et al.,* 2005). Moreover, recent work by Winborn and coworkers shows that AT3 binds to Lys^{48}- and Lys^{63}-linked ubiquitin chains, yet preferentially cleaves Lys^{63}-linkages especially in mixed linkage chains (Winborn, B. J. *et al.,* 2008).

Our data, when viewed from the standpoint of the aforementioned achievements, strongly support the hypotesis that AT3 participates in misfolded protein transport to aggresomes via microtubules. On the other hand, they also raise the issue of whether and how Lys^{48}- and Lys^{63}-linked ubiquitin chains are involved in this phenomenon. To address this issue we first assessed by SPR the binding affinity of either ubiquitin chains with AT3, which showed that it bound to both of them with close to nanomolar affinity. Not surprisingly, Lys^{63}-linked ubiquitin showed however a heterogenous

ligand binding pattern that yielded different affinity values. This may be well accounted for by the heterogeneity of the polyUb sample that actually contains a mixture of polyUb spanning from two to seven residues, and/or by the multiple binding sites on the AT3 molecule, as supported by recent reports showing that AT3 can bind ubiquitin through both UIMs and the JD (Nicastro, G. *et al.*, 2009).

More importantly, we also found that Lys^{48}-polyubiquitin and tubulin binding to AT3 are mutually exclusive, whereas Lys^{63}-polyubiquitin binds to AT3 without any detectable displacement by tubulin. These findings suggest a model whereby AT3 sorts polyubiquitinated substrate protein to either proteasome or aggresome, depending on either Lys^{48}- or Lys^{63}-polyubiquitin tagging, respectively (Pickart and Fushman, 2004; Lim *et al.*, 2005; Tan *et al.*, 2007). According to the model, Lys^{48}-polyubiquitin binding to AT3 would prevent the latter from being sorted to aggresomes along with its cargo protein. In contrast, this seems to be the fate of AT3 when bound to Lys^{63}-tagged protein.

With regard the model above depicted, also noteworthy is the capability of AT3 of binding HDAC6 with high affinity, as shown by our SPR experiments. In keeping with our results, previous work reports that HDAC6 is indispensable for aggresome formation, as it binds polyubiquitinated protein and interacts with the dynein complex, which transports misfolded protein cargo to aggresomes via microtubules (Kawaguchi et al., 2003). Burnett and Pittman (2005) also show that AT3, along with HDAC6, colocalizes with both

aggresomes and preaggresome particles. On the whole, these results point to a cargo protein transport mechanism to aggresome that envisages the formation of a ternary complex consisting of AT3, HDAC6 and Lys[63]-tagged protein. This complex would migrate along microtubules by a dynein-driven mechanism whose details, however, have still to be elucidated.

We also investigated the mode of AT3/tubulin binding by producing several truncated human and murine AT3 variants and determining their affinity towards tubulin. In this way, in the human form we identified three tubulin-binding sites: in the Josephin domain (site 1), in the disordered stretch (site 2), and at the C-terminus at the very end of the polypeptide chain (site 3). However, the latter was apparently absent in the murine variant.

Based on our results, the role of the polyQ tract in tubulin binding is still unclear. In the case of human AT3, the variants truncated immediately upstream and downstream of the 24-residues long polyQ (AT3/Q24/291Δ and AT3/Q24/323Δ, respectively) displayed comparable affinity, suggesting that the polyQ does not play a significant role in the interaction. In contrast, when comparing two variants of murine AT3, truncated immediately upstream and downstream of the 5/6 residues long polyQ (AT3/Q6/291Δ and AT3/Q6/296Δ, respectively) we found that the latter bound to tubulin with a 40-fold higher affinity. Even more surprisingly, full-length murine AT3 displayed an affinity comparable to that of AT3/Q6/291Δ, hence much lower than that of AT3/Q6/296Δ. A

possible interpretation of these conflicting results is that the first 5-6 glutamine residues in the polyQ do actually play a role in tubulin binding, but that the tract downstream might interfere with the interaction of site 2 with tubulin. This might also explain why human truncated forms longer than AT3/Q24/291Δ have lower affinities than the latter, mostly below detection limit. However, full-length human AT3 also has site 3 that should lock the entire C-terminal disorderd domain on tubulin surface, thus preventing misfolding of the disordered tract with resulting interference of the disordered tract downstream of the first glutamines of the polyQ, which in turn would interfere with its binding capacity. So the occurrence of site 3 might also explain why human AT3 can afford a polyQ tract much longer than in the murine counterpart without impairing affinity towards tubulin.

Finally, to better assess the role of the site 3, i.e. the ten last residues (358-368) at the C-terminus of human AT3/Q24, we replaced the tracts 359-362 or 363-367 by the murine counterparts. These mutants did not exhibit detectable association/dissociation kinetics, which confirms the crucial role of site 3 in preserving a strong interaction with tubulin.

In our future research we intend to develop further mutants to better clarify the mode of interaction between AT3 and tubulin. In particular, the characterization of a truncated human AT3 containing only 5-6 glutamines should help understand whether such a short stretch can ensure tight binding, irrespective of the tract downstream as in the

murine form. Furthermore, small-angle x-ray scattering experiments are in progress to provide insight into the structure of the complex and the binding surfaces of the two proteins.

5 References

Albrecht, M., Golatta, M., Wullner, U., Lengauer, T. (2004) Structural and functional analysis of ataxin-2 and ataxin-3. *Eur. J. Biochem.* 271: 3155–3170.

Albrecht, M., Hoffmann, D., Evert, B.O., Schmitt, I., Wullner, U., and Lengauer, T. (2003) Structural modeling of AT-3 reveals distant homology to adaptins. *Proteins* 50: 355-370.

Altschuler, E.L., Hud, N.V., Marimas, J.A., Rupp, B. (1997) Random coil conformation for extended polyglutamine stretches in acqueous soluble monomeric peptides. *J. Pept. Res.* 50: 73-75.

Antony, P. M. A., Mantele, S., Mollenkopf, P., Boy, J., Kehlenbach, R. H., Riess, O., Schmidt, T. (2009) Identification and functional dissection of localization signals within ataxin-3. *Neurobiol. Dis.* 36: (2) 280-292.

Bates, G.P., Mangiarini, L., Wanker, E.E., Davies, S.W. (1998) Polyglutamine expansion and Huntington's diseasez. 26: 471-475.

Berke, S.J., Chai, Y., Marrs, G.L., Wen, H., and Paulson, H.L. (2005) Defining the role of ubiquitin interacting motifs in the polyglutamine disease protein, ataxin-3. *J. Biol. Chem.* 280: 32026-32034.

Bevivino, A.E., Loll, P.J. (2001) An expanded glutamine repeat destabilizes native ataxin-3 structure and mediates formation of parallel beta–fibrils. *Proc. Natl. Acad. Sci. USA* 98: 11955-11960.

Boeddrich, A., Gaumer, S., Haake, A., Tzwetkov, N., Albrecht, M., Evert, B.O., Müller, E.C., Lurz, R., Breuer, P., Schugardt, N., Plaßmann, S., Xu, K., Warrik, J.M., Suopanki, J., Wüllner, U., Frank, R., Hartl, U.F., Bonini, N.M. and Wanker, E.W. (2006) An arginine/lysine-rich motif is crucial for VCP/p97- mediated modulation of ataxin-3 fibrillogenesis. *EMBO J.* 25: 1547-1558.

Bradford, M. (1976) *Anal. Biochem.* 72: 248-253.

Burnett, B., Li, F., Pittman, R.N., (2003) The polyglutamine neurodegenerative protein ataxin-3 binds polyubiquitylated proteins and has ubiquitin protease activity. *Hum. Mol. Genet.* 12: 3195-205.

Burnett, B., Li, F., Pittman, R. N., (2005) The polyglutamine neurodegenerative protein Ataxin-3 regulates aggresome formation *Proc. Natl. Acad. Sci. U S A.* 12: 4330-4335.

Calabresi, V., Guida, S., Servadio, A., Jodice, C. (2001) Phenotypic effects of expanded ataxin-1 polyglutamines with interruptions in vitro. *Brain Res. Bull.* 56(3-4): 337-342.

Chai, Y., Wu, L., Griffin, J.D., Paulson, H.L. (2001) The role of protein composition in specifying nuclear inclusion formation in polyglutamine disease. *J. Biol. Chem.* 276: 44889-44897.

Chai, Y., Berke, S. S., , Cohen, R. E.,Paulson, H. L. (2004) Poly-ubiquitin binding by the polyglutamine disease protein ataxin-3 links its normal function to protein surveillance pathways *J. Biol. Chem.* 279: 3605-3611.

Chan, H.Y., Warrick, J.M., Gray-Board, G.L., Paulson, H.L., Bonini, N.M. (2000) Mechanisms of chaperone suppression of

polyglutamine disease: selectivity, synergy and modulation of protein solubility in Drosophila *Hum. Mol. Genet.* 9: 2811-2820.

Chen, Z. J. (2005) Ubiquitin signalling in the NFkB-pathway. *Nat. Cell. Biol.* 7: 758-765.

Chou, A.-H., Yeh, T.-H., Ouyang, P., Chen, Y.-L.,Chen, S.-Y., and Wang, H.-L., (2008) Polyglutamine-expanded ataxin-3 causes cerebellar dysfunction of SCA3 transgenic mice by inducing transcriptional dysregulation. *Neurobiol. Dis.* 31(1): 89-101.

Costa M. C., Silva J. G., Miranda C. J., Sequeiros J., S antos, M.M., Maciel P. (2004) Genomic structure, promoter activity, and developmental expression of the mouse homologue of the Machado–Joseph disease (MJD) gene. *Genomics* 84 361–373.

Courey, A.J., Tjian, R. (1988) Analysis of SP1 in vivo reveals multiple transcriptional domains, including a novel glutamine-rich activation motif. *Cell* 5: 887-898.

Cummings, C.J. and Zoghbi, H.Y. (2000) Trinucleotide repeats: mechanisms and pathophysiology. *Annu. Rev. Genomics Hum. Genet.* 1, 281-328.

Cummings, C.J. and Zoghbi, H.Y. (2000) Fourteen and counting: unraveling trinucleotide repeats. *Annu. Rev. Genomics Hum. Genet.* 9(6), 909-916.

Donaldson, K.M., Li, W., Ching, K.A., Batalov, S., Tsai, C.C., & Joazeiro, C.A. (2003) Ubiquitin-mediated sequestration of normal cellular proteins into polyglutamine aggregates. *Proc Natl Acad Sci USA* 100, 8892-8897.

Doss-Pepe, E. W., Stenroos, E. S., Johnson, W. G., Madura, K., (2003) Ataxin-3 interactions with rad23 and valosin-containing protein and its associations with ubiquitin chains and the proteasome are consistent with a role in ubiquitin-mediated proteolysis. *Mol. Cell. Biol.* 23: 6469-83.

Durr, A., Stevanin, G., Cancel, G., Duyckaerts, C., Abbas, N., Didierjean, O., Chneiweiss, H., Benomar, A., Lyon-Caen, O., Julien, J., Serdaru, M., Penet, C., Agid, Y., Brice, A. (1996) Spinocerebellar Ataxia 3 and Machado-Joseph disease: clinical, molecular and neuropathological features. *Ann. Neurol.* 39: 490-499.

Ellisdon, A. E., Pearce, M. C., Bottomley, S., P. (2007) Mechanisms of Ataxin-3 misfolding and fibril formation: kinetic analysis of a disease-associated polyglutamine protein. *J. Mol. Biol.* 368: 595-605.

Ellisdon, A. E., Thomas, B., Bottomley, S., P. (2006) The two-stage pathway of Ataxin-3 fibrillogenesis involves a polyglutamine-indipendent step. *J. Biol. Chem.* 281: 16888-16896.

Evert, B.O., Wullner, U., Klockgether, T. (2000) Cell death in polyglutamine diseases. *Cell Tissue Res.* 301: 189-204.

Evert, B.O., Araujo, J., Vieira-Saecker, A.M., de Vos, R.A., Harendza, S., Klockgether, T., Wullner, U. (2006) Ataxin-3 represses transcription via chromatin binding, interaction with histone deacetylase, and histone deacetylation. *J Neurosci.* 44: 11474-11486.

Fujigasaki, H., Uchihara, T., Koyano, S., Iwabuchi, K., Yagishita, S., Makifuchi, T., Nakamura, A., Ishida, K., Toru, S., Hirai,

S., Ishikawa, K., Tanabe, T., Mizusawa, H. (2000) Ataxin-3 is translocated into the nucleus for the formation of intranuclear inclusions in normal and Machado-Joseph disease brains. *Exp. Neurol.* 165: 248- 256.

Fujigasaki, H., Uchihara, T., Takahashi, J., Matsushita, H., Nakamura, A., Koyano, S., Iwabuchi, K., Hirai, S., and Mizusawa, H. (2001) Preferential recruitment of ataxin-3 independent of expanded polyglutamine: an immunohistochemical study on Marinesco bodies. *J. Neurol. Neurosurg. Psychiatry* 71: 518-520.

Garcìa-Mata, R., Bebök, Z., Sorscher, E.J., and Sztul, E.S. (1999) Characterization and dynamics of aggresome formation by a cytosolic GFP-Chimera. *J. Cell. Biol.* 146: 1239-1254.

Gaspar, C. , Lopes-Cendes, I., Hayes, S., Goto, J., Arvidsson, K., Dias, A., Silveira, I., Maciel, P., Coutinho, P., Lim, M., Zhou, Y. X., ,Soong, B. W., ,Watanabe, M., Giunti, P., Stevanin, G., Riess, O., Sasaki, H., Hsieh, M., Nicholson, G. A., Brunt, E., Higgins, J. J., Lauritzen, M., Tranebjaerg, L., Volpini, V., Wood, N., Ranum, L., Tsuj, S., Brice, A., Sequeiros, J., Rouleau, G. A., (2001) Ancestral Origins of the Machado-Joseph Disease Mutation: A Worldwide Haplotype Study. *Am. J. Hum. Genet.* 68: 523–528.

Gygi, S. P., Rist, B., Gerber, S. A., Turecek, F., Gelb, M. H., Aebersold R.(1999) Quantitative analysis of complex protein mixtures using isotope-coded affinity tags. *Nat. Biotechnol.* 17: 994–9.

Greenland, K. J., Zajac, J. D. (2004) Kennedy's disease: pathogenic and clinical approaches. *Int. Med. J.* 34(5): 279-286.

Goswami, A., Dikshit, P., Mishra, A., Nukina, N., and Jana, N.R. (2006) Expression of expanded polyglutamine proteins suppresses the activation of transcription factor NFkB. *J. Biol. Chem.* 281: 37017- 37024.

Gusella, J.F., MacDonald, M.E.. (2000) Molecular genetics: unmasking polyglutamine triggers in neurodegenerative disease. *Nat. Rev. Neurosci.* 1: 109- 115.

Haacke, A., Hartl, F. U., Breuer, P. (2007) Calpain inhibition is sufficient to suppress aggregation of polyglutamine-expanded Ataxin-3. *J. Biol. Chem.* 282: 18851-18856.

Harries, P. A., Palanichelvam, K., Schoelz, J. E., Nelson, R. S. (2009) The cauliflower mosaic virus protein p6 forms motile inclusions that traffic along actin microfilaments and stabilize microtubules. *Plant Physiol.* 149: 1005-1016.

Hashida, H., Goto, J., Suzuki, T., Jeong, S., Masuda, N., Ooie, T., Tachiiri, Y., Tsuchiya, H., and Kanazawa, I., (2001) Single cell analysis of CAG repeat in brains of dentatorubral-pallidoluysian atrophy (DRPLA). *J. Neurol. Sci.* 190(1-2): 87-93.

Hickey M.A., Chesselet M.F. (2003) The use of transgenic and knock-in mice to study Huntington's disease. *Cytogenet. Genome Res*. 100, 276-286.

Higashiyama, H., Hirose, F., Yamaguchi, M., Inoue, Y.H., Fujikake, N., Matsukage, A. and Kakizuka, A. (2002) Identification of ter94, *Drosophila* VCP, as a modulator of polyglutamine-induced neurodegeneration. *Cell Death Differ.* 9: 264-273.

Hofmann, K. & Falquet, L. (2001) A ubiquitin interacting motif conserved in components of the proteasomal and lysosomal protein degradation systems. *Trends Biochem Sci* 26, 347-350.

Ikeda, H., Yamaguchi, M., Sugai, S., Aze, Y., Narumiya, S., Kakizuka, A. (1996) Expanded polyglutamine in the Machado-Joseph disease protein induces cell death in vitro and in vivo. *Nat. Genet.* 13: 196-201.

Jardim, L. B., Pereira, M. L., Silveira, I., Ferro, A., Sequeiros, J. R.(2001) Neurologic findings in Machado-Joseph disease: relation with disease duration, subtypes, and (CAG)n. *Arch Neurol.* 58(6): 899-904.

Johnsson, B.; Lofas, S.; Lindquist, G. Immobilization of proteins to a carboxymethyldextran-modified gold surface for biospecific interaction analysis in surface plasmon resonance sensors. *Anal. Biochem.* 1991, *198*,:268-277.

Johnston, J.A.,Ward, C.L., and Kopito, R.R. (1998) Aggresomes: A cellular response to misfolded proteins. *J. Cell. Biol.* 143: 1883-1898.

Kadonaga, J.T., Carner, K.R., Masiarz, F.R, Tjian, R. (1987) Isolation of cDNA encoding transcription factor SP1 and functional analysis of the DNA binding domain. *Cell* 6: 1079-1090.

Kawaguchi, Y., Okamoto, T., Taniwaki, M., Aizawa, M., Inoue, M., Katayama, S., Kawakami, H., Nakamura, S., Nishimura, M., Akiguchi, I. et al. (1994) CAG expansions in a novel gene for

Machado-Joseph disease at chromosome 14q32.1. *Nat. Genet.* 8: 221-228.

King, J., and Laemli, U.K., (1971) Polypeptides of a tail fibres of bacteriophage T4. *J. Mol. Biol.* 62: 465-477.

Klement, I.A., Skinner, P.J., Kaytor, M.D., Yi, H., Hersch, S.M., Clark, H.B., Zoghbi, H.Y., Orr, H.T. (1998) Ataxin-1 nuclear localization and aggregation: role in polyglutamine-induced disease in SCA1 transgenic mice. *Cell* 95: 41-53.

Kondo, H., Rabouille, C., Newman, R., Levine, T.P., Pappin, D., Freemont, P. and Warren, G. (1997) p47 is a cofactor for p97 mediated membrane fusion. *Nature* 388: 75-78.

Kumar, M. D. S., Gromiha, M. M.(2007) PINT: protein–protein interactions thermodynamicdatabase. *Nucleic Acids Res.* 34: D195–8.

Kunkel, T.A. (1993) Nucleotide repeats. Slippery DNA and diseases. *Nature* 365: 207-208.

Kushner, S.R., (1978) in Genetic. Engineering: Proceedings of the International Symposium on Genetic Engineering, Milan (Boyer, H.W. & Nicosia, S. eds.) p.17, Elsevier, Amsterdam.

Li, F., Macfarlan, T., Pittman, R.N., Chakravarti, D. (2002) Ataxin-3 is a histone-binding protein with two independent transcriptional corepressor activities. *J. Biol. Chem.*.277: 45004-45012.

Lim, K. L., Dawson, V. L., Dawson, T. M. (2005) Parkin-mediated lysine 63-linked polyubiquitination: a link to protein

inclusions formation in Parkinson's and other conformational diseases?. *Neurobiol. Aging* 27: 524-529.

Liu, Y., Gotte, G., Libonati, M., Eisenberg, D. (2001) A domain-swapped RNase A dimer with implications for amyloid formation. *Nat. Struct. Biol*. 8: 211-214.

Madura, K. (2002) The ubiquitin-associated (UBA) domain: on the path from prudence to prurience. *Cell Cycle* 1, 235-244.

Malmqvist, M. BIACORE: an affinity biosensor system for characterization of biomolecular interactions. *Biochem. Soc. Trans.* 1999, 27, 335-340.

Mandel, J.L. (1997) Human genetics. Breaking the rule of three. *Nature* 386: 767-769.

Mao, Y., Senic-Matuglia, F., Di Fiore, P.P., Polo, S., Hodsdon, M.E., and De Camilli, P. (2005) Deubiquitinating function of ataxin-3: insights from the solution structure of the Josephin domain. *Proc. Natl. Acad. Sci. U S A*. 102: 12700-12705.

Marchal, S., Shehi, E., Harricane, M.C., Fusi, P., Heitz, F., Tortora P., and Lange, R. (2003) Structural instability and fibrillar aggregation of non-expanded human ataxin-3 revealed under high pressure and temperature. *J. Biol. Chem.* 278: 31554-31563.

Masino, L., Pastore, A. (2001) A structural approach to trinucleotide expansion deseases. *Brain Res. Bull.* 56: 183-189.

Masino, L., Musi, V., Menon, R.P., Fusi, P., Kelly, G., Frenkiel, T.A., Trottier, Y., Pastore, A. (2003) Domain architecture of

the polyglutamine protein ataxin-3: a globular domain followed by a flexible tail. *FEBS Lett.* 549: 21-25.

Matteoni, R., and Kreis, T.E. (1987) Translocation and clustering of endosomes and Lysosomes depends on microtubules. *J. Cell Biol.* 105: 1253-1265.

Mauri, P., Scarpa, A., Nascimbeni, A. C., Benazzi, L., Parmagnani, E., Mafficini, A., (2005) Identification of proteins released by pancreatic cancer cells by multidimensional protein identification technology: a strategy for identification of novel cancer markers. *FASEB J.* 19: 1125-1127.

Mauri, P. and Dehò, G. (2008) A proteomic MudPIT approach to the analysis of RNA degradosome composition in *Escherichia coli*. *Methods Enzymol.* 447: 99-117.

Michlewski, G. and Kryzosiak, W. J. (2005) Molecular Architecture of CAG Repeats in Human Disease Related Transcripts. *Cerebellum* 4(1):19-24.

Nagayama, K. and Matsomoto, T. (2008) Contribution of actin filaments and microtubules to quasi-in situ tensile properties and internal force balance of cultured smooth muscle cells on a substrate. *Am. J. Physiol. Cell. Physiol.* 295: 1569-1578.

Nicastro, G., Menon, R.P., Masino, L., Knowles, P.P., McDonald, N.Q., and Pastore, A. (2005) The solution structure of the Josephin domain of ataxin-3: Structural determinants for molecular recognition. *Proc. Natl. Acad. Sci. U S A.* 102: 10493-10498.

Nicastro, G., Masino, L., Esposito, V., Menon, R., De Simone, A., Fraternali, F., Pastore, A. (2009) Josephin Domain of Ataxin-3 contains two distinct Ubiquitin-binding sites. *Biopolymers* 91(10): 1203-1214.

Orr, H. T., Zoghbi, Y. H. (2000) Reversing Neurodegeneration: A Promise Unfolds. *Cell*, 101, 1–4.

Paulson, H.L. (1999) Protein fate in neurodegenerative proteinopathies: polyglutamine diseases join the (mis)fold. *Am. J. Hum. Genet*. 64: 339-345.

Paulson, H.L., Perez, M.K., Trottier, Y., Trojanowski, J.Q., Subramony, S.H., Das, S.S., Vig, P., Mandel, J.L., Fischbeck, K.H., and Pittman, R.N. (1997) Intranuclear inclusions of expanded polyglutamine protein in spinocerebellar ataxia type 3. *Neuron* 19: 333-344.

Perutz, M.F., Johnson, T., Suzuki, M., Finch, J.T. (1994) Glutamine repeats as polar zippers: their possible role in inherited neurodegenerative diseases. *Proc. Natl. Acad. Sci. USA* 91: 5355-5358.

Perutz, M.F. (1996) Glutamine repeats and inherited neurodegenerative diseases: molecular aspects. *Curr. Opin. Struct. Biol*. 6: 848-858.

Perutz, M.F., Finch, J.T., Berriman, J., Lesk, A. (2002) Amyloid fibers are water-filled nanotubes. *Proc. Natl. Acad. Sci. USA* 99: 5591-5595.

Pickart, C. M. and Fushman, D. (2004) Polyubiquitin chains: polymeric proteins signals. *Curr. Opin. Chem. Biol.* 8: 610-616.

Pozzi, C., Valtorta, M., Tedeschi, G., Galbusera, E., Pastori, V., Bigi, A., et al. (2008) Study of subcellular localization and proteolysis of ataxin-3. *Neurobiol Dis.* 30:190–200.

Rape, M., Hoppe, T., Gorr, I., Kalocay, M., Richly, H., and Jentsch, S. (2001) Mobilization of processed, membrane-tethered SPT23 transcription factor by CDC48 (UFD1/NPL4), a ubiquiyin selective chaperone. *Cell* 107: 667-677.

Rathinasmy, K. And Panda, D. (2008) Kinetic stabilization of microtubule dynamic instability by benomyl increases the nuclear transport of p53. *Biochem. Pharmacol.* 76: 1669-1680.

Regonesi, M. E., Del Favero, M., Basilico, F., Briani, F., Benazzi, L., Tortora, P., Mauri, P., Dehò, G. (2006) Analysis of the *Escherichia coli* RNA degradosome composition by a proteomic approach. *Biochimie* 88: 151-161.

Ricchelli, F., Fusi, P., Tortora, P., Valtorta, M., Riva, M., Tognon, G., Chieregato, K., Bolognin, S., Zatta, P. (2007) Destabilization of non-pathological variants of Ataxin-3 by metal ions results in aggregation/fibrillogenesis. *Int. J. Biochem. Cell Biol.* 39: 966-977.

Richards, R.I., Sutherland, G.R. (1997) Dynamic mutation: possible mechanisms and significance in human disease. *Trends Biochem. Sci.* 22: 432-436.

Ross, C.A. (1995) When more is less: pathogenesis of glutamine repeat neurodegenerative diseases. *Neuron* 15: 493-496.

Ross, C.A., Poirier, M.A., Wanker, E.E., Amzel, M. (2003) Polyglutamine fibrillogenesis: the pathway unfolds. *Proc. Natl. Acad. Sci. USA* 100: 1-3.

Sakahira H., Breuer P., Hayer-Hartl,M. K., Ulrich H. F. (2002) Molecular chaperones as modulators of polyglutamine protein aggregation and toxicity. *Proc. Natl. Acad. Sci. USA,* 99, 16412–16418.

Sambrook, J., Fritish, E.F. & Maniatis, T. (1989) Molecular Cloning: a Laboratory Manual, second edition, Cold Spring Harbor Laboratory Press.

Sánchez, I., Mahlke, C., Yuan, J. (2003) Pivotal role of oligomerization in expanded polyglutamine neurodegenerative disorders. *Nature* 421(6921): 373-9.

Scheel, H., Tomiuk, S., Hofmann, K. (2003) Elucidation of ataxin-3 and ataxin-7 function by integrative bioinformatics. *Hum. Mol. Genet.* 12: 2845-2852.

Scherzinger, E., Sittler, A., Schweiger, K., Heiser, V., Lurz, R., Hasenbank, R., Bates, G.P., Lehrach, H., Wanker E.E. (1999) Self-assembly of polyglutamine-containing huntingtin fragments into amyloid-like fibrils: implications for Huntington's disease pathology. *Proc. Natl. Acad. Sci. U.S.A.* 8: 4604-4609.

Schuck, P., Minton, A. P. (1996) Kinetic analysis of biosensor data: elementary tests for self-consistency. *Trends Biochem. Sci.* 21: 458-460.

Shehi, E., Fusi, P., Secundo, F., Pozzuolo, S., Bairati, A., and Tortora, P. (2003) Temperature-dependent, irreversible formation of amyloid fibrils by a soluble human ataxin-3 carrying a moderately expanded polyglutamine stretch (Q36). *Biochemistry* 42: 14626-14632.

Sipe, J. D. and Cohen, A. S. (2000) Review: History of the amyloid Fibril. *J Struct Biol* 130: 88–98.

Tait, D., Riccio, M., Sittler, A., Scherzinger, E., Santi, S., Ognibene, A., Maraldi, N. M., Leherach, H., Wanker, E. E. (1998) Ataxin-3 is transported into the nucleus and associates with the nuclear matrix. *Hum. Mol. Genet.* 7: 991-997.

Tan, J. M., Wong, E. S. Kirkpatrick, D. S., Pletnikova, O., Ko, H. S., Tay, S. P., Ho, M.W., Troncoso, J., Gygi, S. P., Lee, M. K., Dawson, V. L., Dawson, T. M. (2007) Lysine 63-linked ubiquitination promotes the formation and autophagic clearance of protein inclusions associated with neurodegenerative diseases. *Hum. Mol. Genet.* 17: 431-439.

Tanaka, F., Reeves, M. F., Ito, Y., Matsumoto, M., Li, M., Miwa, S., Inuka, A., Yamamoto, M., Doyu, M., Yoshida, M., Hashizume, Y., Terao, S., Mitsuma, T., Sobue, G. (1999) Tissue-specific somatic mosaicism in Spinal and Bulbar Muscular Atrophy is

dependent on CAG-repeat length and androgen receptor–gene expression level. *Am. J. Hum. Genet*. 65: 966–973.

Tarlac, V., and Storey, E. (2003) Role of proteolysis in polyglutamine disorders. *J. Neurosci. Res.* 74: 406-416.

Taylor, J.P., Tanaka, F., Robitschek, J., Sandoval, C.M., Taye, A., Markovic-Plese, S., Fischbeck, K.H. (2003) Aggresomes protect cells by enhancing the degradation of toxic polyglutamine-containing protein. *Hum Mol Genet.* 12:749-57.

Tsang, T. M., Woodman, B., Mcloughlin, G. A., Griffin, J. L., Tabrizi, S. J., Bates, G. P., Holmes, E., (2006) Metabolic Characterization of the R6/2 Transgenic Mouse Model of Huntington's Disease by High-Resolution MAS ^{1}H NMR Spectroscopy. *J. Proteome Res.* 5(3): 483-492.

Valiron, O., Caudron, N., Job, D. (2001) Microtubule dynamics. *Cell. Mol. Life Sci.* 258: 2069–84.

Wolters, D. A., Washburn, M. P., Yates 3rd, J.R. (2001) An automated multidimensional protein identification technology for shotgun proteomics. *Anal. Chem.* 73:5683–90.

Wang, G., Ide, K., Nukina, N., Goto, J., Ichikawa, Y., Uchida, K., Sakamoto, T., and Kanazawa, I. (1997) Machado-Joseph disease gene product identified in lymphocytes and brain. *Biochem. Biophys. Res. Commun.* 233: 476-479.

Wang, G., Sawai, N., Kotliarova, S., Kanazawa, I., Nukina, N. (2000) Ataxin-3, the MJD1 gene product, interacts with the two

human homologs of yeast DNA repair protein RAD23, HHR23A and HHR23B. *Hum. Mol. Genet.*.9: 1795-1803.

Wigley, W.C., Fabunmi, R.P., Lee, M.G., Marino, C.R., Muallem, S., DeMartino, G.N., and Thomas, P.J. (1999) Dynamic association of proteasomal machinery with the centrosome. *J. Cell. Biol.* 145: 481-490.

Winborn, B. J., Travis, S. M., Todi, S. V., Scaglione, K. M., Xu, P., Williams, A. J., Cohen, R. E., Peng, J., Paulson, H. L. (2008) The deubiquitinating enzyme Ataxin-3, a Polyglutamine Diseases Protein, edits Lys[63] linkages in mixed linkage ubiquitin chains. *J. Biol. Chem.* 239: 26436-26443.

Ye, Y., Meyer, H.H., and Rapoport, T.A. (2003) Function of the p97-Ufd1-Npl4 complex in retrotranslocation from the ER to the cytosol: dual recognition of nonubiquitinated polypeptide segments and polyubiquitin chains. *J. Cell. Biol* 162: 71-84.

Zhong, X., and Pittman, R.N. (2006) Ataxin-3 binds VCP/p97 and regulates retrotranslocation of ERAD substrates. *Human Molecular Genetics.* 15: 2409-2420.

Zoghbi, H.Y., Orr, H.T. (2000) Glutamine repeats and neurodegeneration. *Ann.. Rev. Neurosci.* 23: 217-247.

Zoghbi, H. Y., Orr, H. T. (2009) Pathogenic mechanisms of a polyglutamine-mediated neurodegenerative disease, spinocerebellar ataxia type1. *J Biol Chem.* 284(12): 7425-9.

Zuccato, C., Tartari, M., Crotti, A., Goffredo, D., Valenza, M., Conti, L., Cataudella, T., Leavitt, B.R., Hayden, M.R., Timmusk, T.,

Rigamonti, D., Cattaneo, E. (2003) Huntingtin interacts with REST/NRSF to modulate the transcription of NRSE-controlled neuronal genes. *Nat. Genet*. 35: 76-83.